GRAIN BOUNDARY CONTROL OF SILICON NITRIDE CERAMICS

Linda Christina Zarnon

Department of Mining and Metallurgical Engineering

McGill University

Montreal, Canada

June 1989

A Thesis Submitted to the Faculty of Graduate Studies

and Research in Partial Fulfillment of

the Requirements for the Degree of

Master of Engineering

To Simon

ABSTRACT

A systematic study of grain boundary control in silicon nitride ceramics was carried out. Three series of compositions with varying amounts of additives were sintered to near-theoretical density to achieve a two-phase system consisting of β silicon nitride or β′ sialon and a Y-SiAlON glass Optimum heat treatment conditions to crystallize the glassy grain boundary phase to $Y_3Al_5O_{12}$ (YAG) were determined to be 1400°C and one hundred hours for most compositions However, devitrification of the glass to garnet had a detrimental effect on the room temperature strength This decrease in strength is attributed to the volume shrinkage associated with the formation of YAG, which results in the debonding of the garnet crystal from the surrounding grains

RESUME

On a effectue une etude systématique du contrôle du joint de grain dans les céramiques de nitrures de silice Trois groupes de compositions differentes comprenant chacun des quantités variables d'additifs ont eté frités jusqu'a atteindre approximativement la densite théorique, le but de cette operation étant d'obtenir un systeme binaire composé de β nitrure de silice ou β' sialon et une phase vitreuse Y-SiAlON Les conditions de traitement thermique optimales permettant la cristallisation de la phase vitreuse se trouvant aux joints de grain en $Y_3Al_5O_{12}$ (YAG) ont été determinees et sont 1400°C et cent heures pour la plupart des compositions Cependant, la dévitrification du verre en "garnet" a eu un effet néfaste sur la resistance mecanique a température ambiante Cet affaiblissement de la resistance mecanique est attribuable à la contraction associée à la formation de YAG qui induit une décohésion des cristaux de "garnet" des grains avoisinnants

ACKNOWLEDGEMENTS

I would like to express my sincere gratitude to my thesis supervisor, Professor R.A L Drew, for invaluable direction and a much admired driving force for research Many thanks to the people who are part of the Department of Mining and Metallurgy for making my years at McGill very memorable, and a special thanks to Professors J J Jonas and R I L Guthrie for use of their Xerox systems.

I would also like to thank the people at NRC for TEM sample preparation and JEOL, U S A for endless hours of help in analyzing TEM samples, in particular Mr J Lehman

Finally, and most importantly I thank my husband, Simon, for believing in me and giving me the confidence to achieve a dream

TABLE OF CONTENTS

LIST OF FIGURES

LIST OF TABLES

CHAPTER 1

INTRODUCTION

Ceramic materials have long been recognized [1-4] as potential candidates in structural and engineering applications due to their excellent mechanical properties and chemical stability at high temperatures. Some of these applications include advanced heat engines, heat exchangers and wear-resistant parts. Ceramics which have been suggested for these applications include silicon nitride, silicon carbide, and toughened zirconia, as these show excellent mechanical properties and chemical stability, even at elevated temperatures.

Silicon nitride (Si_3N_4) in particular has received much attention because of its superior mechanical, thermal, and thermomechanical properties which are important in high temperature applications For example, the use of this ceramic would permit gas turbine operation at temperatures considerably above the limits imposed by the strength of the superalloys currently used[5]. However, the densification of silicon nitride requires the use of sintering aids, which results in the formation of a polyphase material The second phase, which can be glassy and/or crystalline, remains at the grain boundaries, the melting point of which is the limiting factor in the high temperature application of the material.

Since the discovery in 1972 [6,7] of a range of Si_3N_4-based ceramics called Sialons, much promise exists in raising the operational temperature limit of the ceramic. Certain additives are known to form solid solutions with Si_3N_4, and it was originally believed that these sintering aids could be accommodated (completely or in part) within the Si_3N_4 lattice, thereby eliminating or at least reducing the amount of grain boundary phase. A new

science has emerged from this which has become known as Grain Boundary Engineering (GBE) [8,9].

Grain boundary engineering deals with the control of the grain boundary phase through two methods: (1) the careful control of additives which can be substituted within the matrix; this thereby limits the amount of glassy grain boundary phase, and (2) altering the residual glass by heat treatment to form crystalline phases which show superior refractoriness over the glass. The overall aim of GBE is to tailor the grain boundary phase such that the overall mechanical properties of the resulting sialon are improved, especially at elevated temperature.

CHAPTER 2

LITERATURE REVIEW

2.1 THE NATURE OF SILICON NITRIDE

2.1.1 Bonding

The covalent nature of silicon nitride accounts for its chemical inertness, high hardness and strength at high temperatures. These properties are rarely seen in metals due to the relatively weak metallic bonds present which deteriorate at elevated temperatures. This strong directional bonding in Si_3N_4 also accounts for the fact that, unlike metals, this ceramic does not melt but decomposes close to 1900°C and 0.1 MPa of N_2 [4], the reaction being:

$$Si_3N_{4(s)} \rightarrow 3Si_{(l)} + 2N_{2(g)} \qquad (2.1)$$

This dissociation can occur at much lower temperatures in vacuum or inert atmospheres and becomes an important consideration in the sintering process.

Also due to the high degree of covalent bonding in Si_3N_4, self-diffusion coefficients of Si and N are very low, even near the dissociation temperature and, as a consequence, full densification cannot easily be attained by firing without the addition of sintering aids.

2.1.2 Crystal Structure and Morphology

Si_3N_4 crystallizes in two hexagonal modifications [10]: α and β (Figure 2.1), the difference between the two structures being that the c/a ratio of α is almost twice that of β, as seen in Table 2.1. Silicon atoms are located in the center of irregular nitrogen tetrahedra, each nitrogen atom belonging to three tetrahedra. The $Si_{12}N_{16}$ unit cell of the α structure comprises of alternating, mirror-inverted Si_3N_4 layers in the sequence ABCD, resulting in a

	α	β
Structure	hexagonal	hexagonal
a-axis (nm)	0.775-0.777	0.759-0.761
c-axis (nm)	0.516-0.569	0.271-0.292
c/a	~0.70	~0.37
decomposition temperature	1900°C	1900°C
theoretical density ($g.cm^{-3}$)	3.168-3.188	3.19-3.202

Table 2.1. Physical characteristics of silicon nitride [4].

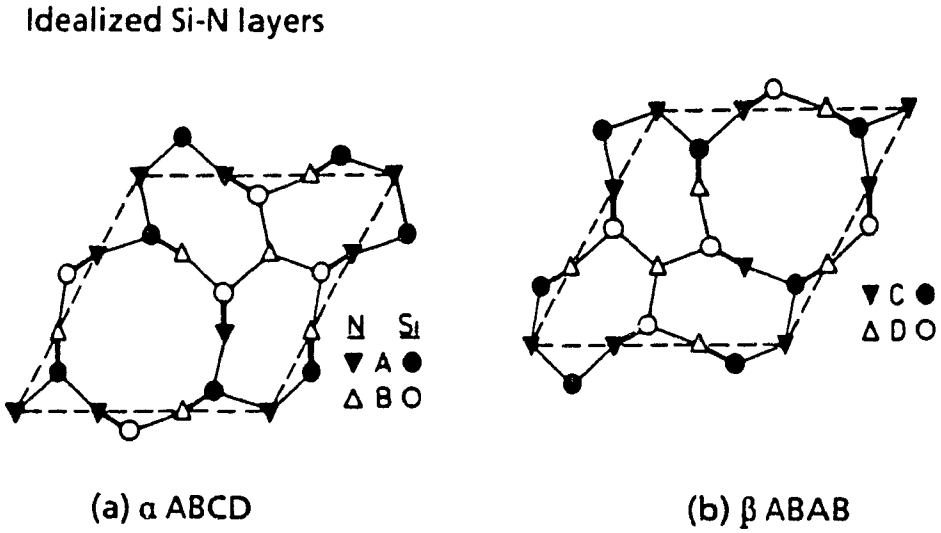

Figure 2.1. Idealized structure of (a) α- Si_3N_4 ;(b) β- Si_3N_4 [6].

closed structure which is twice as long in the c-direction as the β modification. The β structure, with the Si_6N_8 unit cell, is based on that of phenacite (Be_2SiO_4) [11] and consists of Si_3N_4 layers which alternate in the sequence ABAB, forming hexagonal tunnels in the c-axis direction. These tunnels allow for a more open structure than the α modification

The formation of the α phase is thought to be associated with certain ceramic reaction routes during nitridation of silicon [4,12] The phase was believed by some [13,14] to be a form of silicon oxynitride having the formula $Si_{23}N_{30}O$. This is a defect structure in which one in thirty nitrogen atoms are replaced by oxygen. However, this hypothesis was shown to be incorrect [15-17] since α and β powders have been produced which do not contain any oxygen. In this case the α structure consists of only Si and N atoms. However, exact chemistry of the α phase still has not been unequivocally established.

The thermodynamic relationship between α and β structures is also uncertain. The two polymorphs of α and β were originally thought to be low and high temperature modifications [18], respectively; however, both can be synthesized concurrently over a wide temperature range [19] It has been suggested that the α to β transformation proceeds during the densification of Si_3N_4 in the presence of a liquid phase, i.e the β structure is more stable at temperatures greater than 1500°C [19]. This conversion process will be discussed in a subsequent section. It has also been suggested [15] that the β phase could revert back to α, but this has never been observed, perhaps due to the sluggishness of the reverse transformation.

2 2 DENSIFICATION METHODS

Several processing techniques [4] exist for the production of Si_3N_4 components, these are summarized in Table 2 2 The choice of route depends upon the properties required in the dense silicon nitride component Of the methods outlined, only three produce high density ceramics, i e >97% dense, which are of interest on a technological scale, namely (1) hot pressing, (2) hot isostatic pressing (HIP), and (3) sintering Advantages and disadvantages of each route will be discussed in the following sections

2 2 1 Hot Pressing

Typical processing conditions for hot pressing of Si_3N_4 are given in Table 2 2 Hot pressing, or pressure sintering, is analogous to sintering except that high pressures and temperatures are applied simultaneously The applied pressure, typically on the order of 30 MPa, accelerates the kinetics of densification at the sintering temperature by increasing the contact pressure between particles and rearranging the particles to improve packing.

Advantages of this process include [15,20,21]. (a) a reduction in the sintering time and the temperature, which minimizes grain growth, (b) a smaller amount of sintering aids, (c) a minimization of porosity by the removal of large pores, which leads to an improvement in mechanical properties, (d) ultra-fine starting powders are not required, and (e) suppression of the decomposition of Si_3N_4

Disadvantages brought on by axial application of pressure include [4] (a) preferred orientation, or texturing, of the β crystals aligned perpendicular to the hot-pressing direction, leading to anisotropic mechanical properties , (b) shrinkage due to densification is high, in the order of 30% [21], and (c) expensive process due to the short lifetime of the dies and the difficulty in

	Reaction-bonding RBSN	Hot-pressing HPSN	Sintering SSN	Sintering SRBSN	Hot-isostatic Pressing
Starting materials	Si-powder	Si_3N_4-powder + additives	Si_3N_4-powder + additives	Si-powder + additives	1 Si_3N_4 (powder + additive) compacts HIPSN
Processing steps	Moulding		Moulding	Moulding	2
	Nitridation ≧ 1420°C ≦ 72 h	Hot-pressing ≦ 1700°C ≧ 0 5 h ~30MNm-2	Sintering ≦ 1750°C ≧ 1 h p_{N2} ≐ 0 1MPa	Nitridation ≐ 1420°C ≦ 72 h	RBSN-parts with additives (HIPRBSN)
			HIP 3	HIP 2	3
				Sintering ≦ 1750°C ≧ 1 h p_{N2} ≐ 0 1MPa	Pre-sintered Si3N4 parts (HIPSSN)
				HIP 4	4
Final Product	Final part	Machining of the final part	Final part	Final part	Post sintered RBSN (HIPSRBSN)
Shrinkage (%)	0	~30	~15	~5	~15
Post machining	None	Intensive	low	low	low
Final porosity (%)	≐ 20	~0	<3	<5	~0
Flexural strength (MNm 2)	~300 RT ~ 1400°C	≐ 700 RT ~ 1000°C	≐ 700 RT ~ 1000°C	≦ 700 RT ~ 1000°C	≐ 700 RT ~ 1000°C

Table 2 2 Overview and characteristics of processing steps and typical conditions of the various techniques for Si_3N_4 ceramics Note RBSN-reaction bonded silicon nitride, HPSN-hot pressed silicon nitride, SSN-sintered silicon nitride, HIP-hot isostatically pressed silicon nitride

making the process automated to achieve high-speed production. However, the most important limitation, by far, is shape complexity since fabrication is limited to simple geometries with one axis of symmetry requiring subsequent diamond-machining

2 2 2 Hot Isostatic Pressing

Hot isostatic Pressing (HIP), originally developed for the processing of metals and composites, has also been used to improve the mechanical properties of ceramics The process involves the simultaneous application of high pressures and high temperatures (up to 2000°C)[22] to consolidate a compact or to remove residual porosity from pre-sintered materials Typical pressures are around 300 MPa [4], more than one order of magnitude higher than in uniaxial hot pressing, via a gas (Ar, He)

The resulting ceramic shows enhanced properties [4,22]. (a) a resulting near net-shape body of isotropic properties due to application of uniform pressure, (b) smaller amount of sintering aids are required due to enhanced densification at these high pressures, and (c) a more uniform and fine grained microstructure All of these characteristics combined result in an improvement in high-temperature properties and an increase in reliability Despite all the advantages of HIPping, the method is still in the developmental stage, the major limitation of the process being extremely high cost

2 2 3 Sintering of Silicon Nitride

Pressureless sintering of Si_3N_4 is accomplished by liquid phase sintering through the addition of liquid-forming species, and relies entirely on the existing free surface energy of the powder, in conjunction with the liquid phase, as the driving force for densification, i.e. no pressure is applied to drive the reaction as is the case in hot pressing. As a result, more stringent

requirements must be met in the process [4,23] (Table 2.2): (1) a finer starting powder is necessary to reduce the diffusion distances between particles; and (2) the partial pressure of the gases above the sintering bed must be controlled to avoid decomposition of Si_3N_4. The second requirement is fulfilled through the use of a powder bed made up of silicon nitride (to suppress decomposition and vaporization of the constituents by creation of a gas equilibrium in the immediate surroundings) and boron nitride which reduces fritting of Si_3N_4.

One main advantage of pressureless sintering is that there is no shape limitation. Intricate component parts can thus be green formed and sintered to near net shape. However, even by this densification method, a final machining step may still be required. The linear shrinkage associated with pressureless sintering is very high, typically in the order of 15-25% [23].

2.3 LIQUID PHASE SINTERING

Liquid phase sintering is the densification of a solid in the presence of a liquid phase. In order for complete densification to occur, three requirements must be met:

(1) an appreciable amount of liquid must be present

(2) a significant solubility of the solid in the liquid

(3) complete wetting of the solid by the liquid.

2.3.1 The Driving Force for Sintering

The driving force for the densification process is best explained in terms of the surface energies (γ) associated with the system. For wetting of the solid and complete penetration of the liquid between the grains, the following relationship must hold [24]:

$$\gamma_{SV} > \gamma_{LV} > \gamma_{SS} > 2\,\gamma_{SL} \qquad (2.2)$$

where the subscripts refer to solid (S), liquid (L), and vapour (V) phases. The solid-vapour interface (γ_{SV}) can be ignored since it is assumed that the liquid completely wets the solid. If this were not the case, then the solid particles would be joined at the contact points and material transfer within the solid would not result in densification.

As the packing efficiency of a solid is at best 74% (i.e. a close-packed arrangement of mono-sized spheres), a certain amount of residual porosity will always exist, forming a solid-vapour interface [25], as illustrated in Figure 2.2. During the sintering stage the tendency is to eliminate these pores; consequently the high surface energy, γ_{LV}, is the driving force for densification.

The negative pressure in each pore (P_o) is given by the relation[24]:

$$P_o = \frac{-2\gamma_{LV}}{r_p} \qquad (2.3)$$

where r_p is the pore radius. There is an equal and opposite pressure exerted by the small radii of curvature in capillary depressions at the surface. Since the distance separating these capillary depressions between the the solid particles and the pores is small (0.1-1μm), these pressures act as the driving force for densification, i.e. the desire is to eliminate the pores. Initially, these pressures tend to rearrange the particles to maximize packing. Through this rearrangement, the solid particles become joined, although separated by a thin liquid film, (Figure 2.3). These bridges that are formed carry most of the compressive stress at the contact points. It is the capillary pressure of the liquid, P, which holds these spheres together, the pressure given by:

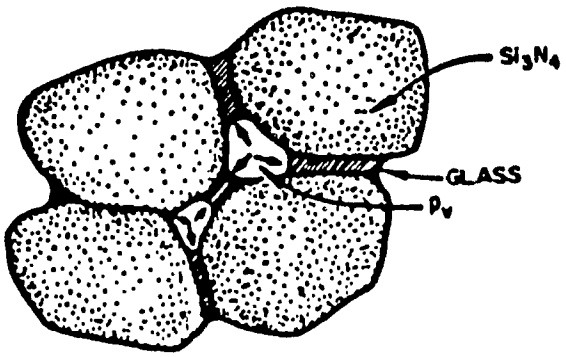

Figure 2.2. Model of liquid-phase sintering involving volatile reaction [25].

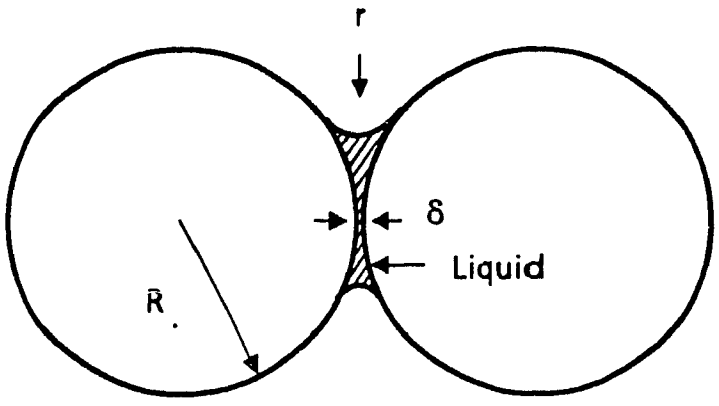

Figure 2.3. Spherical particles held together by liquid capillary pressure [24].

$$P = \frac{-\gamma_{LV}}{r} \qquad (2.4)$$

where r is the radius of the pore. The solid particles do not come into contact with each other but, rather, remain separated by 5-40 nm due to the repulsive forces between them. The liquid film also acts as a binder between the particles

The capillary pressure, which can be substantial (as high as 12 MPa for silicate systems [26]) is also equilibrated by the compressive forces at the contact area. This pressure results in an increase in solid phase activity, a, at the contact points, given by the relationship:

$$ln \frac{a}{a_o} = \frac{K 2\gamma_{LV} V_o}{r_p R T} \qquad (2.5)$$

where the constant K relates the maximum contact area pressure to the overall hydrostatic pressure; V_O is the volume of the solid and liquid phases, R is the gas constant, and T the temperature This increase in activity at the contact points acts as the driving force for material transfer and results in the particle centers moving closer together. This, in turn, increases the density

Thus, it is the tendency to reduce the surface area of the pores in the liquid phase that provides the driving force for sintering

2.3 2 The Sintering Process

Liquid phase sintering is the primary mechanism of densification for most alumino-silicates Complete and rapid sintering of these systems will result if the liquid phase fulfills the requirements mentioned in the previous section, i.e. enough liquid present to completely wet the solid, and solubility of the solid in the liquid Kingery[24] proposed a simple model for the densification mechanism, illustrated in Figure 2 4 [27]

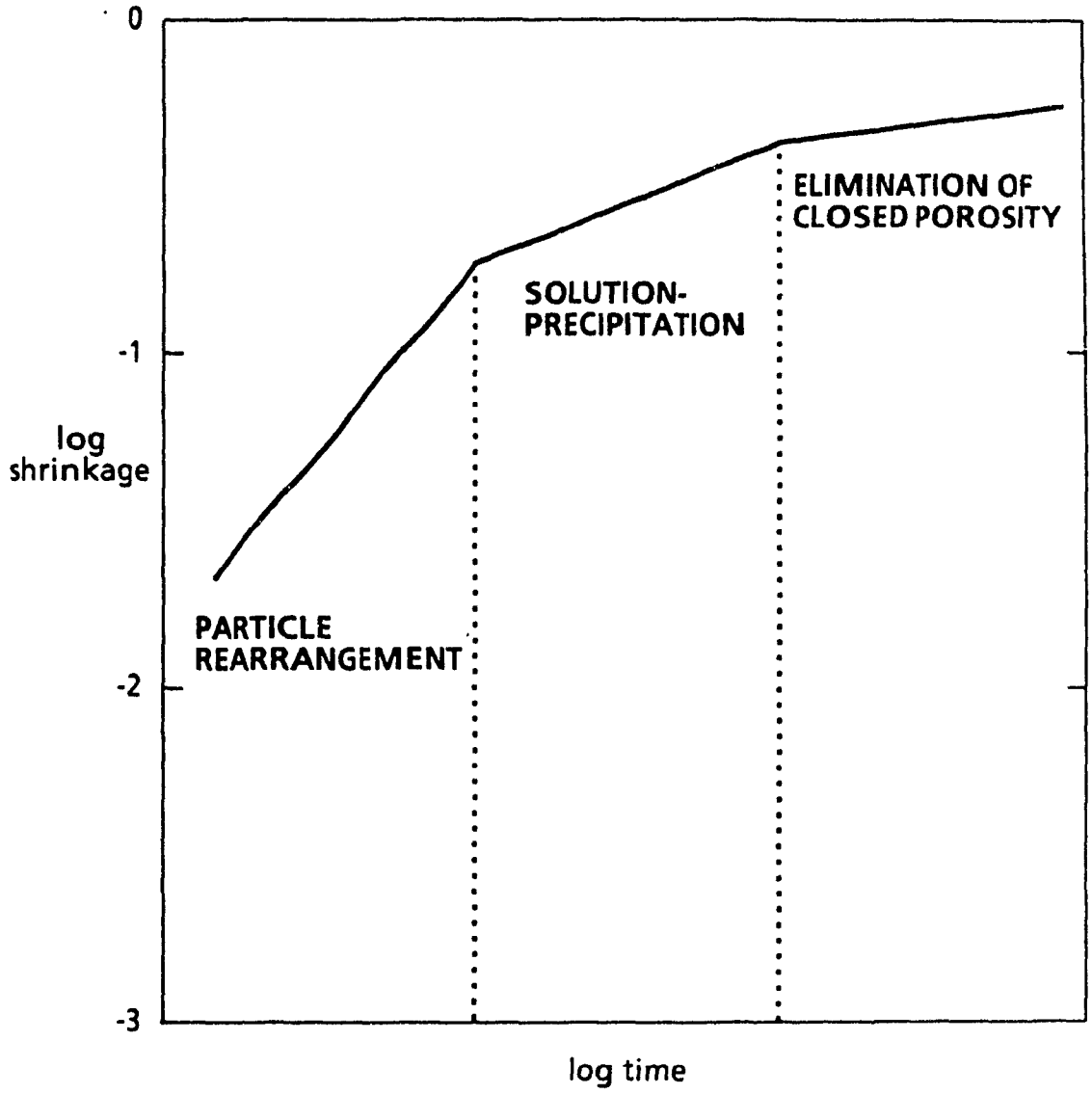

Figure 2.4. Kingery model of liquid phase sintering.[27]

The process can be divided into three steps:

(i) particle rearrangement,

(ii) solution-diffusion-precipitation, and

(iii) coalescence

2.3.2.1 Particle Rearrangement

The start of liquid phase sintering is marked by a rapid increase in the shrinkage rate of the material. This shrinkage is associated with the formation of a liquid phase which coats the solid particles, thus facilitating the sliding of particles over one another. The extent of rearrangement of the particles depends on three factors:

(1) the volume of the liquid phase, i.e. whether enough liquid is available to completely wet the particles and fill the interstices between the particles;

(2) the viscosity of the liquid at the sintering temperature, i.e. whether the viscosity is low enough to allow the sliding of the solid particles over one another; and

(3) the size and shape of the particles in the liquid phase in order to maximize particle/particle impingement.

If the liquid completely wets the solid, each interparticle space becomes a capillary in which substantial capillary pressure is developed. For sub-micron particle sizes, capillaries with diameters in the range of 0.1 to 1 μm develop pressures in the range of 1-12 MPa for silicate systems [26]. Hence, the smaller the particles, the greater the pressure which, in turn, leads to a more rapid densification of the material. This, combined with creep processes (see above), leads to rapid densification in this stage

The fractional shrinkage in the rearrangement process is given by:

$$\frac{\Delta L}{L_o} = \frac{1}{3}\frac{\Delta V}{V_o} = ct^{1+y} \qquad (2.6)$$

where c is a constant, t the sintering time, and $y \leq 1$. The rate of densification corresponds approximately to viscous flow or creep of the particle in the liquid phase and therefore depends on the volume fraction of the liquid phase present. The less viscous the liquid and the more liquid available, the faster the densification becomes.

Complete densification during the rearrangement process is possible if the volume of the liquid content is sufficient (>35%) to fill all of the interstices.

2.3.2.2 Solution-Diffusion-Precipitation

At the end of the rearrangement process, the densely packed solid particles are in close contact with one another and are separated by a thin film of liquid. Material transfer away from the contact points occurs due to the capillary pressures which force the particles together and enhance dissolution. This leads to a decrease in the center-to-center distances between the particles and therefore results in densification

The shape of the solid particles, i e. whether they are spherical or prismatic, will determine the rate of densification at this stage [24,27] A schematic of the solution-precipitation stage is given in Figure 2 5(a) For spherical particles in contact, material transfer can be controlled by either (a) the diffusion of dissolved particles away from the contact points, or (b) by the solution of particles in the liquid, being a phase boundary reaction. The shrinkage, in the case of diffusion controlled densification, is given by:

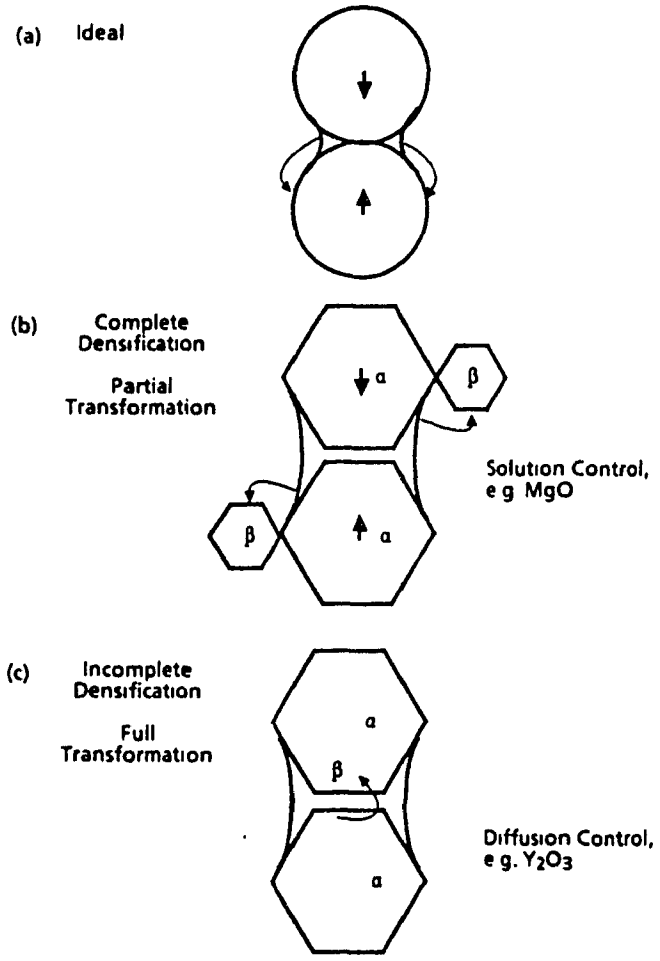

Figure 2.5. Physical representation of liquid phase densification and transformation according to Kingery's stage (ii) solution-precipitation model [27].

$$\frac{\Delta L}{L} = \frac{1}{3}\frac{\Delta V}{V_o} = \left[\frac{6k_2\delta D C_o \gamma_{LV} V_o}{k_1 R T}\right] t r^{-4/3} t^{1/3} \qquad (2\ 7)$$

where δ is the film thickness between the particles, k_1 and k_2 are constants (0-1), V_o is the molar volume of the starting powder, C_o is the solubility of the particles in the liquid, D is the diffusion coefficient in the liquid phase, and r is the initial particle size. The shrinkage due to this process is proportional to the one-third powder of time and inversely proportional to the four-thirds power of the initial particle size.

If the rate controlling step is the phase boundary reaction leading to solution, the sintering equation becomes.

$$\frac{\Delta L}{L} = \frac{1}{3}\frac{\Delta V}{V_o} = \left[\frac{2k_2k_4\delta C_o \gamma_{LV} V_o}{k_1 R T}\right] t r^{-1} t^{1}$$ (2 8)

where the time exponent is increased to 1/2 from 1/3 The densification rate is also slower for solution-controlled densification

For prismatic particles, similar equations for densification apply However, the acicular grains are oriented in a random fashion, leading to a more complex geometric relationship than is the case for spheroidal grains in contact. In the case of a diffusion-controlled process (Fig 2 5(b))

$$\frac{\Delta V}{3V_o} \propto t^{1/5} \qquad (2\ 9)$$

while if the rate controlling step is a solution process (Fig. 2 5(c)), then

$$\frac{\Delta V}{3V_o} \propto t^{1/3} \qquad (2\ 10)$$

2.3.2.3 Coalescence

The coalescence process results in the elimination of closed pores. These internal pores are due to the incomplete wetting of a certain number of grains which are oriented such that the grain boundary energy (γ_{SS}) is smaller than twice the solid-liquid interface energy (γ_{SL}) (see Equation 2.2). In order for densification to take place, material transfer within the solid phase must occur. Thus, the densification rate at this stage is greatly reduced due to the low surface energy associated with γ_{SS}

2.3.2.4 Effect of other Parameters on Densification

The initial particle size is important in all sintering processes as smaller particles lead to higher capillary pressures, and thus more rapid shrinkage However, for reactive liquid phase sintering, the growth of solid particles only has a small effect on the rate of densification. This is because the main driving force for the process is the decreased liquid vapor surface area (γ_{LV}), the controlling parameter, then, is the size of the pores in the liquid phase[24,26] That is, a decrease in the surface area of pores in the liquid phase results in a major decrease in the free energy, thereby providing the driving force for sintering Secondly, the temperature dependence, which is a result of the diffusion coefficient in the liquid phase, is much lower than for other sintering processes as the diffusion coefficient does not change markedly with temperature

In summary, for complete densification, the following criteria must be met.

(i) ultra-fine starting powders must be used to decrease the diffusion distances between particles and increase the thermodynamic driving force

(ii) a high sintering temperature is required to increase diffusion rates and lower the liquid viscosity

(iii) equilibrium between the partial pressure of the reactants must exist to avoid dissociation of the starting material

(iv) an external pressure, in addition to the effective pressure derived from capillary forces, can be used to increase the driving force for sintering, e.g hot pressing or hot isostatic pressing

2 3 3 Liquid Phase Sintering of Si_3N_4 and Sialons

Densification of Si_3N_4 containing an additive is generally attributed to the presence of a liquid formed at high temperatures according to the general reaction [28]:

$$Si_3N_4 + SiO_2 + metal\ oxide + impurities \xrightarrow[Temp]{} Si_3N_4 + oxynitride\ liquid \qquad (2\ 11)$$

SiO_2 is included in the reaction as it is invariably present on the surface of Si_3N_4 powder

The sintering stages for Si_3N_4 [27] are illustrated in Figure 2 6 In the case of sintering of Si_3N_4 ceramics,the mechanism of dissolution involves the breaking of Si-N bonds, where the additives provide a liquid medium which dissolves the α-Si_3N_4. The material is then transferred away from the contact areas, resulting in a movement of the particle centers towards each other, and hence leads to shrinkage The diffusion of the dissolved Si and N in the silicate or oxynitride liquid is much greater than the self-diffusion in Si_3N_4, this therefore leads to an increase in the densification rate

As the sintering temperature is raised above 1400°C, the α phase becomes unstable and thus precipitation of the more stable β phase occurs Precipitation of β-Si_3N_4 occurs at preferred sites or on pre-existing β-Si_3N_4

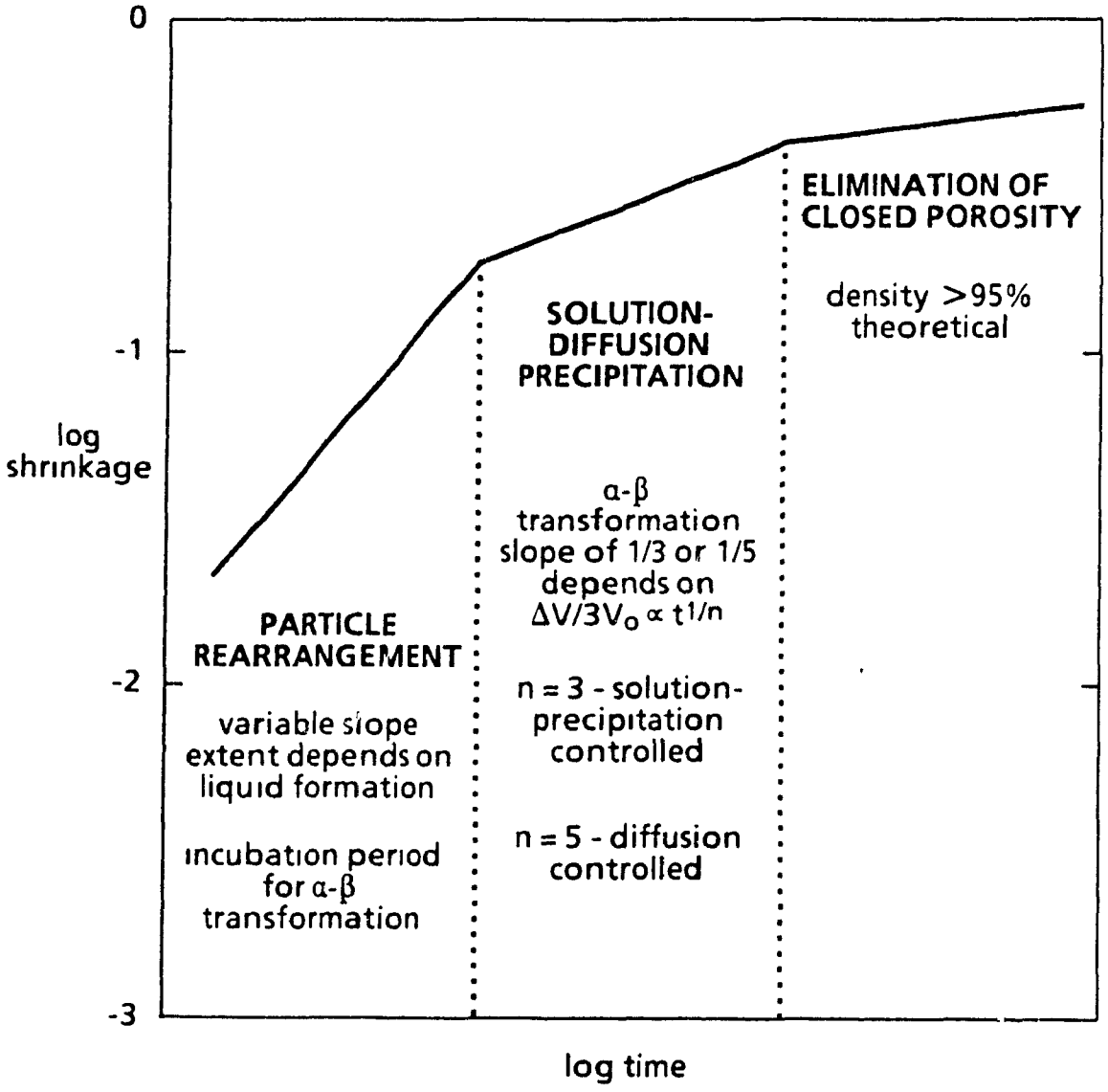

Figure 2.6. Kingery process of densification of Si_3N_4 [27].

particles in the starting material [4] (Figure 2.7). It has been found [29] that starting powders containing >95% α are required to induce the self-precipitation of the β phase. The reason for this is the instability of α with respect to β, which causes enhanced solution of α into the liquid phase. If the starting material contains a large number of β grains, the fine particles start to dissolve and re-precipitate on pre-existing β grains. If, on the other hand, the initial β content is small, then spontaneous nucleation and growth of rod-like β grains will occur This second case is the more desirable, as the resulting grain size is more uniform. The effect of grain morphology on mechanical properties will be reviewed in a later section

The rate of shrinkage in the transformation stage is given by:

$$\frac{\Delta L}{L_o} = \frac{1}{3}\frac{\Delta V}{V_o} = (A\,t)^{1/n} \qquad (2.12)$$

where A is a constant, and n determines the rate-controlling step (see Figure 2.6). If the process depends upon solution of α-Si_3N_4 into or precipitation of β-Si_3N_4 from the liquid, then n = 3 (phase boundary reaction). If, on the other hand, diffusion through the liquid controls the rate of densification, then n = 5. The rate-controlling step therefore determines the rate of shrinkage densification occurs more rapidly if the rate-determining step is dependent upon precipitation of β-Si_3N_4, and it can thus be controlled by the starting materials used, i.e. high α content.

Hampshire and Jack [27] did a comparative study of the densification rates using MgO and Y_2O_3 as sintering aids (Figure 2 8) They found that with magnesia, rapid densification occurred during the rearrangement stage; while during the solution-precipitation stage,they showed that n = 3, suggesting that the process is reaction-controlled (Fig. 2.5(b)) With yttria, on

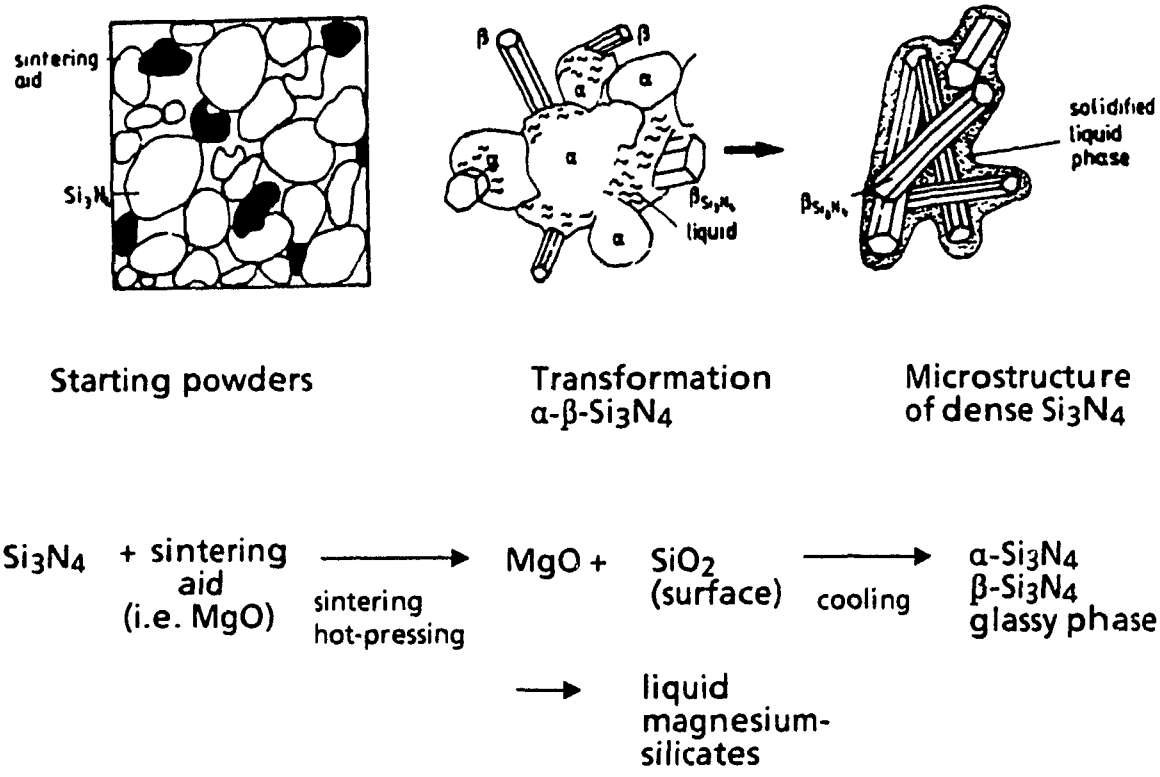

Figure 2.7. Solution-precipitation model for the liquid phase sintering of Si_3N_4 (schematic drawing) [4].

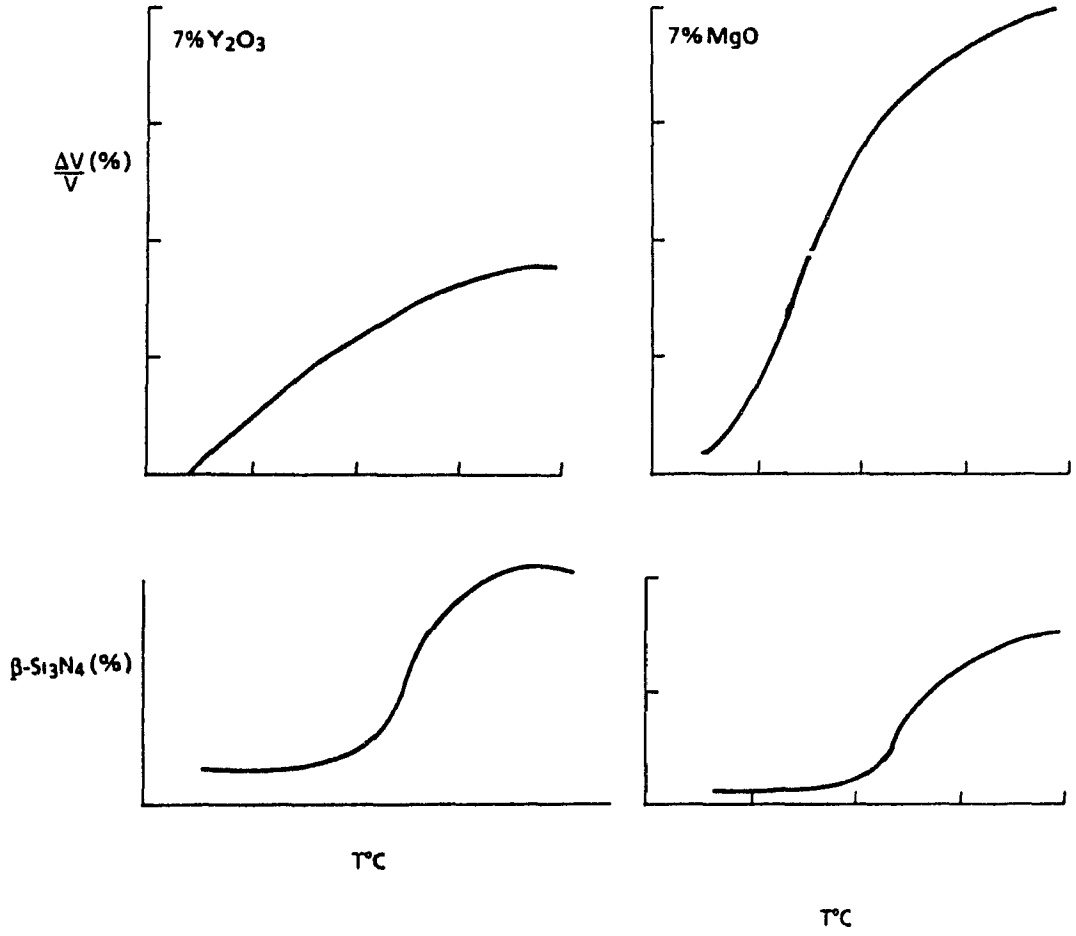

Figure 2.8. Shrinkage and transformation after 30 minutes of various temperatures for pressureless sintering of silicon nitride with Y_2O_3 and MgO [27].

the other hand, the rearrangement process did not contribute significantly to densification Rather, during the solution-diffusion-precipitation stage, diffusion through the liquid was the rate controlling step (Fig 2.5(c)) The difference between these two sintering aids is a result of the smaller liquid volume and higher liquid viscosity of Y_2O_3 over MgO

The densification rate increases rapidly during this stage to near completion with the transformation of α to β-Si_3N_4, as this conversion is thermodynamically favourable at temperatures greater than 1400°C There is, however, an upper limit to this transformation due to particle impingement of the β-Si_3N_4 grains as full conversion is approached

The final stage of densification is the coalescence process, during which the elimination of closed porosity occurs. Grain growth of the β phase also proceeds, with a resulting morphological change from rod-like structures to more equiaxed grains Due to this change in grain shape, excessive grain growth is accompanied by a marked decrease in strength (see later) Furthermore, if the starting material contained a high β-content, then precipitation of the β phase onto these original grains will result in inhomogeneous grain size. That is, the β grains which were present in the starting material will have grown to a far greater extent than those which were precipitated from solution This leads to a deterioration in the mechanical properties

Once the sintering stage has been completed, and the system returns to ambient temperatures, the oxynitride liquids cool to form an amorphous or partly crystalline phase along the grain boundaries and at triple points of the β-Si_3N_4 grains (as shown in Figure 2 7) This glassy grain boundary phase softens at high temperatures and is responsible for the deterioration of mechanical properties (see Section 2 6)

2.4 THE ROLE OF SINTERING AIDS

Densification of Si_3N_4 without any additive has been achieved by hot isostatic pressing (HIP). Prochazka and Rocco [30] were the first to achieve densities of 95% theoretical by hot pressing silicon-rich (~8%) powders at 5GPa and 1500-1600°C for 20 minutes. Yamada et al. [31] obtained near full densities by hot pressing highly pure powders at 1600°C for 1 hour Miyamoto et al. [32] obtained densities greater than 99% by the glass container and HIPing method at 150MPa and 1900-2000°C for 2 hours However, in all cases, the mechanical properties of the sintered silicon nitride were inferior to those achieved by other sintering methods due to the euhedral morphology of the β grains.

Depending on the purity of the starting material, some silica is always present on the surface of Si_3N_4 powder, which reacts with the silicon nitride to form an oxynitride [33] according to:

$$Si_3N_4 + SiO_2 \rightarrow 2Si_2N_2O \qquad (2.13)$$

This oxynitride phase was also observed in some HIPped samples reported by Miyamoto et al.[32]

Through the use of sintering aids, however, full densification and improved mechanical properties can be achieved The function of an additive is to provide conditions for liquid phase sintering, i e. solubility of the solid in the liquid and complete wetting of the solid. This is due to the increase in diffusion coefficients of the ions in the liquid phase The rate and temperature at which densification occurs depends mainly on (a) the amount and (b) type of additive.

2.4.1 Effect on Densification

The effect of liquid volume on densification is illustrated in Figure 2.9 [34]. It is seen that the incremental addition of MgO results in an increasing densification rate since the particles can rearrange themselves with more ease when more liquid is present. In general, increasing the amount of liquid phase by the addition of more sintering aids enhances densification. The liquid phase coats the silicon nitride grains and remains along the grain boundaries. When the volume fraction of the liquid phase is increased, for example from 2 to 10%, the thickness of the liquid layer between the β-Si_3N_4 grain boundaries remains constant, ~1-2nm; the excess liquid is accommodated at triple points between the β-Si_3N_4 grains to form pockets of glass [35]. This volume increase of the grain boundary phase leads to a deterioration of mechanical properties especially at high temperatures, as will be seen in a later section of this chapter.

2.4.2 Types of Additives

Sintering aids are most commonly metal oxides and oxide mixtures which either:

(a) form solid solutions with Si_3N_4, such as BeO, and an equimolar mixture of Al_2O_3 + AlN; or

(b) do not form solid solutions with Si_3N_4, such as MgO, Y_2O_3, Al_2O_3, and ZrO_2

The mechanism for both of these types of sintering aids is the same: the additive reacts with the SiO_2 layer and impurities on the particle surfaces of α-Si_3N_4 to form a eutectic liquid at temperatures between 1300°C and 1700°C, depending on the oxide. Upon cooling, this liquid forms an amorphous or partly crystalline grain boundary phase. The sintering stage can be summarized by the following reaction [2]:

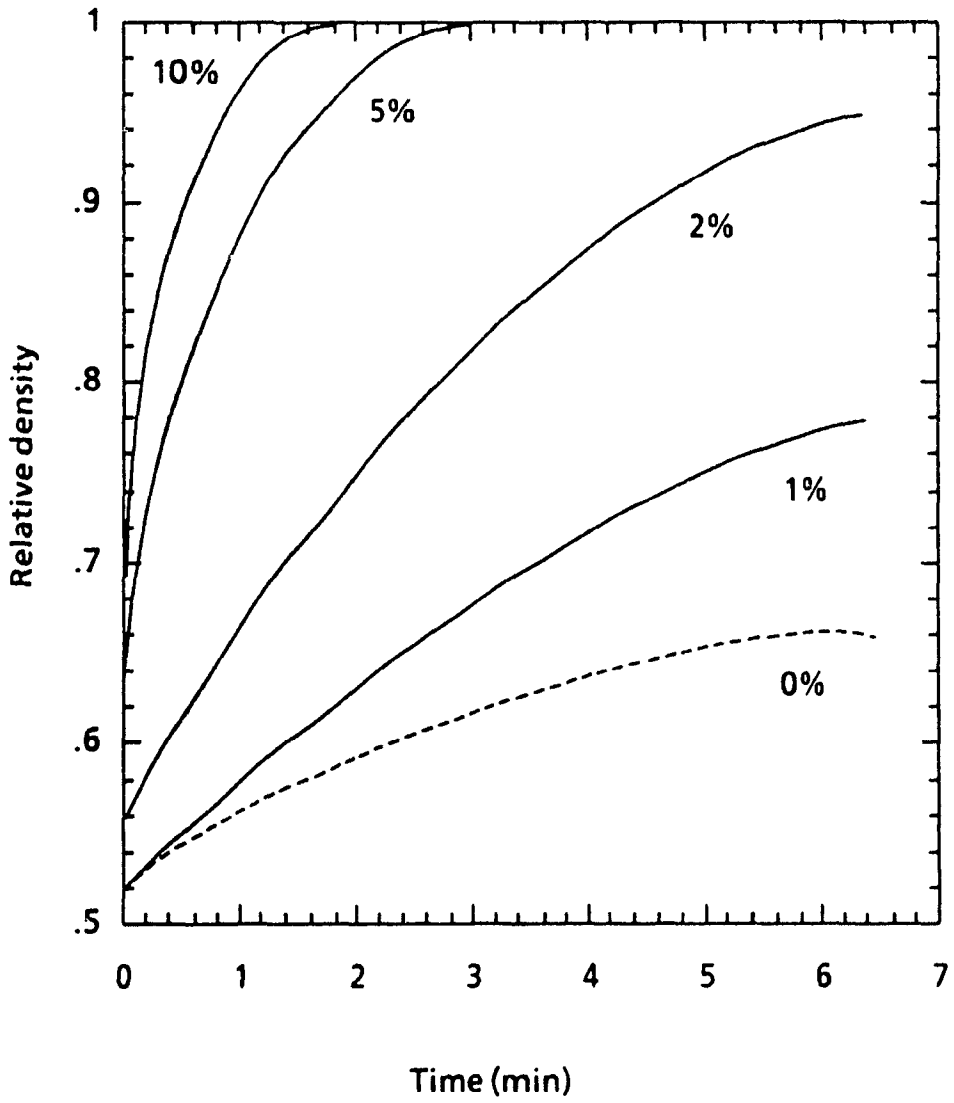

Figure 2.9. Influence of the amount of MgO addition on the densification of Si_3N_4 by hot pressing. T = 1650°C, p = 20 MNm^{-2}. [34]

$$Si_3N_4 + additive + SiO_2 + (impurities) \xrightarrow{1700-2000°C} \beta Si_3N_4 + liquid$$

$$\beta Si_3N_4 + liquid \xrightarrow{cooling} \beta Si_3N_4 + second\ phase(s) \qquad (2.14)$$

Impurities, particularly alkali (Na, K, Ca, Fe), and alkali-earth oxides tend to migrate to the glassy grain boundary phase This results in a further lowering of the glass viscosity, and leads to a decrease in strength and creep resistance of the final product [36] (refer to Section 2.6 on Mechanical Properties)

The rate of densification will therefore be dependent on the type of sintering aid, as the latter will dictate the degree of wetting and the viscosity of the liquid.

2 4.2.1 The Sialon System

The acronym "Sialon" was originally given to a group of new compounds derived from silicon nitride and oxynitride by the simultaneous replacement of silicon and nitrogen by aluminum and oxygen [37] The ability of Si_3N_4 to undergo this substitution can be explained in terms of the similar bond lengths between Si-N (1 75Å) and Al-O (1 75Å), and the difference between Al-N (1 87Å) and Si-O (1 62Å) [14] The extent of solid solutions are illustrated in the respective equivalence diagram in Figure 2 10, which is an idealized behaviour diagram for the Si-Al-O-N system at 1700°C [38] The β'-Sialon phase is the most important solid solution phase within the system It extends along a constant M/X ratio of 3.4, with a homogeneity range of $Si_{6-z}Al_zO_zN_{8-z}$, where z reaches a maximum value of 4.2. Because of its structure, the physical and mechanical properties of the β' are similar to

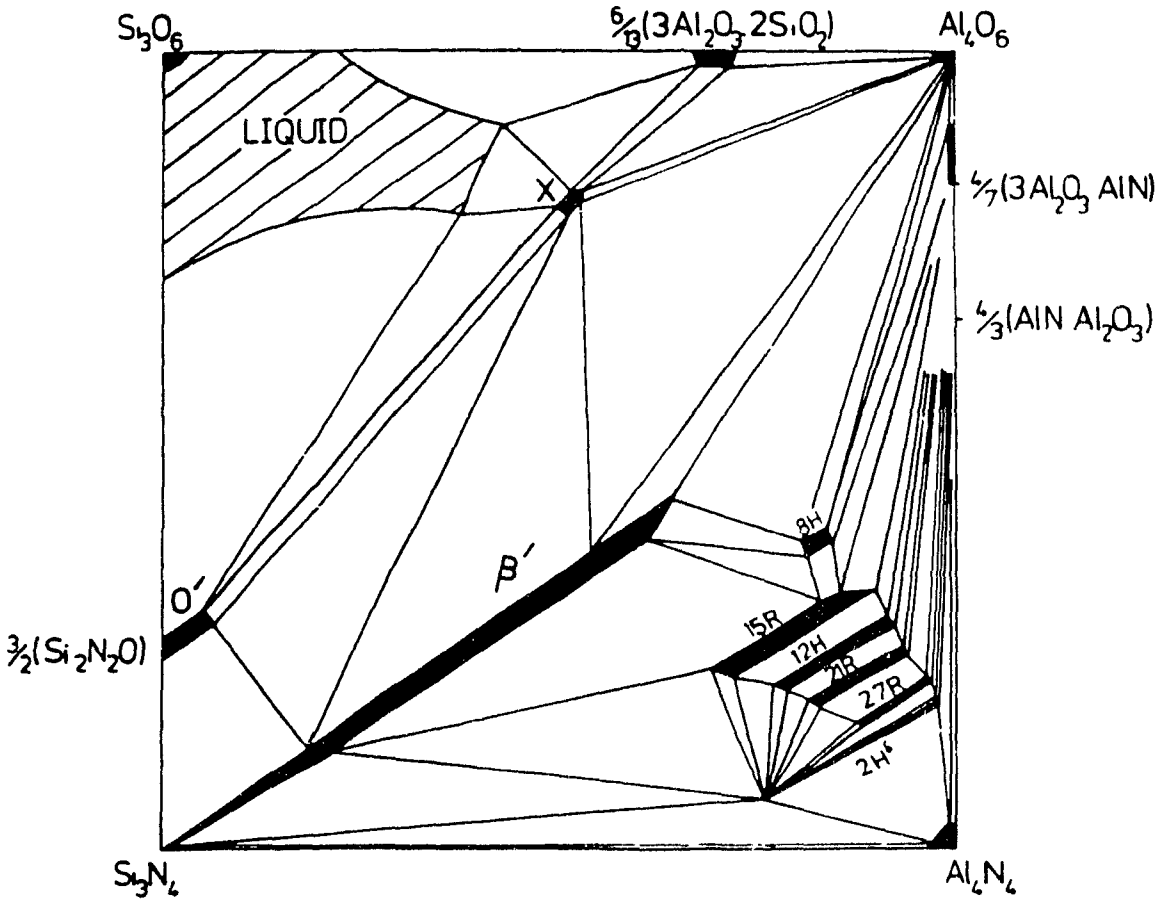

Figure 2.10. Phase relationship of Si_3N_4-Al_2O_3-SiO_2-AlN at 1700°C [14].

those of β-Si_3N_4, but chemically it is closer to aluminum oxide (Al_2O_3). The overall effect of this substitution is a decrease in thermal conductivity, which tends to lower the thermal shock resistance [39] Figure 2 11 illustrates the effect of substitution of Si_3N_4 on thermal expansion the linear coefficient of thermal expansion of the resulting sialon with $z = 3$ ($2.7 \times 10^{-6}°C^{-1}$) is less than that of pure β-Si_3N_4 ($3.5 \times 10^{-6}°C^{-1}$) [40] Also, as the extent of substitution increases, so does the hexagonal unit cell dimension [40], as shown in Figure 2.12

Thompson [41] was the first to characterize the solid solution compounds of 8H, 15R, 12H, 21R and 27R, as compositional polytypes of the AlN structure Each polytypoid is formed by a different repetitive stacking of similar structural layers, with a constant M/X ratio of 3.4 Other phases shown in the behaviour diagram in Figure 2 10 are the O' phase, which is based on the Si_2N_2O-type structure, and the X-phase, of composition close to $3Al_2O_3\ 2Si_3N_4$

Figure 2 13 illustrates the extent of the liquid phase field in the Si-Al-O-N system at 1750°C, a typical sintering temperature [38] It is clear from this that the oxynitride glass is in equilibrium with β', with no eutectics reported to date [15] Upon rapid cooling, this liquid will form an oxynitride glass [42]; however, this glass is unstable and requires a liquid quench at greater than $500°C min^{-1}$ to obtain a completely vitreous product [43] Thus, achieving a single crystalline phase system is at best difficult within the SiAlON system due to the instability of the glass However, the addition of metal oxides (MgO, Y_2O_3) to the system leads to a more extensive and stable glass-forming region, as will be discussed in the next section

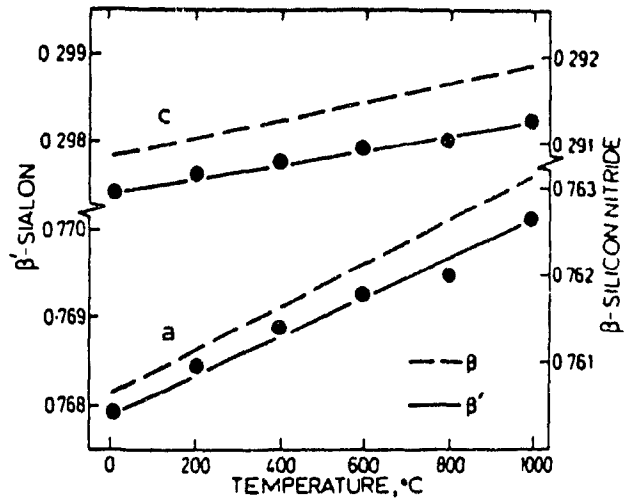

Figure 2.11. Thermal expansion of β'-Sialon (z = 3) and β-silicon nitride [40].

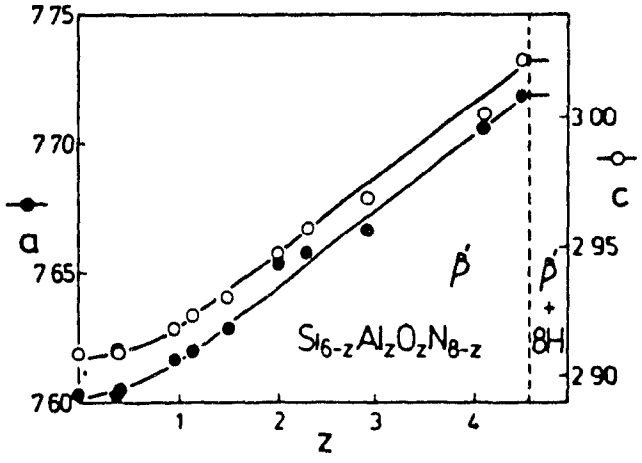

Figure 2.12. Effect of extent of substitution on cell dimensions [40].

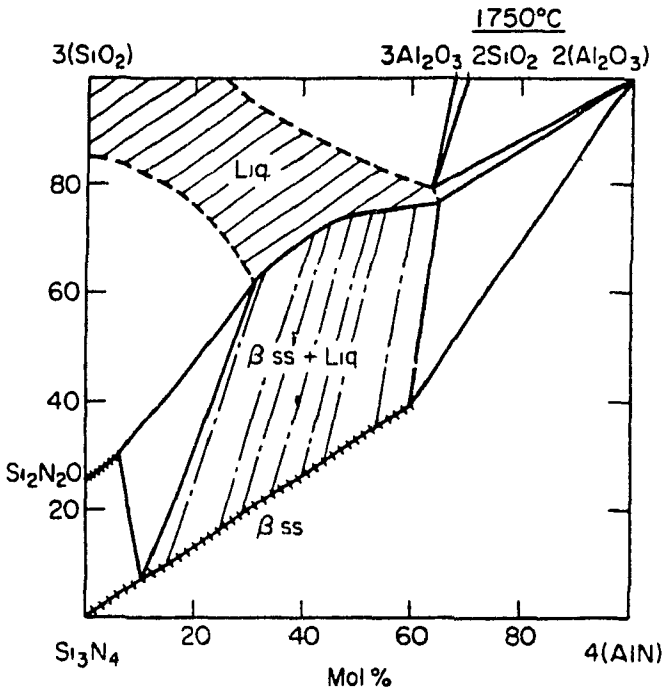

Figure 2.13. Phase relationships at 1750°C indicating extent of liquid field in SiO_2 end of diagram [38].

2.4.2.2 Sintering with Oxide Additives

Sintering aids which do not form solid solutions with Si_3N_4 are used mainly to provide conditions for liquid phase sintering by reducing the viscosity of the glass. Magnesium oxide, the first widely used additive, has been shown to react with the surface layer of silica to form an oxynitride liquid [44]. Impurities in the silicon nitride further reduce the solidus temperature of MgO-SiO_2 from 1547°C to 1450-1500°C [45]

The high temperature strength loss exhibited by MgO-doped Si_3N_4 is attributed to the low softening temperature of the glass phase (850°C-900°C). Richerson [46] has suggested two approaches to improve the high temperature properties of silicon nitride. The first was to reduce the alkali impurities contents in the starting materials and minimize the amount of additive. The second was to use a sintering aid which formed a more refractory intergranular phase.

Gazza [47] showed that the addition of Y_2O_3 to relatively impure α-silicon nitride results in a refractory yttrium silicate grain boundary phase, stable to at least 1600°C; the mechanical properties were also greatly improved

The mechanism for sintering with Y_2O_3 is similar to the others reviewed (see Eq. 2.14) in that the surface silica and some of the nitride react to give an oxynitride liquid As the reaction proceeds, this liquid combines with more Si_3N_4 to give one or more refractory bonding phases in which are accommodated impurities that would otherwise degrade properties[33] The unreacted liquid cools to give a glass and/or crystalline phases Densification of Si_3N_4 with Y_2O_3, however, is slower than with MgO since the rate determining step is solution-precipitation controlled rather than diffusion controlled (see Fig. 2.5) The Y_2O_3-SiO_2 solidus is between 1660°C and 1980°C [48], as seen on the phase diagram in Figure 2 14 In addition, the viscosity of

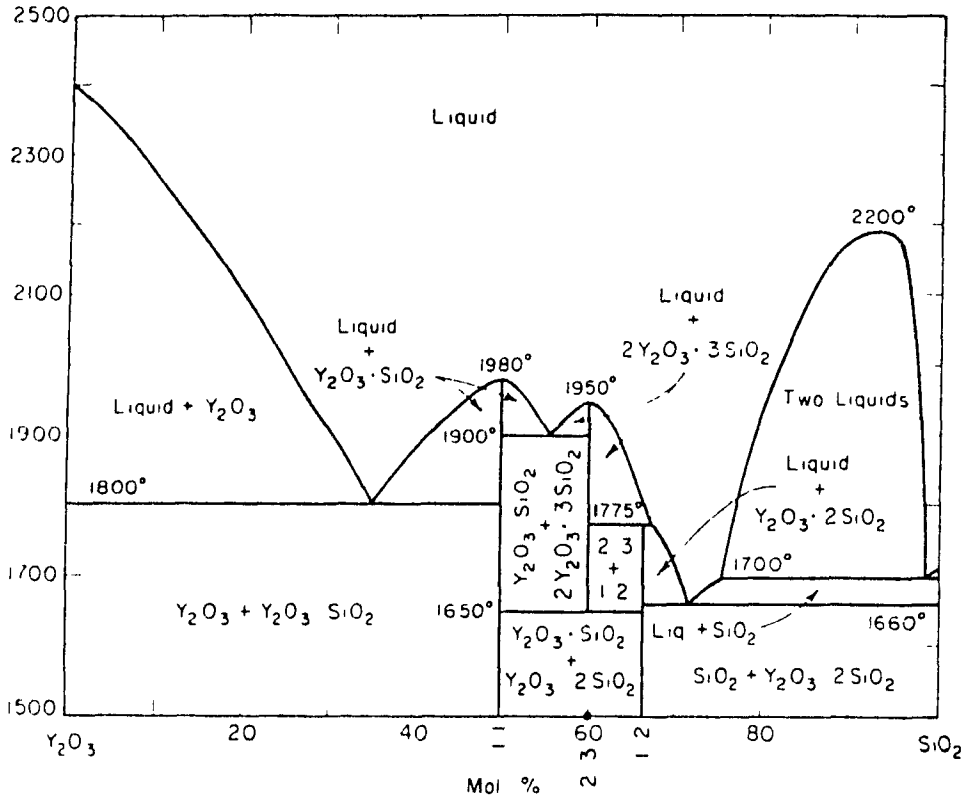

Figure 2 14. System Y_2O_3- SiO_2. [38]

the Y_2O_3-SiO_2 liquid formed is higher and forms less liquid at lower temperatures than MgO-SiO_2.

Subsolidus phase relations in the Y-Si-O-N system are shown in Figure 2.15. Work at Newcastle [38] characterized the four quaternary phases that are possible in the system:N-melilite ($Y_2O_3.Si_3N_4$), N-apatite ($Y_9Si_6O_{21}N_3$), N-YAM ($2Y_2O_3.Si_2N_2O$) and N-α-wollastonite ($Y_2O_3.Si_2N_2O$). Table 2.3 gives the melting points of the quaternary phases.

All of these phases are stable to at least 1600°C, with the exception of N-α-wollastonite, which decomposes above ~1400°C to give mainly Y-phase and melilite, $Y_{10}(SiO_4)_6N_2$ and $Y_2Si_3O_3N_4$, respectively [41]. However, the phases present within this system undergo large molar volume changes in an oxidizing environment, which results in catastrophic strength degradation at elevated temperatures [28]. Thus, the presence of these four quaternary phases is undesirable.

If the system is fabricated within the Si_3N_4-Si_2N_2O-Y_2SiO_7 compatibility triangle (shaded area in Figure 2.15), the oxynitride phases described above can be avoided. The resulting silicate compounds (Y_2O_3 SiO_2, $2Y_2O_3$ $3SiO_2$, $Y_2O_3.2SiO_2$) show improved oxidation resistance and excellent refractory characteristics (refer to Table 2.3 for melting points). Moreover, the highest yttrium silicate, $Y_2Si_2O_7$, shows compatibility with SiO_2, and is therefore a stable phase. The major drawback of this disilicate, however, is the large volume difference between $Y_2Si_2O_7$ and the yttrium silicate glass from which it crystallizes. This volume change, which accompanies crystallization, imposes a high stress on the surrounding Si_3N_4 grains, and results in a deterioration of the mechanical properties [49].

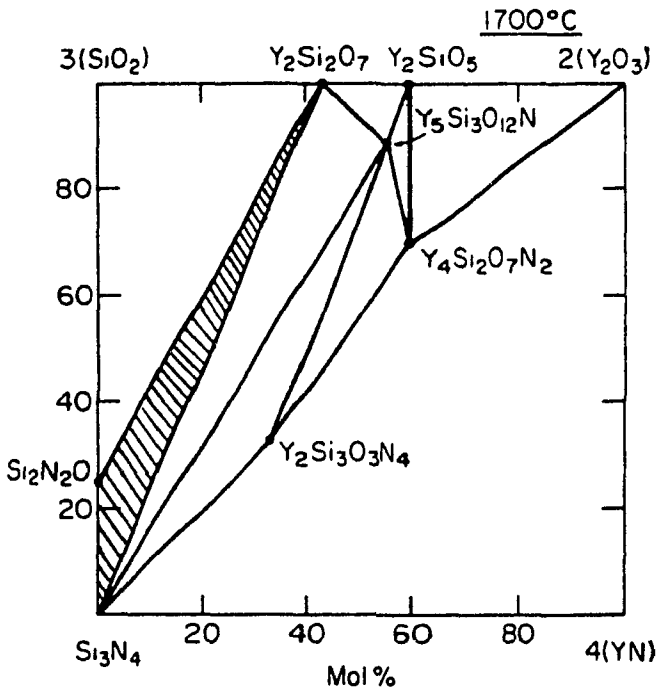

Figure 2.15. Subsolidus phase relationships in Si-Y-O-N system [38].

Phase	Formula	Melting Temperature (°C)
yttrium silicate	$Y_2O_3.SiO_2$	1980
yttrium silicate	$2Y_2O_3.3SiO_2$	1950
YAP	$Y_2O_3.Al_2O_3$ (meta-stable)	1875
YAG (garnet)	$Y_3Al_5O_{12}$	1860
yttrium disilicate	$Y_2O_3.2SiO_2$	1775
N-melilite	$Y_2O_3.Si_3N_4$	1600
N-apatite (H-phase)	$Y_{10}(SiO_4)_6N_2$	1600
N-YAM (J-phase)	$Y_4Al_2O_9$-$Y_4Si_2O_7N_2$ solid solution	1600
N-wollastonite (K-phase)	$YSiO_2N$	1400

Table 2.3. Melting temperatures of typical crystalline phases formed.

Other rare earth systems additives have been studied, i.e. CeO_2[33,50], ZrO_2[33], Nd_2O_3 [15] and La_2O_3 [51]; however, the resulting high temperature properties were not as impressive as for Y_2O_3.

Figure 2.16 shows the effect of the different sintering aids on densification. Si_3N_4 with no additives shows limited densification even at high temperatures, as was discussed in Section 2.3. In the case of Y_2O_3, the lowest melting temperature of Y_2O_3-SiO_2 is very high (1660°C), thus allowing for densification to take place at higher temperatures (if increased N_2 pressure is used to suppress Si_3N_4 decomposition). More importantly, less liquid is formed with the addition of Y_2O_3 than with MgO. Hence, less grain boundary phase is present, and the high temperature strength and creep resistance of the material are improved.

The addition of Al_2O_3 to Si_3N_4 containing Y_2O_3 was shown [20,50,52] to be more effective than simply using Y_2O_3 in assisting the sintering process . Rowcliffe and Jorgensen [53] were the first to show that 95% dense sialons could be achieved using these additives. The behaviour diagram for this system [33] at 1700°C is given in Figure 2 17. The tie lines shown run from the stable Si_3N_4 compounds to the oxide end of the phase diagram. Of the three stable crystalline phases in the system, $Y_3Al_5O_{12}$ (YAG) is the most refractory, with a melting temperature of 1860 °C, in contrast to ~1700°C for (YAM) and (YAP). The two latter phases, as seen earlier, cannot withstand oxidizing environments. However, YAG , with a composition of $Y_3Al_5O_{12}$, is an oxide phase and would not suffer catastrophic strength degradation due to oxidation YAG is therefore seen as the most desirable crystalline grain boundary phase in terms of its excellent refractoriness as well as oxidation resistance

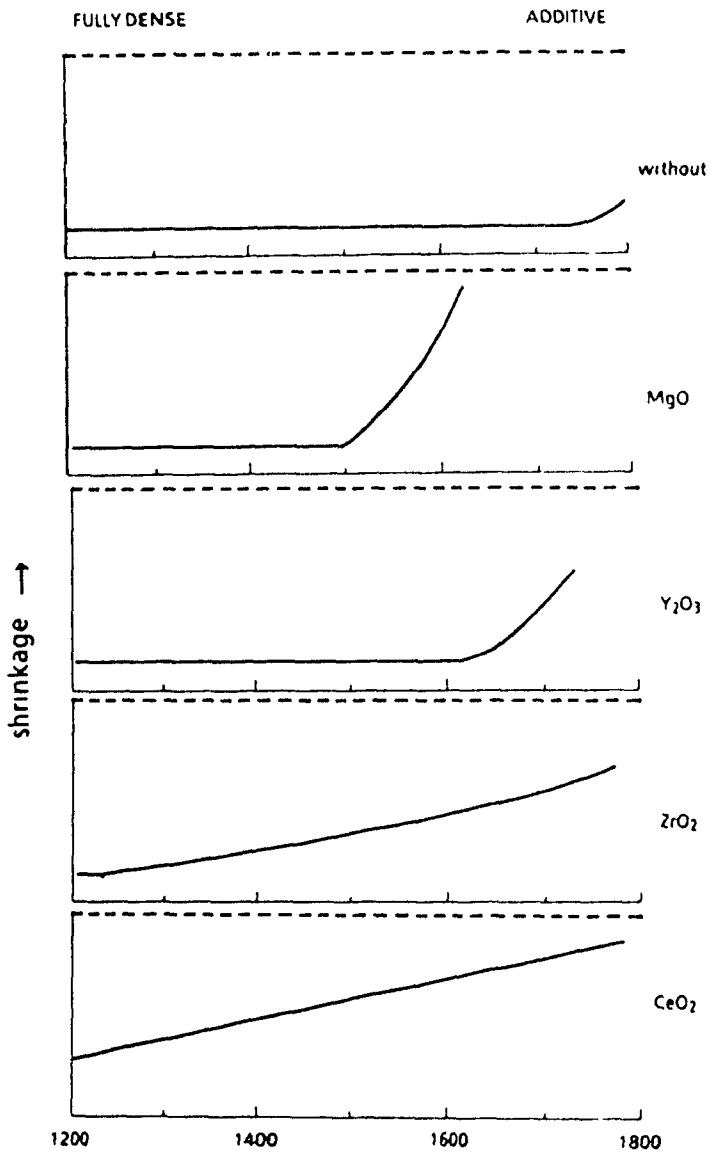

Figure 2 16 Influence of the type of additive on the densification of Si_3N_4 by hot-pressing (schematic plot) [79]

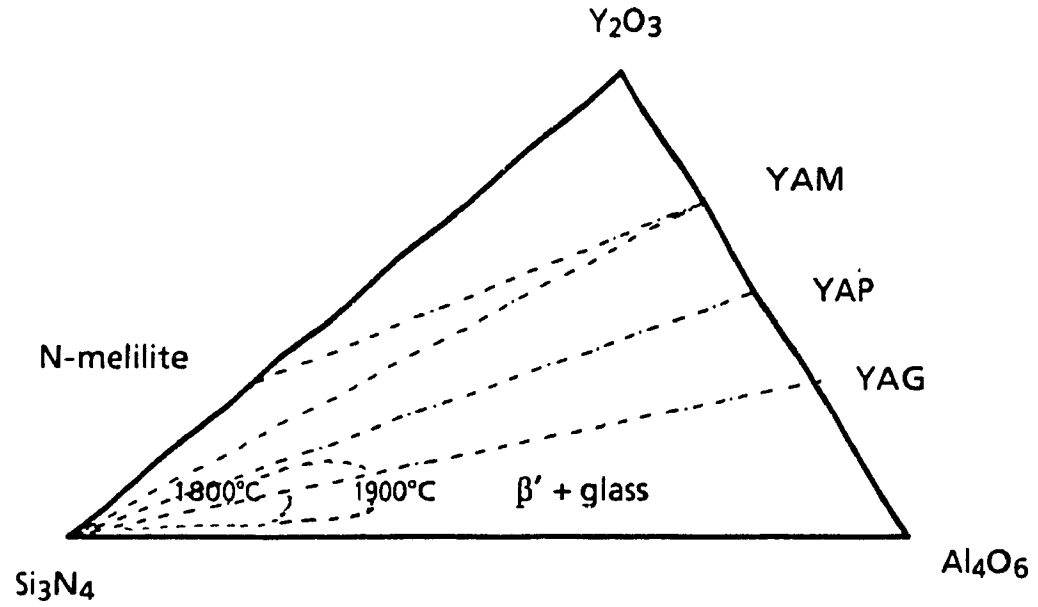

(a)

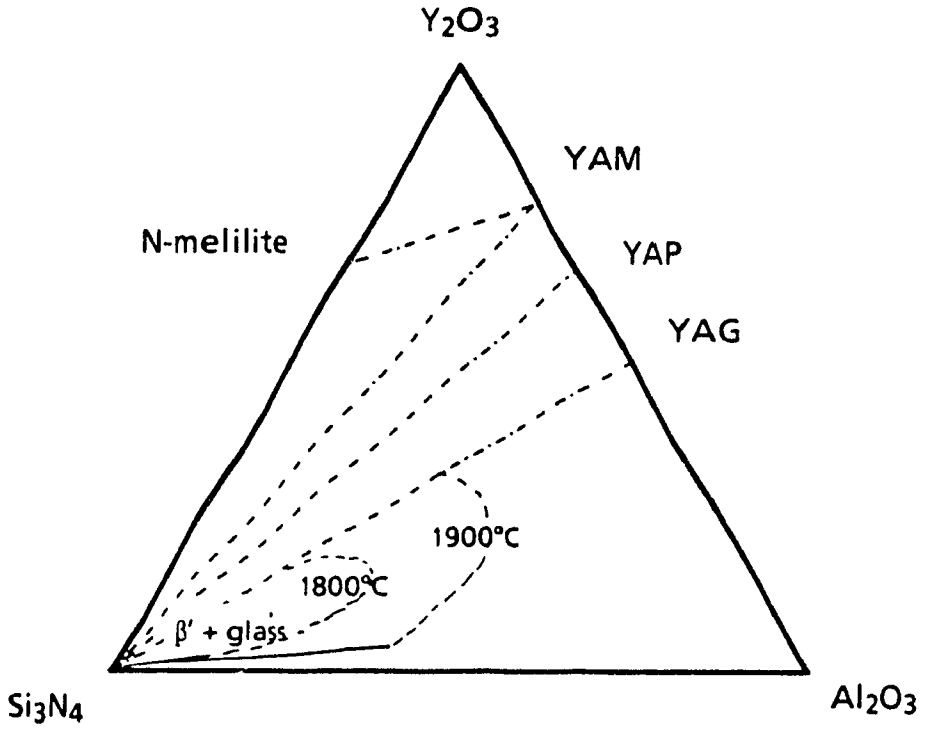

(b)

Figure 2.17. The Y_2O_3-Si_3N_4-Al_2O_3 behaviour diagram showing glass formation after heating to 1900°C: (a) in equivalent concentrations; (b) in weight percent [33].

Also of interest is the ternary oxide system [33] shown in Figure 2 18 Phases present are the yttrium silicates, yttrium aluminates and yttrium aluminum garnet (the most refractory) and were discussed in previous systems The lowest liquid formation temperature is ~1400°C The glass forming region within the oxide system will be discussed in a later section (refer to Section 2.5.2.1)

2.4 3 Non-oxide Sintering Aids

Although oxide additives are the ones most commonly studied, non-oxide additives also exist which do not form a low viscosity grain boundary phase, such as ZrN and Mg_3N_2 Literature on these sintering aids is very limited, and hence will not be discussed

2.4.4 General characteristics of Sintering Aids

In summary, the following characteristics of an additive optimize the high-temperature properties of Si_3N_4.

(i) high softening temperature of the additive-SiO_2 composition

(ii) minimal amount of the liquid phase with relatively low viscosity at the sintering temperature

(iii) good wettability of Si_3N_4 by the liquid phase to promote α/β transformation

(iv) high solubility of nitrogen in the liquid phase

2.5 GRAIN BOUNDARY CONTROL

The use of oxide sintering agents allows for the complete densification of Si_3N_4, as seen in Section 2 4 During sintering, these oxides form a eutectic liquid with silicon nitride, which allows for the dissolution-transformation-precipitation of β-Si_3N_4 to occur Although some Al and O, if used in sintering, can be substituted within the beta lattice to form a solid solution

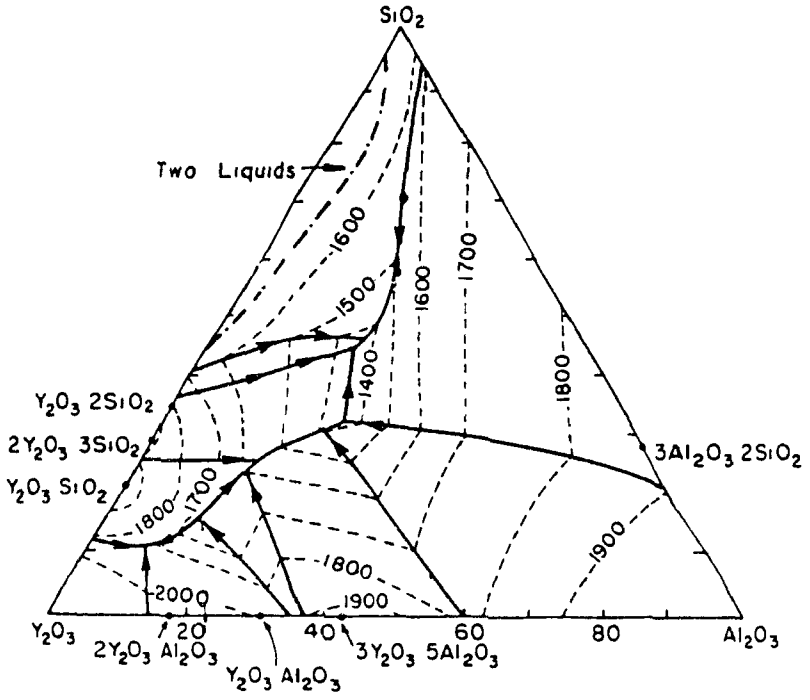

Figure 2.18. System Al_2O_3-Y_2O_3-SiO_2.[34]

of β'-SiAlON, there will almost always be some liquid phase remaining which becomes a glassy grain boundary phase upon cooling This amorphous constituent will result in a degradation in the mechanical properties, especially at elevated temperatures [54]

Two methods of improving the mechanical properties exist, namely by limiting the amount of residual glassy phase through compositional control and/or crystallizing the glass to form a crystalline grain boundary phase

Several approaches to these methods have been considered

1. Transient liquid phase sintering, where the constituents of the glass are absorbed into the β-Si_3N_4 lattice by solid solution [55]
2 Minimizing the amount of additives used in sintering by gas pressure sintering, hot pressing or hot isostatic pressing [56,57]
3 Crystallization of the glass phase by post-sintering annealing treatments in air [58] or in an inert [48] atmosphere

The first two methods involve compositional control of the starting material only The latter technique involves a combination of the two approaches

Post-sintering techniques in air involve the oxidation of the residual glassy phase to form either disilicates or aluminates Naik & Tien [59] showed that, of all the available yttrium-containing phases, β'-Sialon was only in equilibrium with $Y_2Si_2O_7$ and $Y_3Al_5O_{12}$ (YAG) Lange et al [58] and Tsuge et al [60] showed that heat treatment of Si_3N_4 materials in an oxidizing environment after sintering can lead to improved thermomechanical properties Both groups found that the phases formed depended upon the heat treatment schedule, i e temperature, time and cooling rate (as well as starting composition) The optimum composition for crystallized phases lie within the Si_3N_4-Si_2N_2O-$Y_2Si_2O_7$ compatibility triangle (Figure 2 15), as these phases give a polyphase

material with good oxidation resistance and good mechanical properties. However, this method of achieving crystalline grain boundary phases results in substantial gradients in composition and phase content between the immediate surface and the bulk of the material since the oxide scale tends to concentrate the impurity elements, as well as Y and Al cations. Hence, the mechanical properties of the heat treated material are detrimentally affected as the impurities not only act as inclusions but also lower the viscosity of the glass further [36,46].

Most recent research [62-65] has concentrated on the formation of YAG over its disilicate counterpart as it requires the use of less Y_2O_3 additive, and is more refractory As this crystalline phase is an oxide, it also shows excellent oxidation resistance and, in turn, leads to a sialon exhibiting apparently superior high temperature properties to the as-sintered counterpart.

2.5.1 Heat Treatment of Sialons

The high temperature properties of silicon nitride ceramics can be improved by the crystallization of the glassy intergranular phases. The resulting grain boundary would typically be more refractory (T_m = 1860°C) in nature than its glass counterpart with a glass transition temperature (T_g) of 900-1000°C, thus being able to withstand higher temperatures before the mechanical properties begin to deteriorate. As all glasses are metastable with respect to their crystalline products, through proper compositional control of the sintering aids, devitrification of a Y-Sialon glass to $Y_3Al_5O_{12}$ can be achieved.

2.5.1.1 Theory of Glass Formation

By definition, a glass is an inorganic product of fusion which has cooled to a rigid condition without crystallizing [66]. Furthermore, the long-range order

in the atomic arrangement of the amorphous substance does not exist over distances greater than 10 nm [67]

If a pure substance is melted and cooled, a definite freezing point is observed at which solidification occurs, with the formation of crystals It is sometimes possible to cool the liquid below its freezing point without any crystal formation, this process is known as super-cooling The supercooled liquid is in a metastable state since it has a higher free energy than the corresponding crystal, but its structure has a lower free energy than any immediate neighbouring structure

Throughout the supercooling of the liquid, there is no volume change associated with it, unlike the accompanying volume change upon crystallization Rather, the viscosity of the melt increases with decreasing temperatures, and reaches a value so high that the liquid approaches a rigid solid state. With the increasing viscosity of the glass, structural rearrangement becomes less feasible The resulting structure of the glass is "open" , allowing for interstitial accommodation of ions such as Na^{+}, Li^{+}, Mg^{2+}, etc

The formation of a glass depends on several factors [67] including structural and chemical considerations, as well as kinetic effects Only the kinetic influences will be discussed briefly here

Kinetic factors in glass formation are best understood in terms of the probability of formation, as seen in the Time-Temperature-Transformation (TTT) curve in Figure 2 19 A temperature (T_N) exists where the time (t_N) to crystallize a volume fraction of glass is a minimum This temperature is critical if crystallization of the glass is to be avoided. The rate at which crystallization occurs is given by

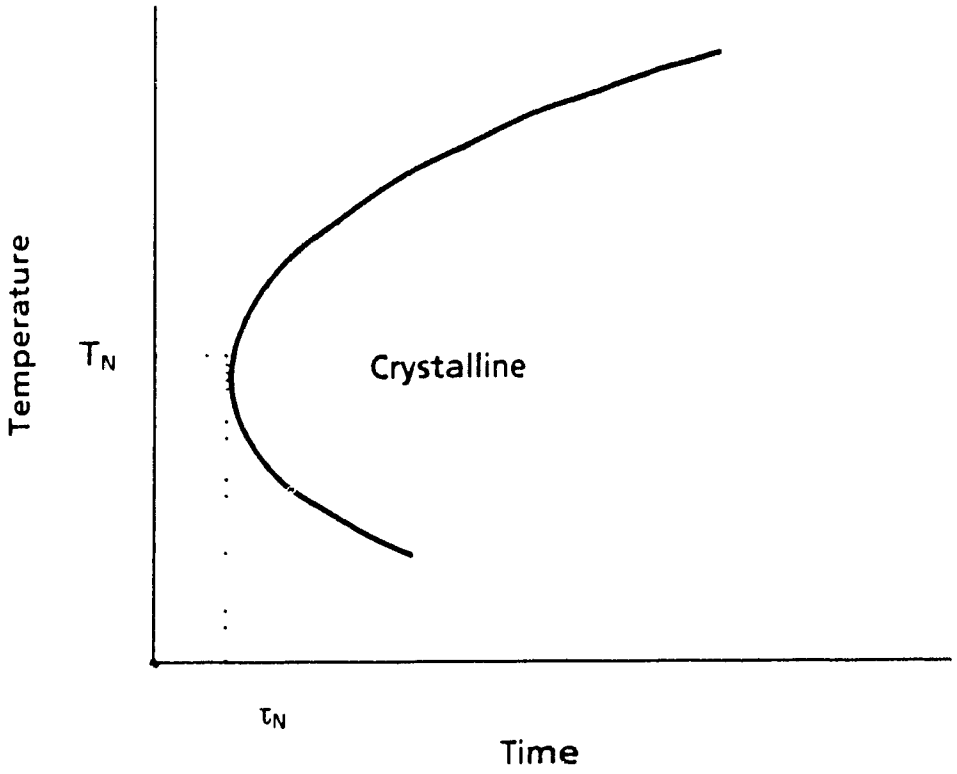

Figure 2.19. The general form of a time-temperature-transformation (T-T-T) curve [67].

$$X_t = 1 - exp\left(-\frac{\pi}{3}U^3 I t^4\right) \qquad (2.15)$$

where X_t is the volume fraction of glass crystallized after time t, U is the crystal growth rate, and I is the nucleation rate. For the formation of a glass to occur, X_t must be kept low by minimizing U and I. Thus, glass formation is governed by the rate of crystal nucleation and growth. These will be discussed in Section 2.5.1.3.

The cooling rate, R_c, of the liquid is also critical in glass formation, and is given by:

$$R_c \approx \frac{\Delta T}{\tau_N} \qquad (2.16)$$

where ΔT is the amount of undercooling from the equilibrium melting temperature. In summary, in order to cool a glass from a liquid, both the cooling rates and crystallization rates must be kept to a minimum

2.5.1.2 The Glass-Forming Region of Y-Si-Al-O-N System

The formation of YSiAlON glasses from melts [68-71] is far more complex (in terms of structural, compositional and kinectic effects) than that of silicate glasses. Both the presence of additional cations (Al^{3+}, Y^{3+}) and anions (N^{2-}) play significant roles in the cooling of the liquid, such that crystallization of the glass is suppressed. Messier [68], for one, did extensive work on glasses which would crystallize to the disilicate phases ($Y_2Si_2O_7$, Y_2SiO_5) He found that compositional control of the nitrogen to oxygen ratios was difficult to maintain. This was primarily due to decomposition processes which were accompanied by nitrogen evolution during formation of the glass However, certain beneficial effects of nitrogen substitution within the silica glass were

apparent, namely that the density, the glass transition temperature (T_g), hardness and elastic modulus all increase with increasing nitrogen content Figures 2 20 and 2 21 illustrate the variation of the glass transition temperature (T_g) and viscosity (η) with nitrogen concentration for different glasses, respectively Both T_g and η increase with increasing nitrogen content Figure 2 22 illustrates the variation of viscosity with temperature for different glass systems It is clear also from this that the Y-Sialon glass has the highest viscosity over its Mg, Ca, and Nd glass counterparts and it can be concluded that Y-based glasses would show improved high temperature properties over these other glasses since the YSiAlON glass would begin to soften at higher temperatures.

Also observed is an increase in the thermal diffusivity with increasing nitrogen content, leading to better thermal shock resistance All of these would therefore result in improved thermomechanical properties

It was originally thought by some authors [69,70] that oxynitride glasses could be made from high nitrogen glass-forming melts in which Si_3N_4, AlN or some other nitrides are appreciably soluble at temperatures below which the nitride has a significant decomposition pressure, typically 1650-1750°C for Si_3N_4 or AlN Further work showed that such extensive incorporation of N in the glass melt was not that easily achieved High nitrogen losses by frothing of the glass and decomposition occurred when attempting to incorporate N into the glass [70]

Most oxynitride glasses contain Si,O and N, and a majority also contain Al - all of which are favorable for oxynitride formation Both oxygen and nitrogen can bond tetrahedrally to Si to form SiX_4 groups (where X = O, N) Likewise, Al will tetrahedrally bond to oxygen and nitrogen, as in alumino-silicate glass systems The most easily synthesized oxynitride glasses contain

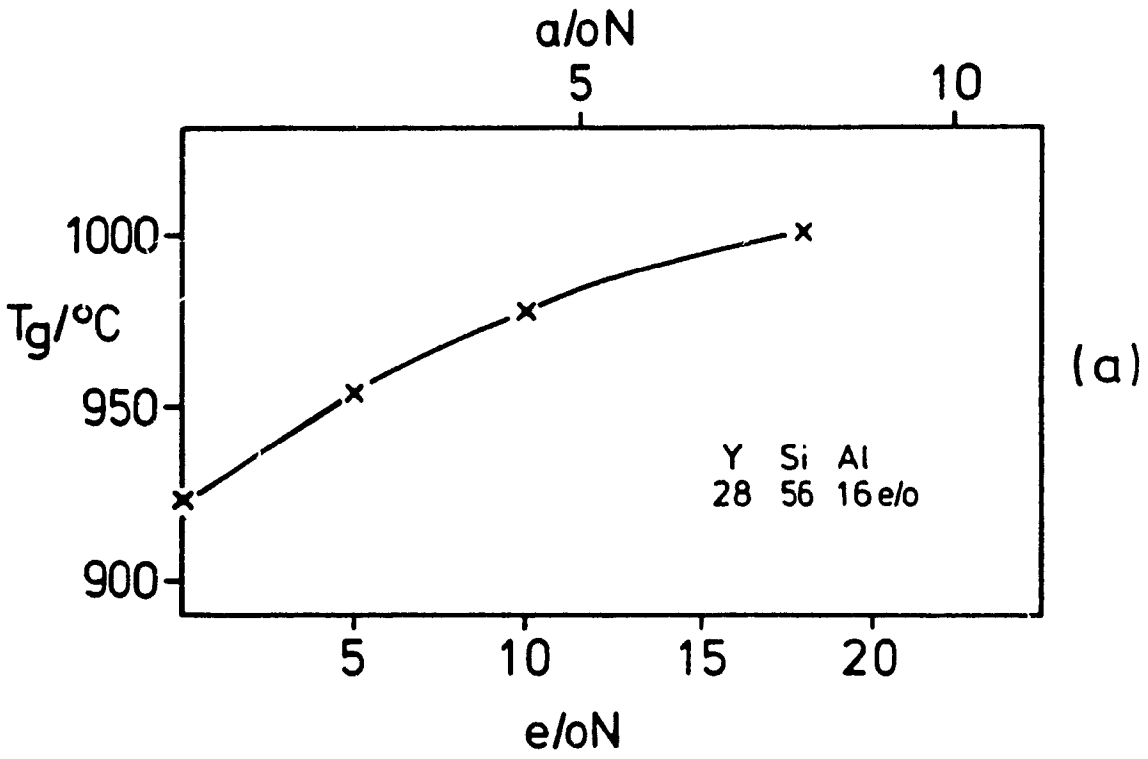

Figure 2.20. Variation of glass transition temperature (T_g) with nitrogen concentration in the Y-Si-Al-O-N system [72].

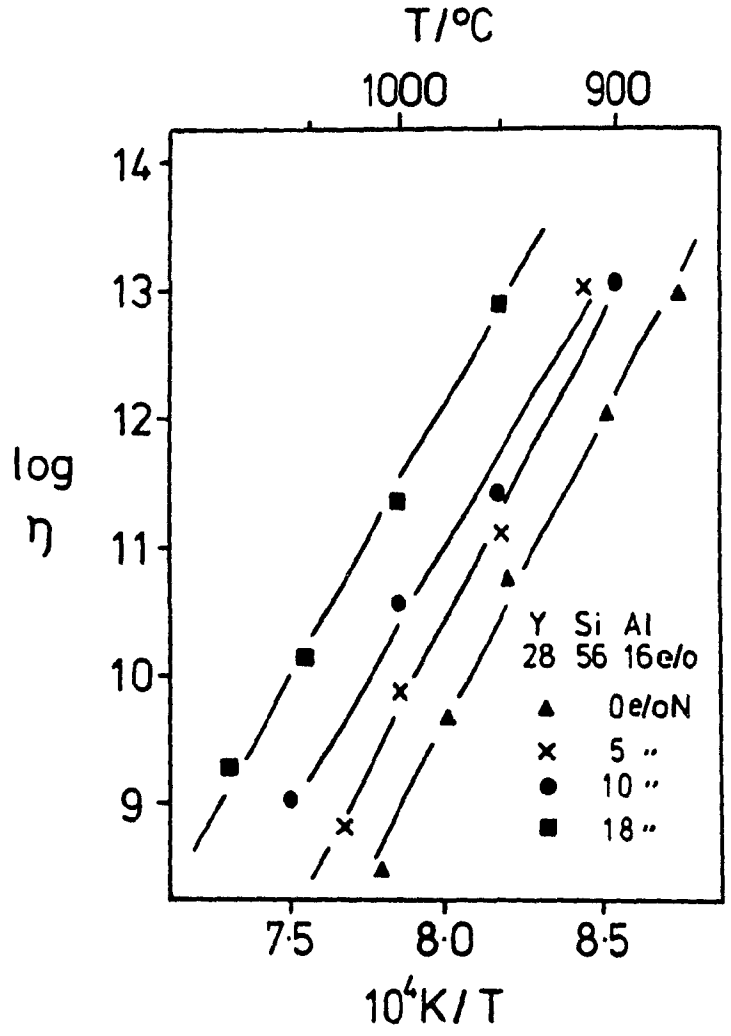

Figure 2.21. Variation of viscosity with temperature for the Y-Si-Al-O-N glasses of different nitrogen concentrations [72].

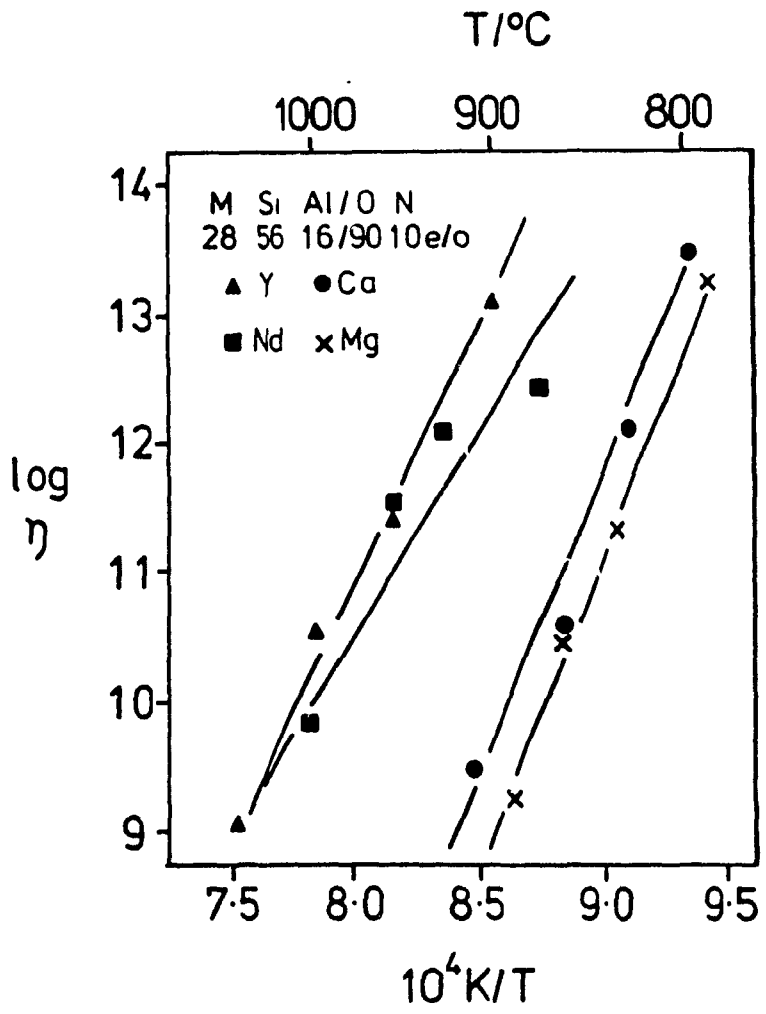

Figure 2.22. Variation of viscosity with temperature for the Y, Nd, Ca and Mg sialon glasses (28M:56Si:16Al) with 10e/o nitrogen concentration[72].

more than four components, i e. Y-Si-Al-O-N glasses. The addition of Al to the Si-O-N glass has several effects, namely it (i) expands the compositional range of glass formation, (ii) lowers the liquidus temperature, (iii) increases the nitrogen solubility , and (iv) suppresses phase separation. All of these effects are desirable in the sintering process of Sialons. It was found that the incorporation of Y into the glass results in a higher softening temperature, but tends to reduce the nitrogen solubility in the glass This is in part due to the more refractory nature of the Y_2O_3-Al_2O_3-SiO_2 system [73]

The formation of Y-sialon glasses from melts cannot be directly compared to the formation of two-component system of β'-Sialon and glass In the latter case, the glass is formed from the sintering aids incorporated to help in the densification of Si_3N_4. Also, the volume of glass is kept to a minimum since it has a detrimental effect on the mechanical properties of the material (see Section 2 6).

The general equation for the formation of this two-phase system is given by·

$$\beta\ Si_3N_4 + sintering\ aids \rightarrow \beta'\ Si_{6-z}Al_zO_zN_{8-z} + YSiAlON\ glass \qquad (2.17)$$

The glass forming region of the YSiAlON system is illustrated in Figure 2.23. This six-component system, called a Janecke prism, consists of the standard Si_3N_4-AlN-Al_2O_3-SiO_2 square (from Figure 2 10), with Y equivalents units along a third dimension The front and back triangular faces represent the nitride and oxide ternary phase diagrams, respectively.

The glass forming region within the system extends from the SiO_2-rich portion of the oxide face towards the nitrogen face. This implies that a certain amount of nitrogen will dissolve in the glass In fact, upto 33e/o N has been found to be accommodated in the Y-Sialon glass, with a composition of

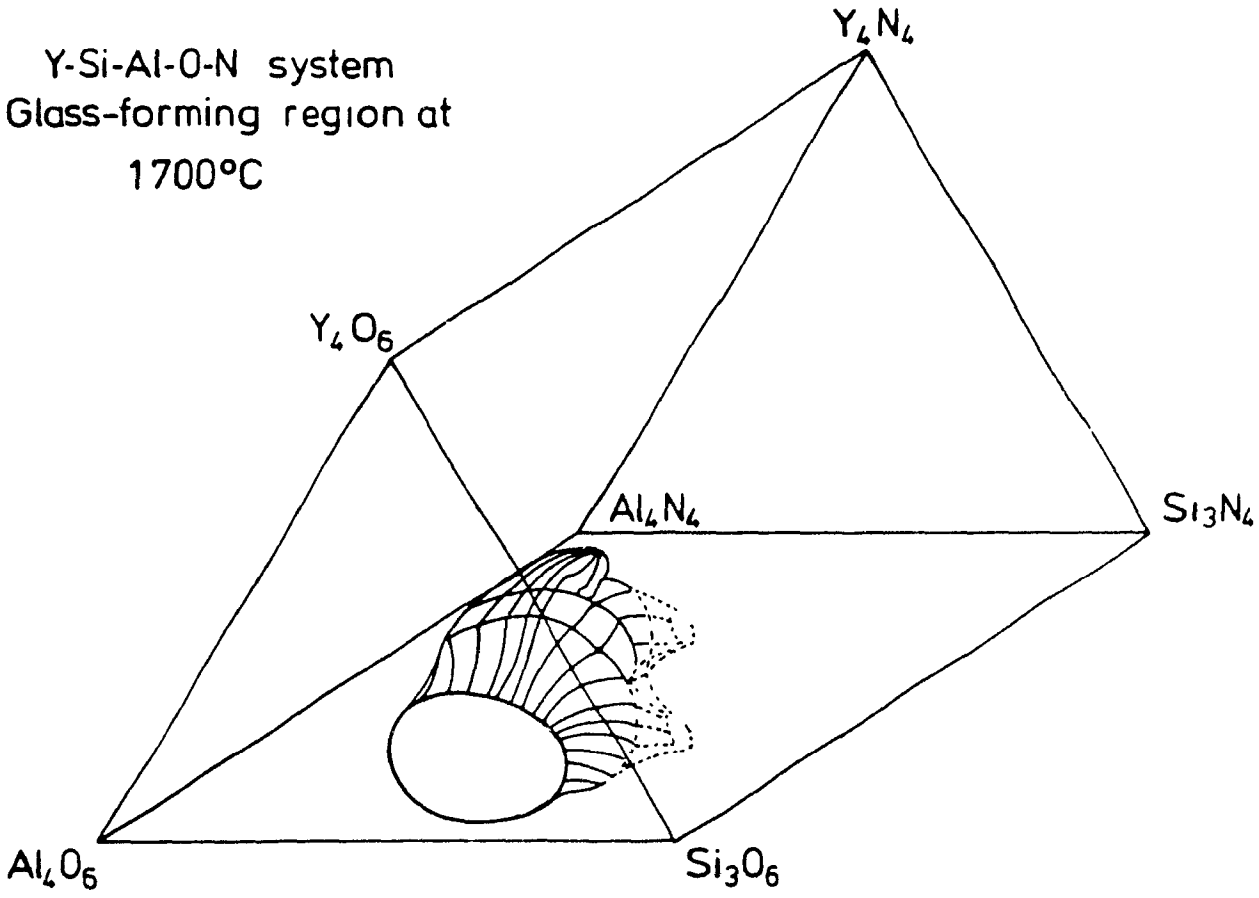

Figure 2.23. The Y-Si-Al-O-N glass-forming region at 1700°C represented in three dimensions [72].

$Y_{15}Si_{15}Al_{10}O_{45}N_{15}$ [71], where one of every four oxygens is replaced by nitrogen The widest part of the glass forming region occurs at 10e/o N [72] as shown in Figure 2 24, and so implies that this is the area of most stable glass formation

It is clear from the above that the glass forming region is rather extensive, but in order to obtain the desired YSiAlON glass which will devitrify to $Y_3Al_5O_{12}$, strict compositional control of the glass must be achieved, i e the glass must lie within a certain N O range for it to crystallize to YAG There are two methods of representing the system of interest, that is β' and Y-SiAlON glass, these are illustrated in Figures 2 25-2 27 The first, developed by Hohnke and Tien [74], is based on an equilateral triangle with the apexes being Si_3N_4, β'_{60} ($Si_2Al_4O_4N_4$), and YAG The liquid forming region extends over most of of the triangle, however, the area of interest is where only β' + liquid are present Although this representation is simple to understand as it is in terms of weight percent of constituents, it is rather misleading since there is a greater compositional difference between Si_3N_4 and YAG than between β'_{60} and YAG A more appropriate representation was developed by Drew et al [75], who mapped out triangular sections of varying e/oN content, i e similar to the triangular faces found on the Janecke prism (Figure 2 24) These sections intersect the larger β-YAG plane (Fig 2 26) to give a region of glass formation shown in Figure 2 27 , which lies above the β-YAG tie line The parallel lines represent constant N.O ratios, increasing from the Si_3N_4 point towards the β'-60 composition

The phases present at a typical sintering temperature of 1700°C are illustrated in Figure 2 28 The liquid forming region at this temperature is much more extensive than the glass region, and extends over much of the system However, in order to obtain a Y-Si-Al-O-N glass upon cooling, the

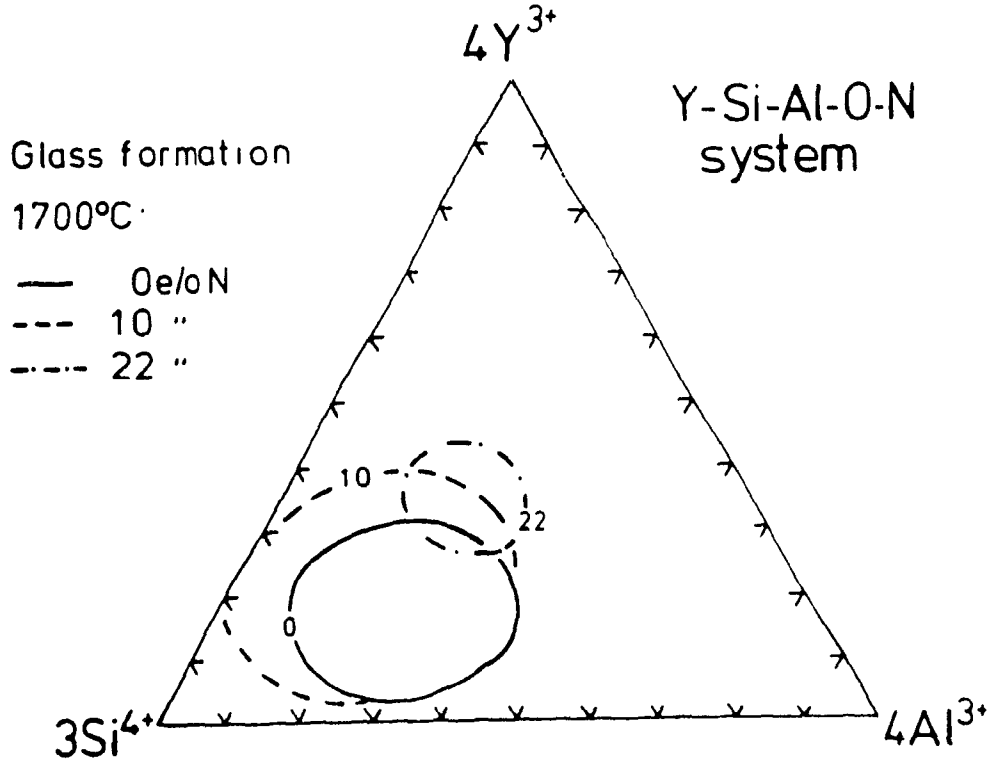

Figure 2.24. The Y-Si-Al-O-N glass-forming regions at 1700°C on the 0, 10 and 22e/o nitrogen planes [72].

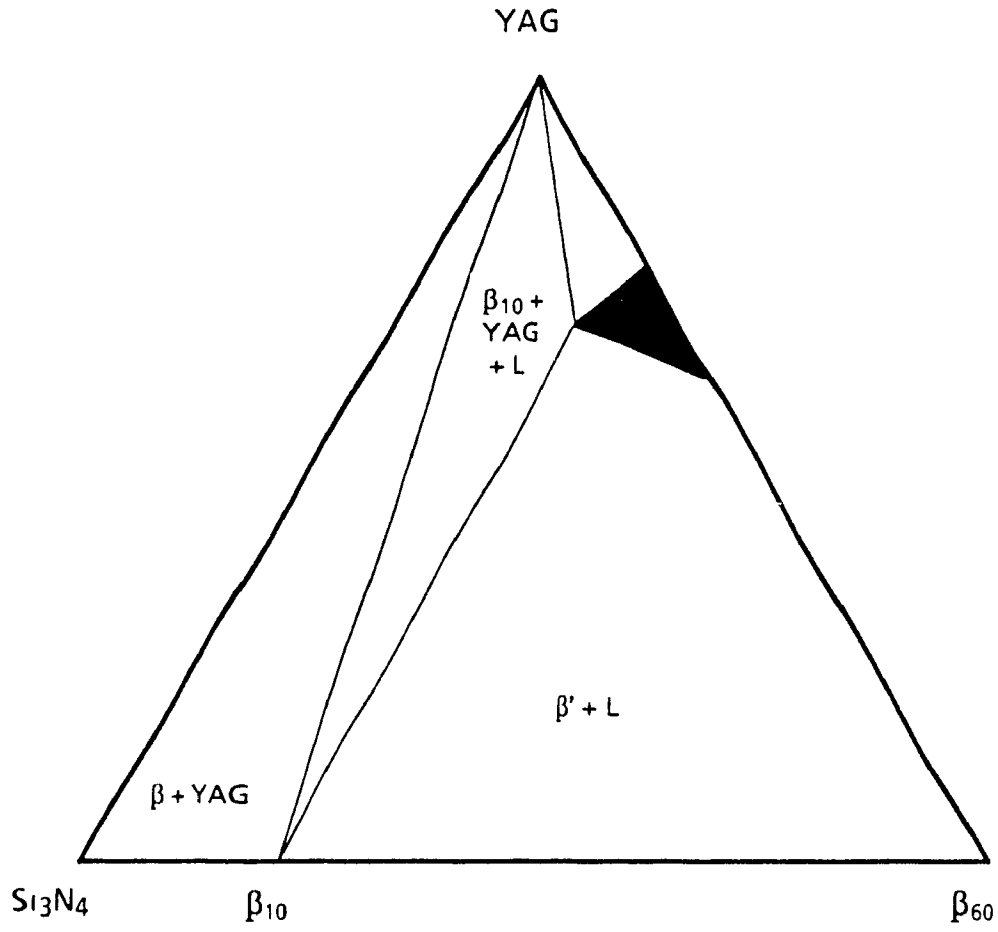

Figure 2.25 Phase relationships in the β'-YAG plane at 1550°C [74].

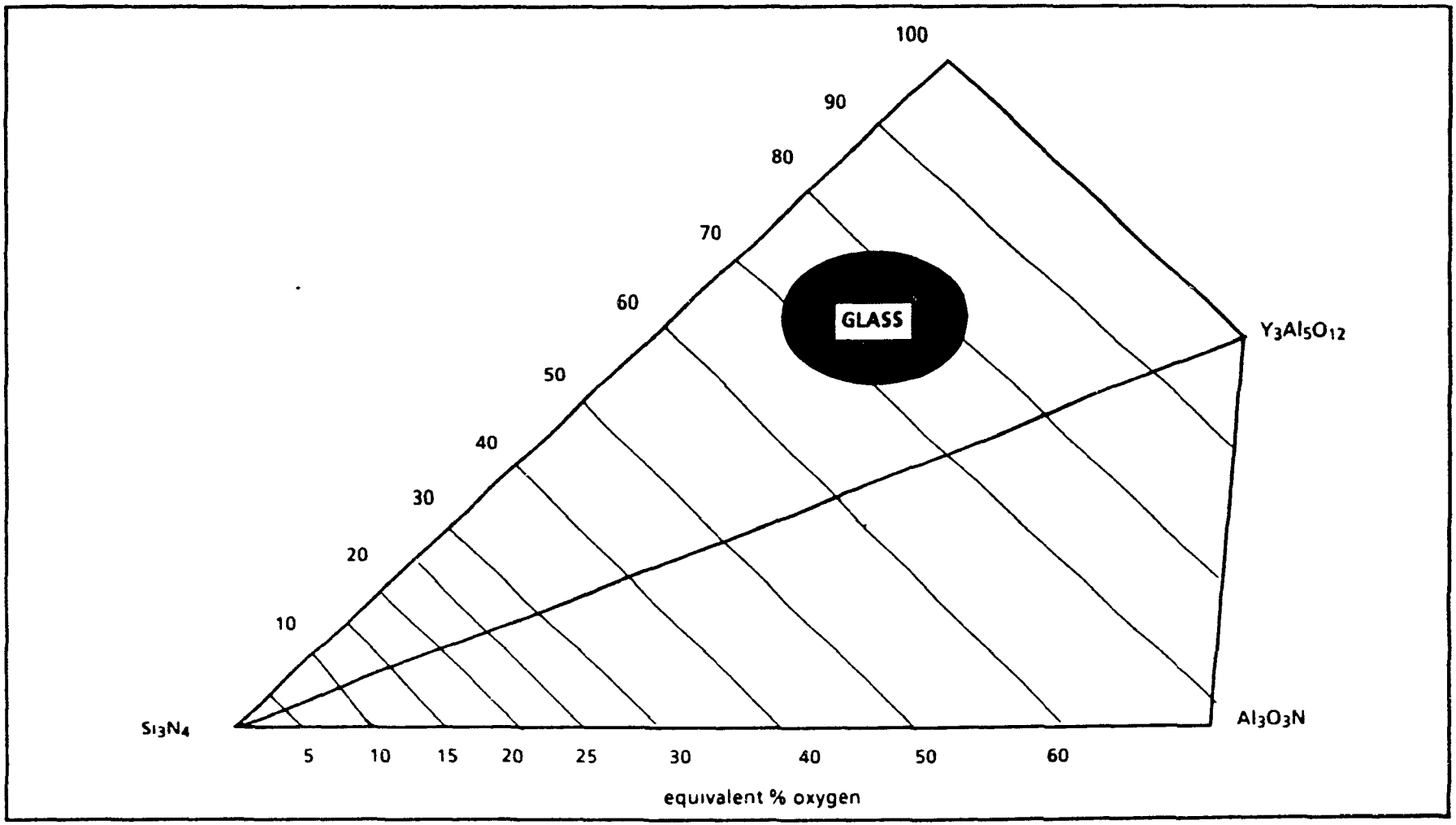

Figure 2 26 Phase relationships in the β'-YAG plane at 1550°C

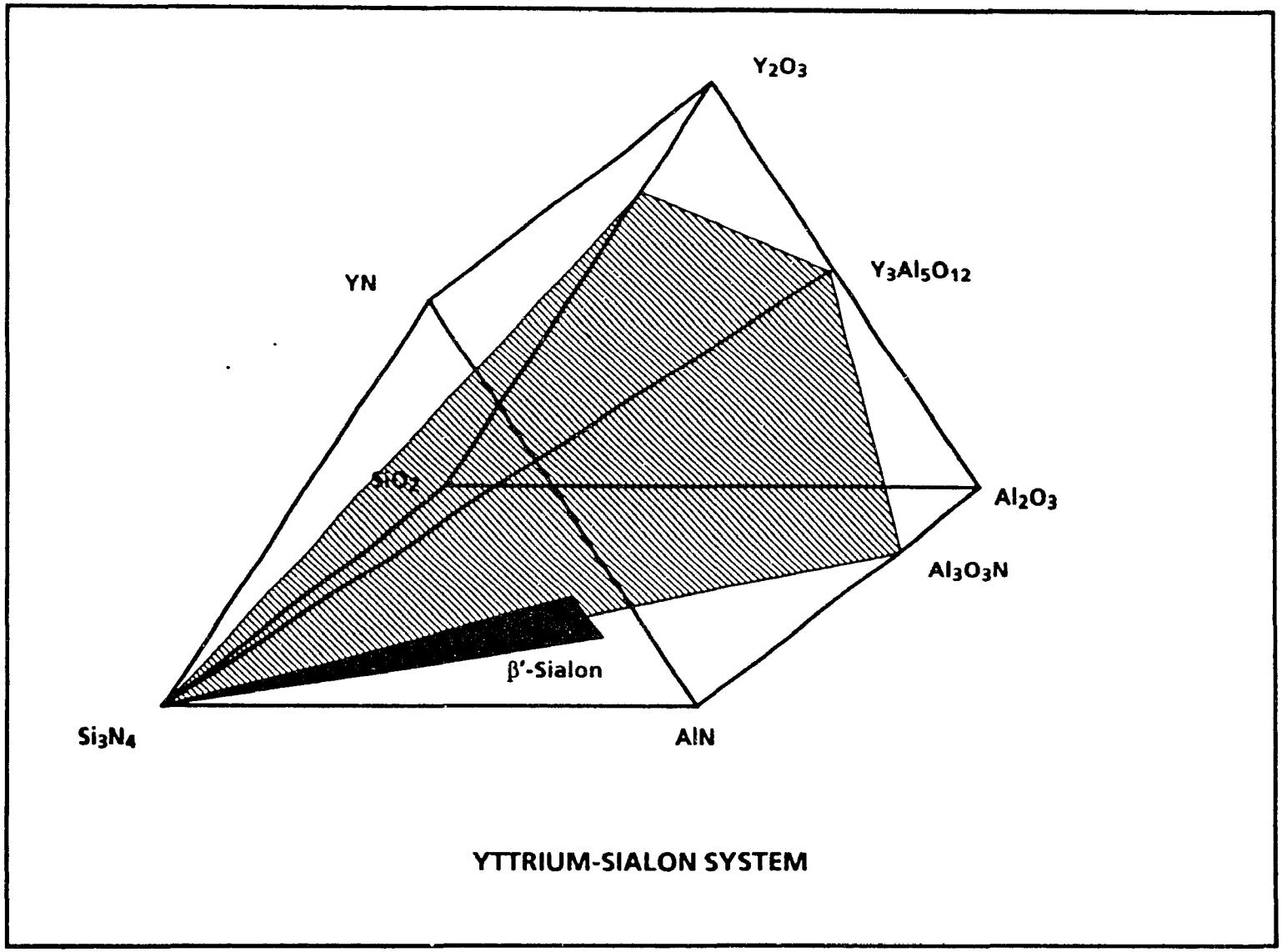

Figure 2.27. Phase relationships in the Y-SiAlON system.

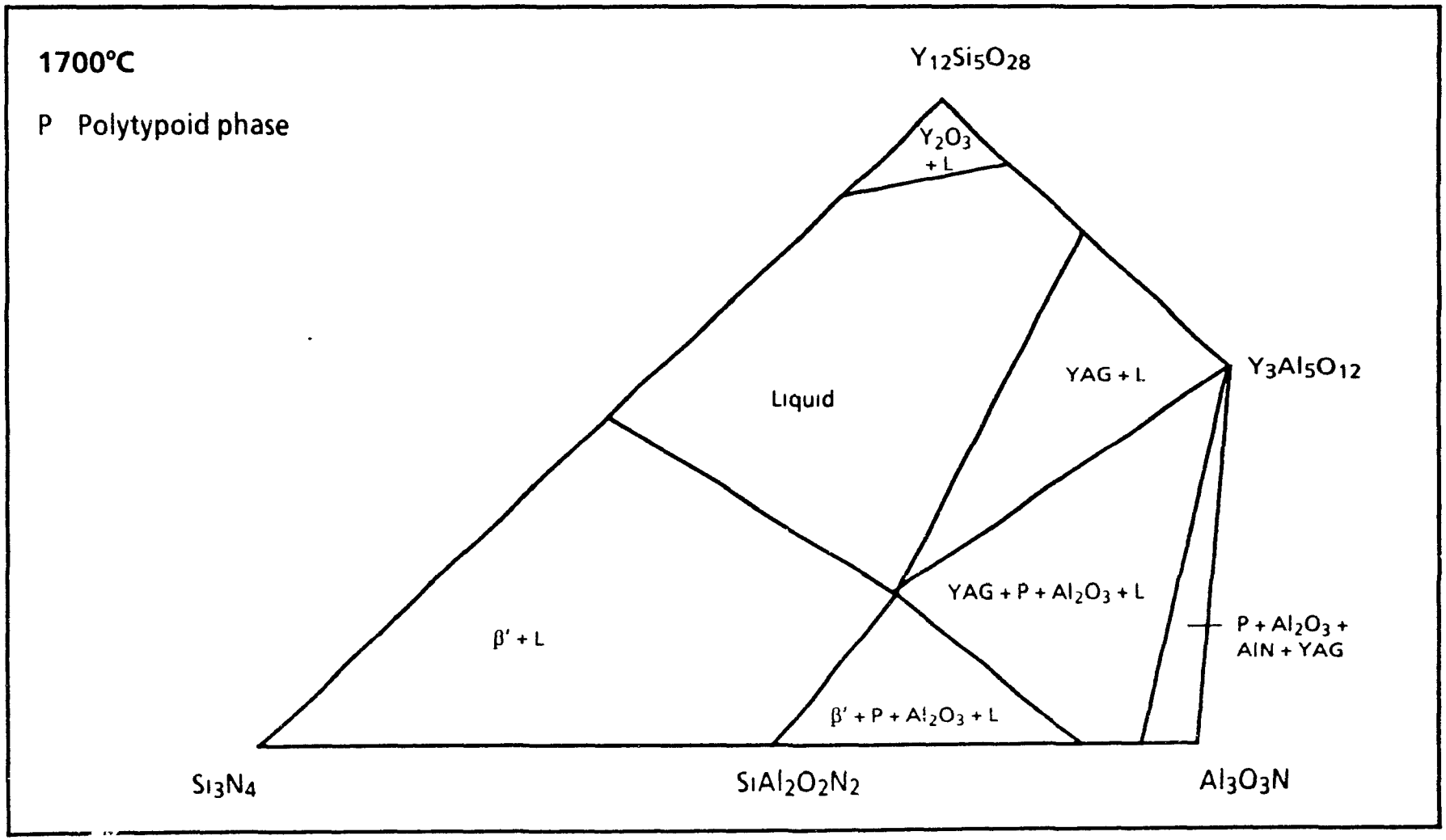

Figure 2.28 Phase relationships in the β'-YAG plane at 1700°C [74].

liquid phase must cool to achieve a glass composition somewhere inside the triangle defined by the β' solid solution line and the YAG composition. This will only occur for higher z value β' compositions as the liquid phase in equilibrium with lower z values will be on the silica side of this triangle [41,71]

In summary, YSiAlON glasses can exist over an extensive range of compositions, containing upto 33e/o N, however, only a limited glass region exists over which the devitrifcation of the glass to YAG will occur.

2.5.1.3 Theory of Crystallization of Glass-Ceramic Systems

The process by which the regular lattice of a crystal is generated from the less well-ordered liquid or glass structure is termed crystallization [67]. This transformation of structures proceeds from distinct centers of nuclei and the crystals begin to grow by depositing material upon these. Thus, the crystallization process can be divided into two distinct stages: nucleation and crystal growth.

Nucleation may be either (a) homogeneous, where the first seeds are of the same constitution as the crystals upon which they grow, or (b) heterogeneous, where the nuclei are chemically different from the crystals on which they are deposited. Heterogeneous nucleation in a glass is unlikely to occur as any foreign matter, such as dirt, would dissolve in the glass. Thus, the emphasis will be on homogeneous nucleation.

Figure 2.29 illustrates the nucleation of crystal growth in a viscous liquid. Below the equilibrium melting temperature, T_1, of a solid, there is a temperature interval called the metastable zone in which nuclei will not form. However, if nuclei are pre-existent in the solution, i.e. seeds, then crystals will grow upon them. Below this metastable zone, crystallization is controlled by two competing factors: the rate of nuclei formation and the crystal growth rate. Nucleation and growth both reach maxima as the

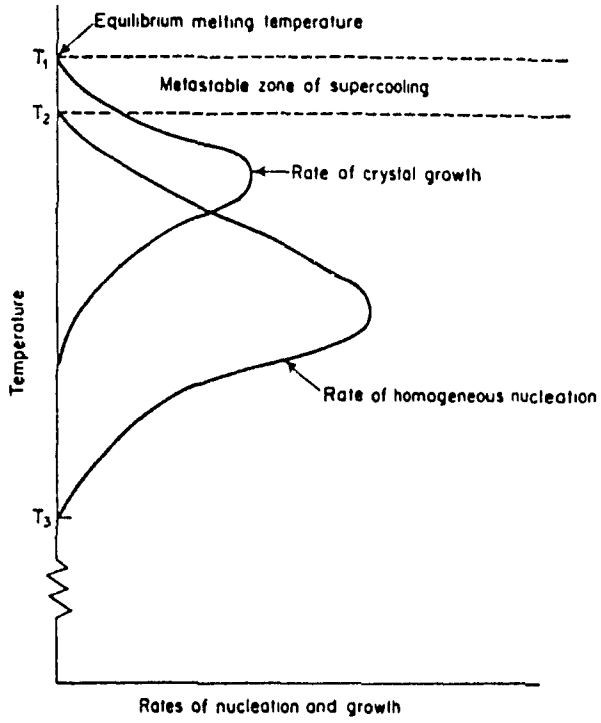

Figure 2.29. Rates of homogeneous nucleation and crystal growth in a viscous liquid [67].

temperature decreases, due to the increasing viscosity of the glass which hinders atomic rearrangement and diffusion processes. Therefore, in order to maximize the number of crystals upon which growth can occur, the nucleation temperature should be chosen such that the rate of nucleation is at a maximum The production of a large number of small crystals is favoured over a small number of large crystals as the former will show superior mechanical properties [68]

At a certain temperature (T_3), the viscosity of the glass is so high that the nucleation rate drops to zero. The general equation for nucleation rate, I, is given by [76]

$$I = \frac{C^{*}}{\eta} exp\left(-\frac{W^{*}}{RT}\right) \qquad (2\ 18)$$

where W^{*} is the thermodynamic barrier to nucleation, R is the gas constant, T is the temperature at which nuclei start to grow, η is the viscosity of the glass, and C is a constant The optimum nucleation temperature, T, generally lies within a temperature range where the viscosity of the glass is between 10^{11}-10^{12} poise [71]

The crystal growth process is critical in determining the morphology of the material produced Crystal growth is dependent upon two factors [67]:

(1) the rate at which the irregular glass structure can be rearranged into the periodic lattice of the growing crystal; and

(2) the rate at which energy released in the phase transformation process can be eliminated A general equation for crystal growth, U, is given by.

$$U = K\frac{\Delta T}{\eta} \qquad (2\ 19)$$

where K is a constant, ΔT is the amount of undercooling from the equilibrium melting temperature upon cooling, and η is the viscosity. It is clear that

viscosity plays a dominant role in the crystal growth process as well An increase in viscosity leads to a rapid decrease in the growth rate

The crystallization of a glass is often accompanied by significant changes in the properties of the resulting material [68]

1 specific gravity changes between the parent glass and the crystalline product are often accompanied by small volume changes (either contraction or expansion, depending on the density of the crystal
2 thermal expansion coefficients of the crystalline phases formed are often markedly different from those of the parent glass
3 improved refractoriness since the composition of the glass progressively changes as the crystals are precipitated. An upper crystallization temperature exists where complete crystallization is achieved, with little residual glass remaining
4. improvement in mechanical properties as the glass is replaced by a crystalline phase

2 5 1.4 Crystallization of Y-Si-Al-O-N Glasses

As stated in previous sections, crystallization of glassy grain boundary phases in sialons through post-sintering heat treatments offers a means of improving the properties of the ceramics The phases which are devitrified, such as YAG, are more refractory in nature than the glass itself, therefore improving the thermomechanical properties However, the addition of nitrogen to a glass results in both an increase the viscosity of the glass and glass transition temperature, ranging from ~920°C for 0e/oN to 1000°C for 20e/oN (Figure 2 21) This, in turn, tends to lower the rate of nucleation and increases the crystallization temperature [76] (Figure 2 27)

The growth of a YAG crystal from the YSiAlON glass is believed by some[54,64,69] to occur by the diffusion of excess Si and N from the glass into

the β′ phase; that is, the glass reacts with the matrix to give a slightly changed β′ composition and a crystalline garnet phase (YAG), according to:

$$\beta' Si_{6-z}Al_zO_zN_{8-z} + YSiAlON\,glass \rightarrow \beta' Si_{6-z+x}Al_{z-x}O_{z-x}N_{8-z+x} + Y_3Al_5O_{12} \quad (2\ 20)$$

where x is the amount of Si and N diffusing back into β′ A schematic diagram showing the growth of YAG is given in Figure 2 30 Leng-Ward and Lewis [64] found that crystallization of YAG increases with increased polytypoid content, the nucleation and growth of YAG is accompanied by excess components (Si,N into the β′ or precipitation of β′ of modified composition)

Greil et al [62] established TTT diagrams for the crystallization of YAG in β′-Sialons (Figure 2 31) They found that crystallization was only detectable below 1450°C, with a maximum rate occurring at 1380°C for β′-Sialons with a 10 wt % YAG content Also, the extent of substitution within the silicon nitride lattice (i e z value) affected the rate of crystallization as the z value of the sialon increased, so did the rate of crystallization (Figure 2 31)

The heat treatment temperature and time will determine whether or not nucleation of the YSiAlON glass to YAG will occur. The temperature will in turn be determined partly by the nitrogen content of the glass since the glass transition temperature increases with the amount of nitrogen present

Figure 2 32 shows phase relationships in the β′-YAG plane at 1050°C [41]; this temperature being slightly above the expected glass transition temperature Spacie et al [63] found that at this annealing temperature, however, no two-phase β′ + YAG region exists Rather, the diagram is predominated by a phase which they labelled B The composition of this phase is Y_2SiAlO_5N, and is close to the YSiAlON glass composition; it would

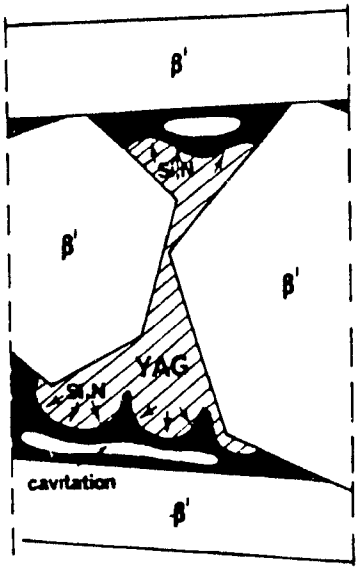

Figure 2.30. Schematic diagram showing growth of crystalline YAG phase and diffusion of Si and N into the amorphous phase [54].

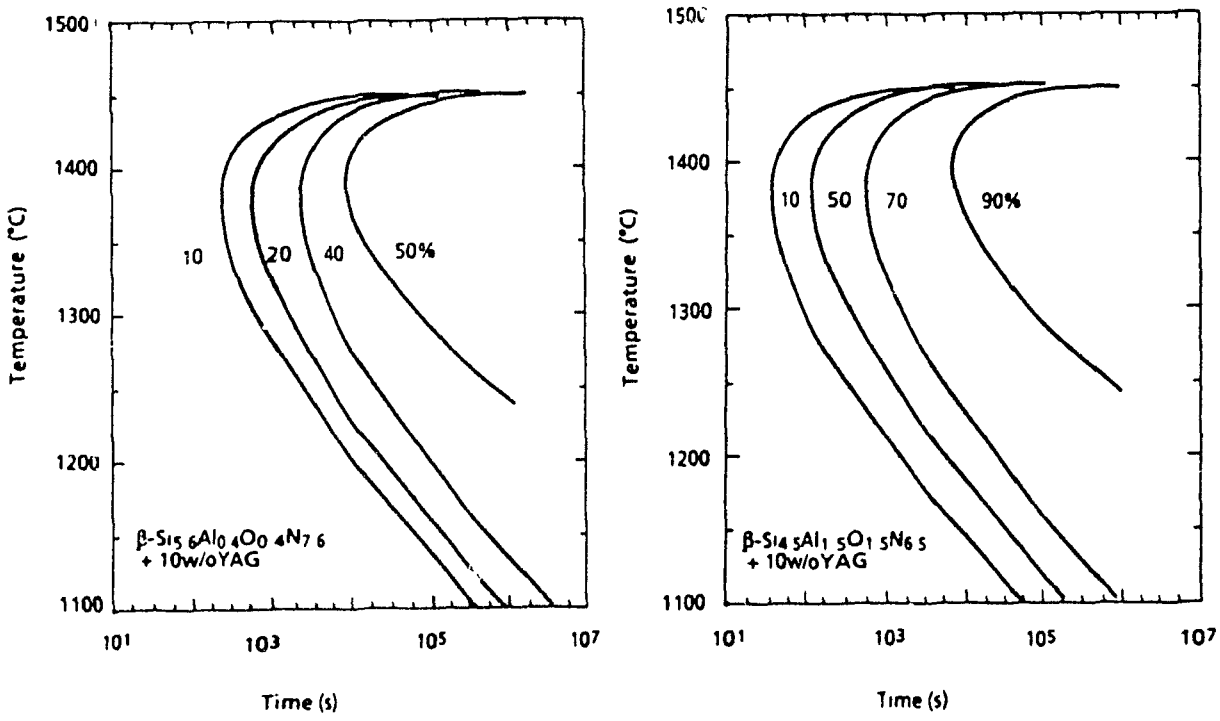

Figure 2.31. TTT-diagram s of YAG crystallization in β-sialon with (a) z = 0.4 and (b) z = 1.5. [62]

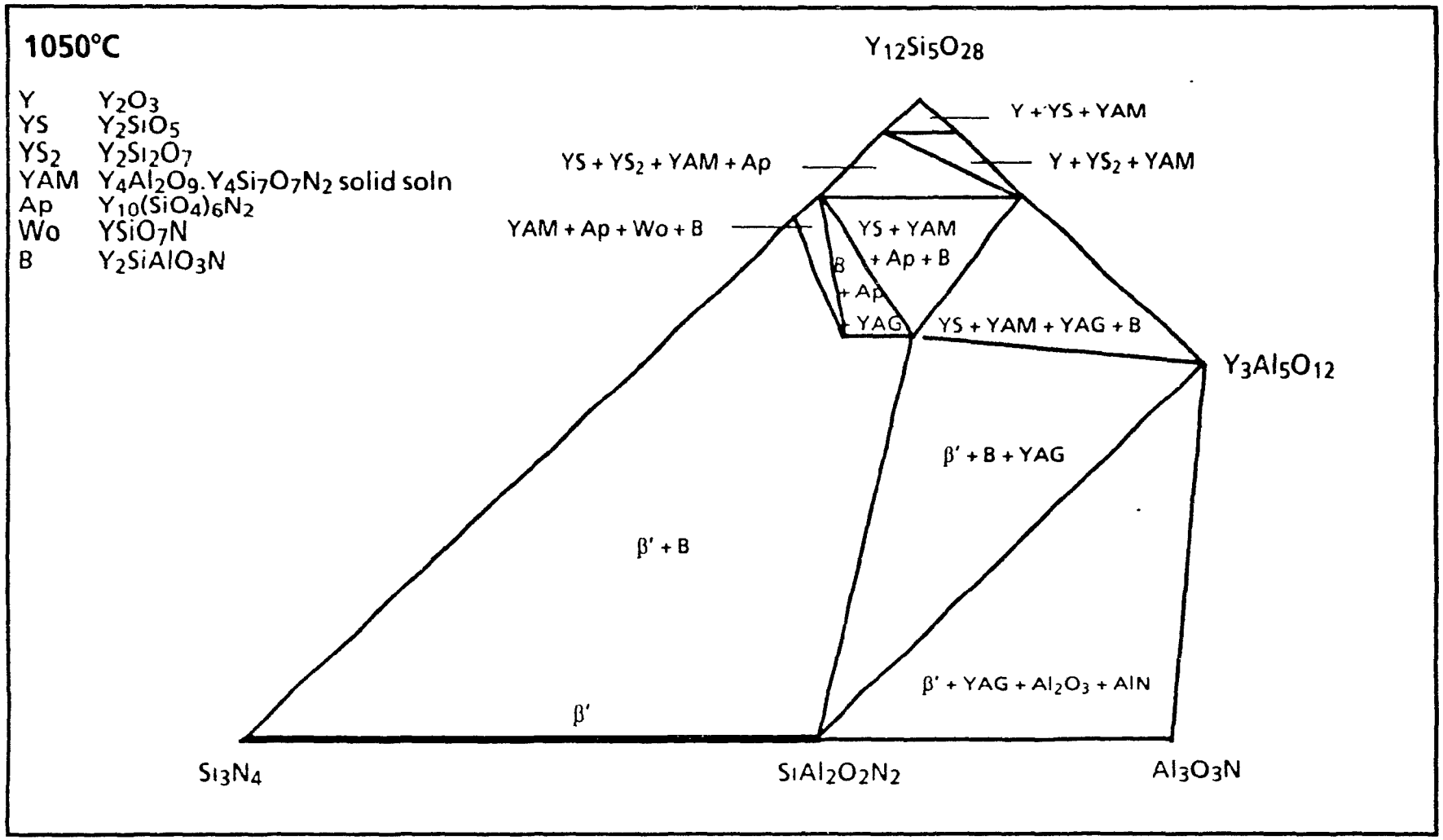

Figure 2 32 Phase relationships in the β'-YAG plane at 1050°C [74]

therefore require little structural rearrangement for the crystals to grow from the glass The other phases present in the system include YAM, YAP, and the yttrium silicates, as reviewed in Section 2 4, most of these quaternary ph-ses are undesirable due to either their low melting points, or to their poor oxidatior resistance

At 1350°C, the stable phase relationships are different [41] (Figure 2 33)· a β' + YAG region is found to exist However, the production of this two-phase system involves careful compositional control as this region is limited The major factor affecting the formation of YAG is the nitrogen content of the glass Leng-Ward & Lewis [64] did an extensive study of glasses containing 0, 10, 20 and 30e/o N which had been heat treated at 1250°C for 40 hours They found that, with increasing nitrogen content, $Y_2Si_2O_7$ was progressively replaced by YAG

Hayashi et al [52] reported that a heat treatment schedule of 1250°C for 72 hours was optimum in achieving devitrification of the glassy phase to YAG At higher temperatures, i e 1400°C, $YSiO_2N$ was the major crystallization phase However, they gave no indication of the starting compositions

2 5 1 5 Heat Treatment Conditions

It is clear from the above that heat treatment of YSiAlON glasses to produce YAG is dependent upon several factors

1 compositional control of the starting material so that the sintered material results in β'-Sialon and a YSiAlON glass
2 a specific heat treatment temperature to optimize the nucleation and growth of YAG from the Y-SiAlON grain boundary glass
3 an optimum heat treatment time to allow for complete grain growth of YAG to occur, thereby minimizing the amount of residual glass.

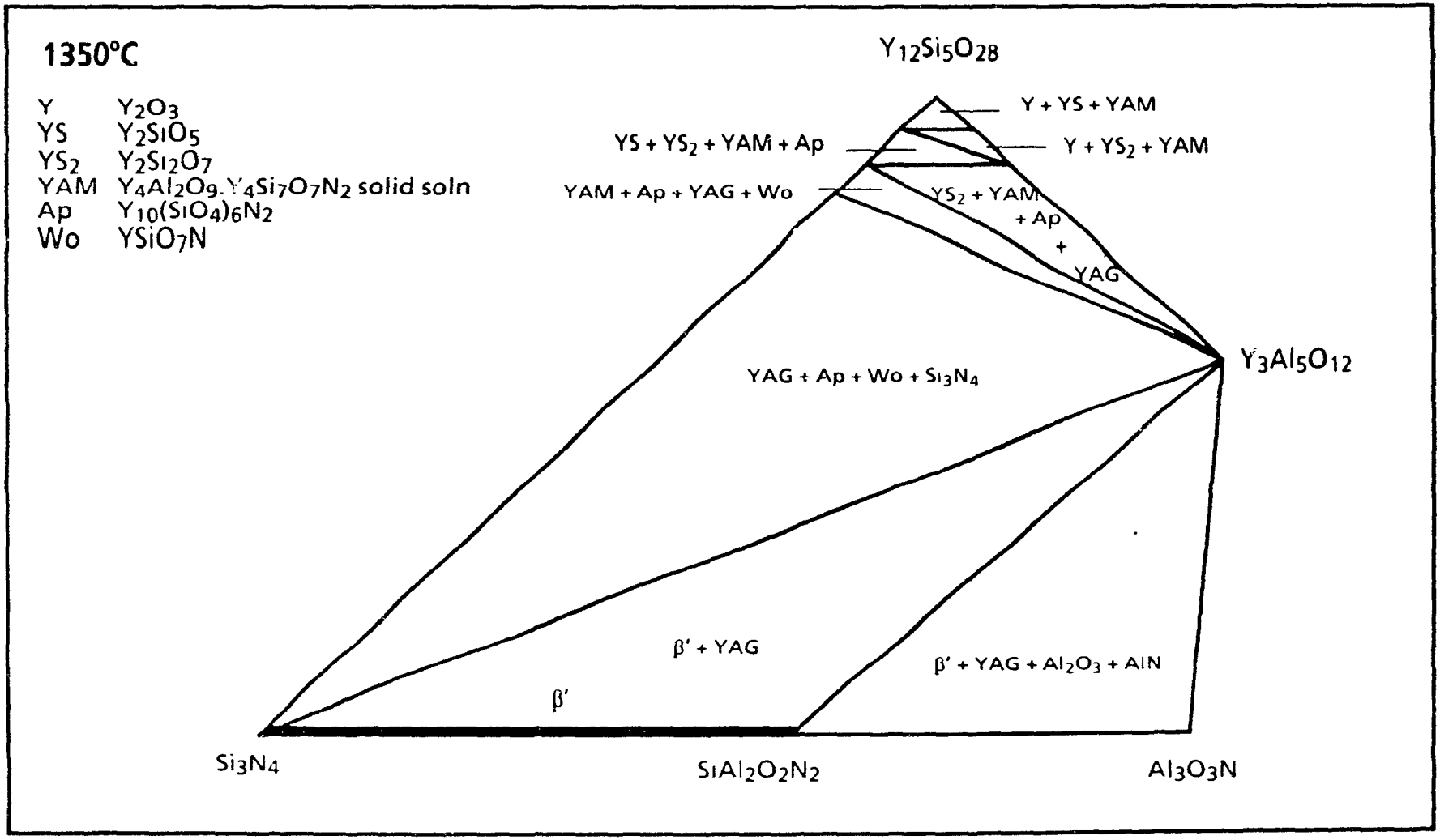

Figure 2 33 Phase relationships in the β'-YAG plane at 1350°C [74]

2.6 MECHANICAL PROPERTIES

The strength of a brittle material is best described in terms of the Griffith fracture equation

$$\sigma = A\sqrt{(\gamma E/c)} \qquad (2\ 21)$$

where γ = the fracture energy

E = Young's modulus

c = the length of the crack that initiates fracture

A = dimensionless number that depends on the mode of stress application, specimen configuration and dimensions, and the type of crack under consideration

Hence, the strength is strongly dependent upon the fracture surface energy, elastic properties and crack size As Si_3N_4, like all ceramics, is brittle in nature, its fracture energy is relatively low (see later)

The Griffith Equation can also be related to the strain energy release rate or toughness, G_c, such that

$$G_c = \frac{\pi c \sigma^2}{E} \qquad (2\ 22)$$

where c is the crack length and σ is the applied stress. A more useful relationship involves fracture toughness, K_c, which can be determined experimentally, Equation 2 22 can be rearranged to

$$\sigma = \frac{K_c}{\sqrt{\pi c}} \qquad (2\ 23)$$

Table 2.4 shows fracture toughness values for various metals and ceramics [77] Although the K_c value of Si_3N_4 is low (4-10 $MPa^{\frac{1}{2}}$) compared to metals, it is higher than most ceramics

It can be said, then, that the strength of Si_3N_4 is mainly dependent on the size and distribution of cracks or flaws present [78] These flaws are most often found within the volume of the sample (as inclusions, pores) and surface flaws (cracks introduced by grinding) Inclusions are most often in the form of impurities in the starting material, i e Fe, Ca, which tend to segregate at the grain boundaries [8] Hence, by using high purity materials, the effect of inclusions can be minimized Also, porosity can be limited through proper sintering conditions; that is, by sintering at high temperatures, to produce full density materials.

2.6 1 Room Temperature Strength

The room temperature strength of Si_3N_4 is not only dependent upon size and distributions of flaws present, but also upon two additional factors, namely the microstructure of the matrix, and the nature of the grain boundary bonding phase

2.6.1.1 Effect of Microstructure on Strength

The strength of a material is related to its grain morphology Figure 2 34 shows the relation of grain size (d) and aspect ratio (R) on the strength of a material It is clear from this that the strength improves as the grain size decreases and the aspect ratio increases [4]. In order to maximize the room temperature strength of silico n nitride, the sintered microstructure should be of sub-micron grain size This can be achieved by using fine starting material and limiting the extent of grain growth in the coalescence process (see Section 2 3.2 3) Not only is the size important, but also the morphology of the grain dictates the resulting strength A rod-like morphology is favoured

Material	K_c (MPa $m^{\frac{1}{2}}$)
Pure ductile metals, e g Cu, Ni, Ag, Al	100-350
High strength steels	50-154
Titanium alloys (Ti6Al4V)	55-115
Si_3N_4	4-10
SiC	3
Al_2O_3	3-5
Soda glass	0 7-0 8

Table 2 4 Fracture toughness of various materials [77]

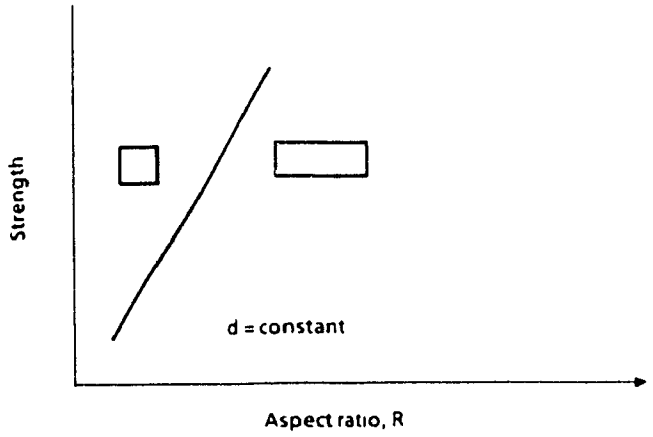

(a)

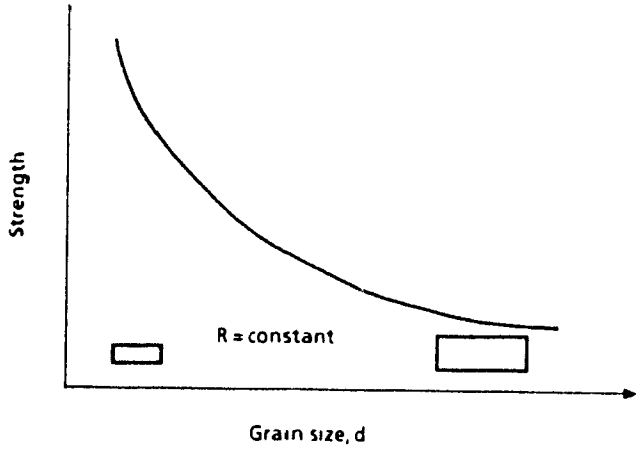

(b)

Figure 2.34. Influence of two typical microstructural variables of dense Si_3N_4: (a) the aspect ratio and (b) the grain size of the β-phase, on the mechanical properties at room temperature (schematic plot) [4].

over equiaxed grain shape, as the former increases the energy required for fracture (γ)

Lange [15] discussed the requirement of a high α-Si_3N_4 starting material if a fibrous microstructure is to be obtained upon sintering He proposed that the resulting aspect ratio, R, of the fibers or acicular microstructure of the transformed β depends on the inital α/β volume fraction ratio

$$R = 1 + \frac{\alpha}{\beta} \tag{2.24}$$

Lange went on to propose that the mechanical properties could thus be controlled through the α/β ratios for the starting materials. Table 2 5 lists the fracture energies and strength of high α phase and high β phase powders[29] It is seen that the α phase starting powder results in the material with the highest fracture energy and strength This increase in strength is attributed to the formation of an elongated grain structure which causes the high fracture energy

Si_3N_4	σ (MPa)	γ (J.m^{-2}x10^{-3})
high α	520-650	29 3-69 5
high β	375	15 8

Table 2.5 Strength and fracture energy of high α and β starting materials [29]

Bowen and Carruthers [79] also showed that the strength of hot pressed Si_3N_4 increases with α/β transformation (Figure 2 35). Microstructural examination of fully converted samples, showing the highest strengths, had a highly acicular grain morphology

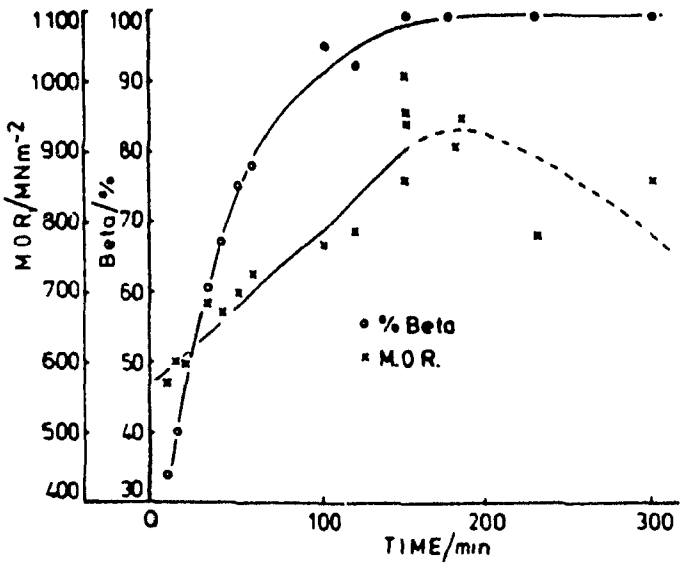

Figure 2.35. Room temperature modulus of rupture and degree of conversion as a function of hot pressing time at 1650°C under 20 MPa for high α-silicon nitride + 5wt.% MgO.[79]

2 6.1 2 *The Effect of the Grain Boundary Phase on Strength*

The mechanical properties of sintered Si_3N_4 is also dependent upon the nature and volume of grain boundary phase present If this intergranular phase is a glass, its strength is much lower than that of the Si_3N_4 itself YSialon glasses, depending upon the composition, have strengths varying from ~150-215 MPa [68], as opposed to ~500-1000 MPa for Si_3N_4 [22] depending on the processing conditions

The volume fraction of the glassy grain boundary phase will also dictate the strength of the resulting sintered Si_3N_4, an increase in the glass content is accompanied by a decrea e in strength. Das & Mukerji [80] observed that a Si_3N_4 containing 20 wt % glass had a lower room temperature strength than one containing 12wt % glass, i e 372 MPa vs 475 MPa, respectively Bonnell et al [65] reported that the toughness of Sialons decreased with increasing YSiAlON and cordierite (MgO-based) glass content (Figure 2 36) More dramatic differences in toughness were observed between the amorphous and samples crystallized to YAG They found that these differences were more pronounced as the amount of additive was increased, and attributed the phenomena to the large residual stresses in the garnet These stresses were thought to arise because the thermal coefficient of YAG is much higher than that of Si_3N_4 The cordierite showed improved room temperature strengths upon annealing due to the formation of the crystalline phase μ-cordierite, however, this phase is metastable

Pugh et al [81] noted a decrease in fracture toughness an , strength with an increase in additive content They attributed this decrease to an increase in the grain boundary phase, as well as porosity due to decomposition during sintering Consistent with other authors [79], they also found that upon devitrification of the glass at 1100°C and 1400°C, a 15% reduction in strength

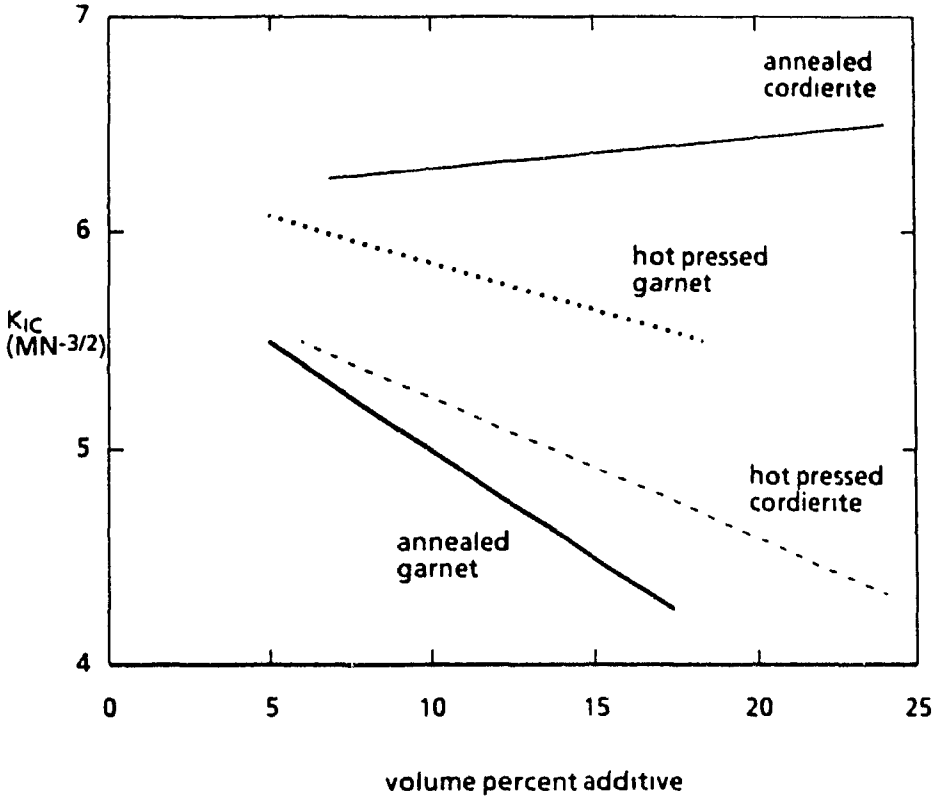

Figure 2.36. Room temperature fracture toughness as a function of the volume fraction of second phase for cordierite and garnet SiAlON.[65]

resulted They attributed this decrease in strength to a volume change of the second phase (YAG) during devitrification. This volume change is due to a density difference between the glass (~3 9 Mgm-3) and YAG (4.55 Mgm-3) which, in turn, leads to the formation of microporosity

2 6 2 High Temperature Mechanical Properties

Most mechanical property studies of Si_3N_4 have been performed at high temperatures, as these conditions simulate the intended application environments of the ceramic. As is true of almost all ceramics, the strength of Si_3N_4 decreases as the temperature is increased (the exception being graphite) [22] The transverse rupture strengths of sintered and crystallized Sialons [54] are shown in Figure 2 37 Although the sintered sialons show superior strengths over their annealed counterparts at low temperatures, their strengths deteriorate dramatically as the temperature reaches ~800°C This degradation in the high temperature thermomechanical properties arises from the presence of the grain-boundary glass phase The amorphous glass begins to weaken as temperatures approach its softening temperature, i e >800°C Conversely, the annealed sialons retain their strength to well over 1000°C This improved strength is due to the reduction of glass content by crystallization, thus the effect of softening of the glass is no longer as critical Also, the crystalline phases formed upon devitrification have excellent refractory properties, i e the melting point of YAG being 1860°C (see Table 2 3) Hayashi et al [52] reported that the flexural strength of specimens devitrified to YAG retained their strength (360 MPa) to 1300°C Clarke et al [58] similarly found that sialons fabricated within the Si_3N_4-Si_2N_2O-$Y_2Si_2O_7$ system and heat treated in air to form Si_2N_2O and $Y_2Si_2O_7$ retained their strength at 1370°C, the strength retention is once again

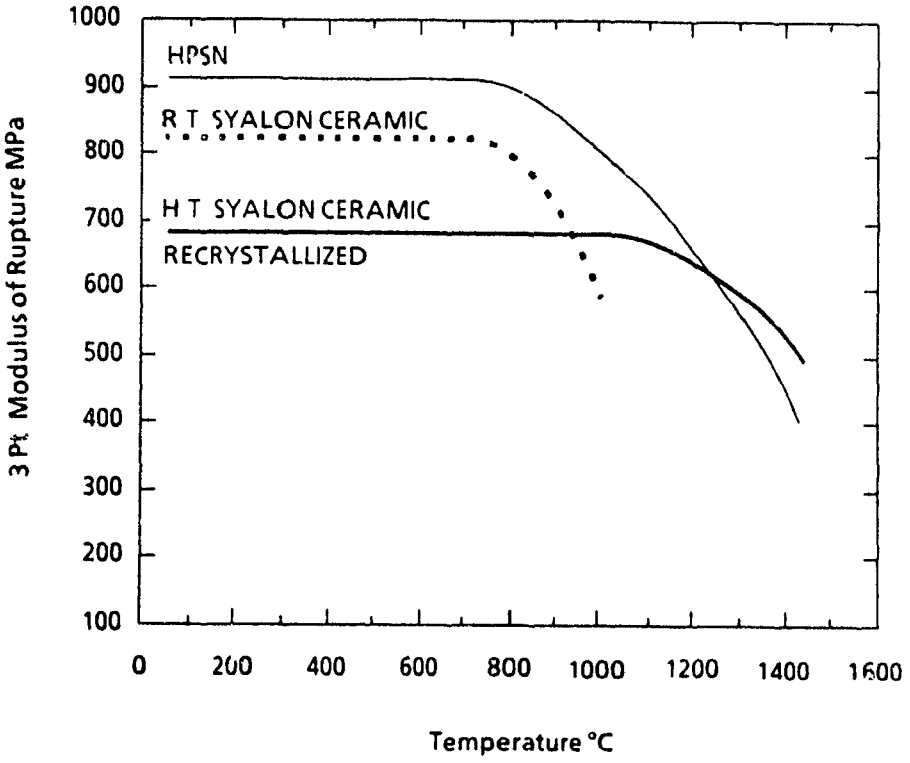

Figure 2.37. Transverse rupture strength of sintered and crystallized sialon as a function of temperature.[54]

related to the refractoriness of the grain boundary phase (see Table 2 3 for melting temperatures).

Like strength degradation, the onset of creep in sialons has also been attributed to the viscous grain boundary phase [82] An empirical expression for creep is given by [83]:

$$\varepsilon = \left(\frac{\sigma}{k_1}\right)\left[1 - exp\left(\frac{-k_1 k_2 t}{\eta}\right)\right] + k_3 \frac{\sigma t}{\eta} \qquad (2\ 25)$$

where ε = creep strain

σ = creep stress

$k_{1,2,3}$ = constants

t = time

η = viscosity

It is clear from this expression that the viscosity of the glassy grain boundary phase affects creep as the viscosity of the glass decreases, the creep strain increases. As seen in Section 2 5, the viscosity of the glass is controlled by the nitrogen content, i.e the viscosity increasing with nitrogen content (Figure 2 20). Butler et al. [54] found that the lowest nitrogen-containing materials exhibit extremely high creep rates, as the intergranular glass is very fluid (Figure 2 38); high nitrogen-containing materials exhibit intermediate creep rates, attributed to the increased viscosity of the glass with higher nitrogen levels The lowest creep rates were achieved when the intergranular phase was crystallized, as little residual glass remains in the grain boundary.

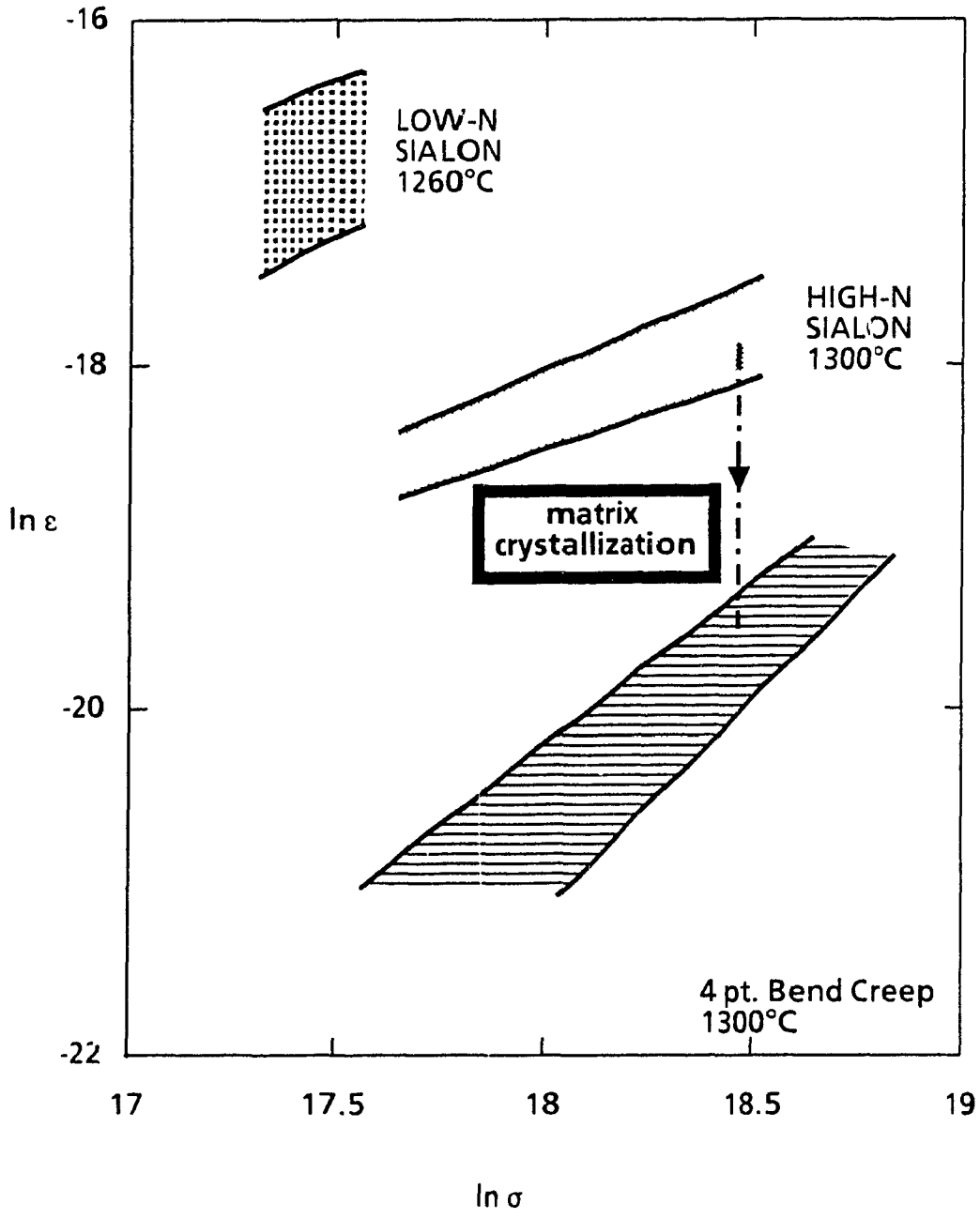

Figure 2.38. Comparison of creep rates of nitrogen ceramic materials with varying composition and microstructure.[54]

2.7 SUCCESS OF GRAIN BOUNDARY ENGINEERING TO DATE

From the above literature review, it has been shown that grain boundary control, viz. limiting the glass phase and/or crystallization, is essential in producing sialons with good mechanical and thermomechanical properties Success to date has been limited in that most of the publications on GBE are ambiguous. Thomas et al. [84] have just recently applied for a patent for the development of a silicon nitride ceramic that shows no loss of strength at 1000°C. The report simply mentions that minimum amounts of additives were used in sintering, thereby minimizing the grain boundary phase. This oxynitride glass was further crystallized to yttrium silicate, the exact heat treatment conditions not being elaborated upon. The ceramic was reported to have a room temperature strength of 532 MPa (which is not spectacular in view of results obtained in this and other studies), and retained 71% of its strength at 1300°C.

The key to producing high strength and creep resistant sialons lies primarily in limiting the amount of grain boundary phase present, whether glassy or crystalline. However, the crystallization of the glass is important with respect to limiting creep at high temperatures.

CHAPTER 3

SCOPE OF PRESENT STUDY

The pressureless sintering of silicon nitride can only be achieved by the use of sintering aids. These additives, typically oxides, allow for densification by providing a liquid phase in which the α-Si_3N_4 dissolves and reprecipitates as the β phase. However, when this liquid cools to a glass it remains as a grain boundary phase which exhibits poor mechanical properties, especially at elevated temperatures Devitrification of the glass to a crystalline phase has been shown to result in improved thermomechanical properties; however an in-depth study of the effect of compositional variation and heat treatment on the devitrification of Y-Sialon glass has not been published.

The primary objective of the study was to achieve the binary system of β'-sialon and YAG. Although $Y_3Al_5O_{12}$ and $Y_2Si_2O_7$ are both stable phases with respect to β', YAG was chosen as the devitrification product based on its higher melting temperature It was therefore postulated that improved high temperature properties would result.

The two variables used in the present study were:

1. composition - different amounts of additives (Al_2O_3, Y_2O_3, AlN) were incorporated into α-Si_3N_4 such that the liquid phase formed upon sintering had different Y/Al/Si/O/N ratios. Some compositions were chosen such that the cation/anion ratio was constant, but with varying N:O content, and vice versa.
2. heat treatment temperature and time - such that the maximum rate of nucleation and growth of YAG from the glass was achieved.

Finally, the effect of the nature and volume of the grain boundary phase on room temperature strengths was evaluated. Samples with a constant

volume of grain boundary phase but increasing amounts of YAG were tested to observe the relationship between the strength and amount of YAG present. Transmission and high resolution electron microscopy were used to identify the sources of variation in strength of various compositions which had undergone different degrees of crystallization

The morphologies of as-sintered samples were studied by scanning electron microscopy The grain boundary phases and general morphologies in both as sintered and heat treated samples were examined by high resolution electron microscopy. It was hoped to link the observed strength measurements to the general microstructures and compositions of the grain boundary phases.

CHAPTER 4

EXPERIMENTAL PROCEDURE

4.1 COMPOSITIONS

The effect of compositional control was studied in terms of two variables: firstly the z value, in order to see if the extent of substitution of Al/O (or z value) within the Si_3N_4 lattice can be controlled, and the effect that the z value has on devitrification; and secondly, the liquid volume to see if the amount of liquid phase plays a role on devitrification. Sialon compositions were chosen such that they lie within the Si_3N_4-YAG-Al_3O_3N region illustrated in Figure 4 1 The compositions studied were divided into three series. More specifically, with increasing additive content

(i) Series I had an increasing liquid content and increasing z value;

(ii) Series II had a constant liquid content and increasing z value; and

(iii) Series III had an increasing liquid content and a constant z value equal to zero Compositions within this series lie along the Si_3N_4-YAG tie line

Compositions were chosen within each of these three series such that they had increasing oxygen content with increasing amounts of additives. For example, composition Ia contained 10 equivalent percent (e/o) oxygen and 90 e/o nitrogen with ~11 wt.% additives, while composition Id had 25 e/o oxygen and 75 e/o nitrogen with ~31wt.% additives The effect of cation content (Y^{3+}, Al^{3+}, Si^{4+}) could also be studied since each composition within a series contained the same O/N ratio as a composition within the other series That is, compositions Ia and IIb each had 10e/o O; Ib, IIb, and IIIc had 15e/o O, and so on; the yttrium content for equivalent O/N ratios increased from Series I to III.

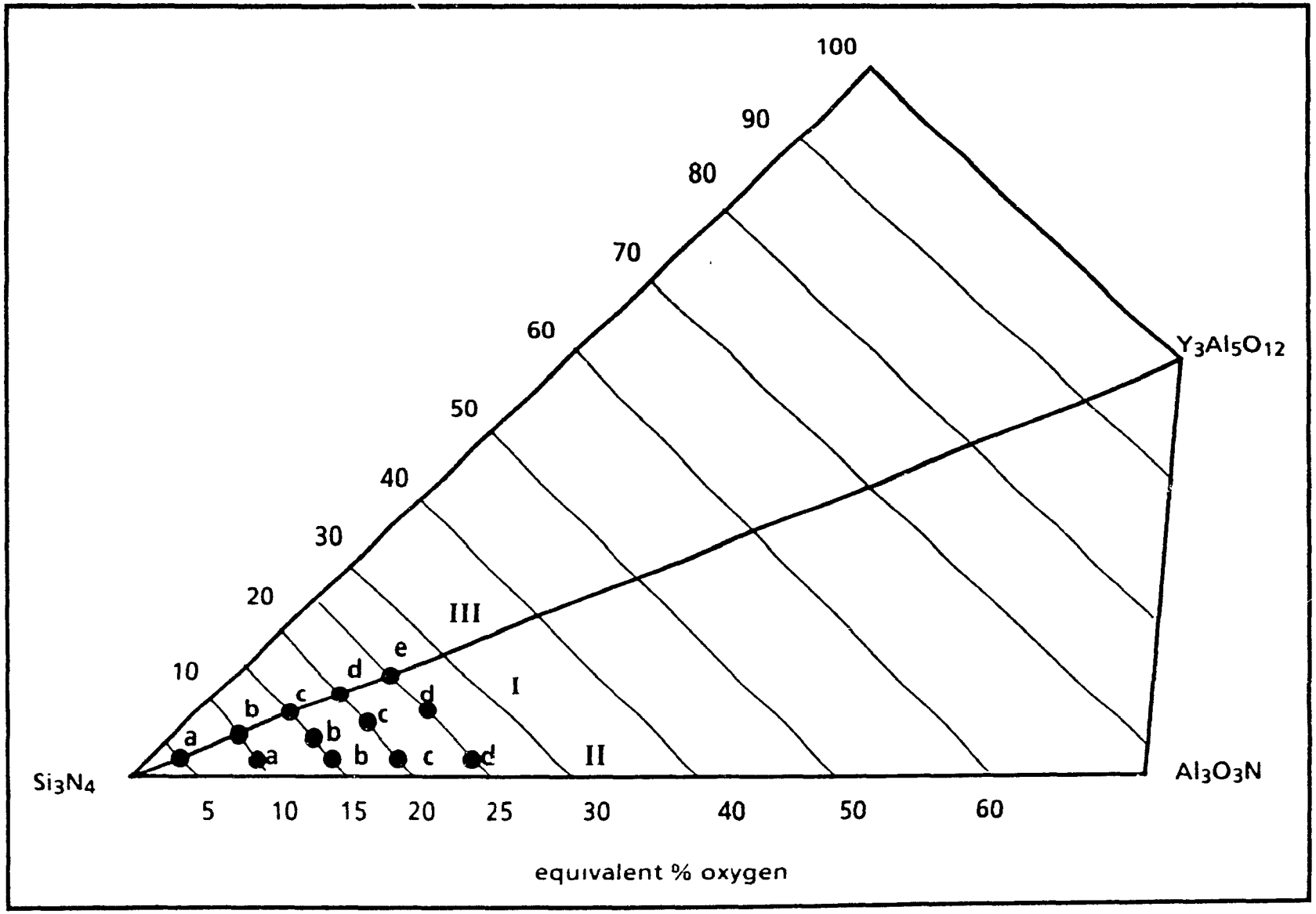

Figure 4.1. Compositions studied within the Si_3N_4-Al_3O_3N-YAG boundaries.

A second method of representing the compositions is based on equilateral triangles of Si^{4+}-Al^{3+}-Y^{3+}, with constant O/N content. Thus, compositions with equal oxygen content were mapped out on the same triangle, as shown in Figures 4.2(a)-(e). The anion ratios for all compositions ranged from 10e/oO (90e/oN) to 25e/oO (75e/o N). The actual amount of the starting materials required, i.e. Si_3N_4, Al_2O_3, Y_2O_3 and AlN, were calculated from these triangles by converting the equivalent percent cations (Y^{3+}, Al^{3+}, Si^{4+}) and anions (O^{2-}, N^{3-}) to weight percent compound. A sample calculation is given in Appendix A. Compensations were made for the surface layer of SiO_2 inherent on the Si_3N_4 powder, this was based on the manufacturer's listed oxygen content which was typically between 1.90-2.0 wt %. The exact constituents of each composition are given in Tables 4.1-4.3.

All of the compositions lie in the Si_3N_4-rich portion of the Janecke prism, shown in Figure 2.26, and are within the Si_3N_4-YAG boundaries. Assuming that the phase diagram is correct, the only expected devitrification phase of these compositions is YAG.

The theoretical amount of YAG formed upon heat treatment was calculated based on the assumption that all Y^{3+} present in the starting material went into forming $Y_3Al_5O_{12}$. Thus, the accompanying Al^{3+} and O^{2-} required to form one mole of YAG were determined by atomic ratios, i.e. $3Y^{3+}$ $5Al^{3+}$ $12O^{2-}$. Any remaining Al^{3+} and O^{2-} not required for the formation of YAG was assumed to substitute into the Si_3N_4 lattice to form β' SiAlON. Since the number of Al atoms going into the β' phase is equal to the z value, the theoretical composition of $Si_{6-z}Al_zO_zN_{8-z}$ could be determined (see Appendix A).

As it was assumed that only $Si_{6-z}Al_zO_zN_{8-z}$ and YAG are present upon devitrification, i.e. no residual glass remains, the weight percents of the Sialon

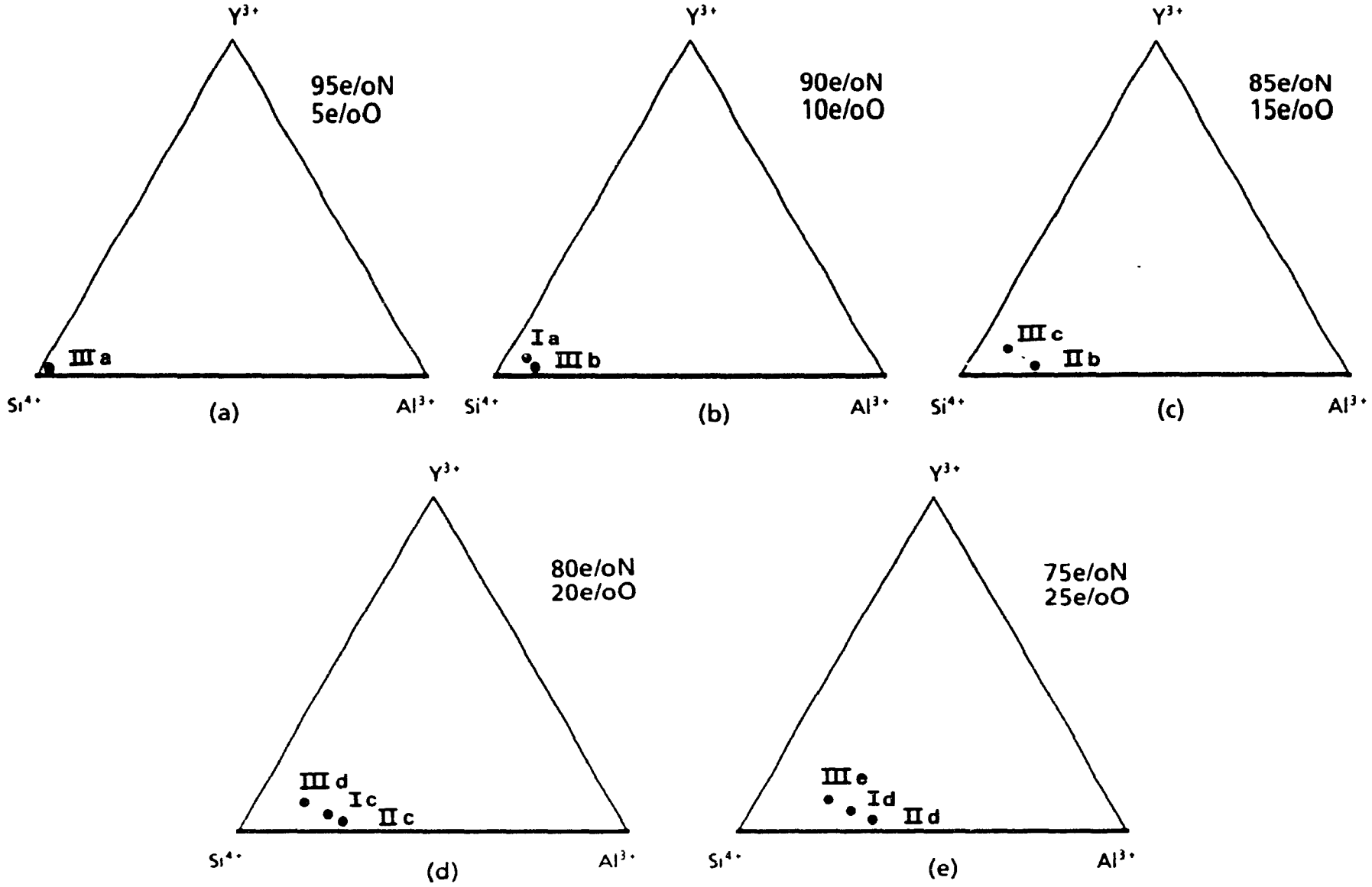

Figure 4 2. Cation equivalence triangles for compositions with varying O/N contents
(a) 95e/oN, 5e/oO, (b) 90e/oN, 10e/oO, (c) 85e/oN, 15e/oO, (d) 80e/oN, 20e/oO, (e) 75e/oN, 25e/oO.

(wt.%)	Ia	Ib	Ic	Id
α-Si_3N_4	88 74	82.06	74 07	68.03
Additives	11 26	17.94	25 93	31 97
Al_2O_3	4.97	9 16	12.17	16 42
Y_2O_3	4 56	6.78	11.16	13 17
AlN	1.72	2.00	2 60	2 38

Table 4.1 Compositions within Series I - Increasing liquid volume and z value with increasing additive content.

(wt.%)	IIa	IIb	IIc	IId
α-Si_3N_4	88.74	82.01	75.51	68 94
Additives	11.26	17.99	24 49	31 06
Al_2O_3	4.97	10.57	16 03	21 64
Y_2O_3	4.56	4.90	5 08	5 25
AlN	1.72	2.52	3 38	4 17

Table 4.2. Compositions within Series II - Constant liquid volume and increasing z value with increasing additive content

(wt.%)	IIIa	IIIb	IIIc	IIId	IIIe
α-Si_3N_4	94.59	87 43	80 61	74.07	67 83
Additives	5 41	12 57	19 39	25.93	32 17
Al_2O_3	0 26	3.50	6.62	9 53	12 31
Y_2O_3	4 23	8 23	12 00	15.69	19 21
AlN	0 91	0 84	0.77	0.71	0 65

Table 4.3. Compositions within Series III - Increasing liquid volume and z = 0 with increasing additive content.

and YAG were calculated A sample of these calculations is given in Appendix A.

Tables 4.4-4 6 list the theoretical z values and YAG contents as well as the theoretical density (ρ_{th}) for all of the compositions The theoretical z values ranged from zero to a maximum of two for the higher additive content compositions. Compositions within Series I had a theoretical z value ranging from 0 5 to 1, within Series II from 1 1 to 2 0, and a z value of 0 for Series III since no substitution was expected in the silicon nitride lattice The theoretical YAG contents for Series I increased from 14 wt % for Ia to 33 wt.% for Id, for Series II, all compositions were calculated to contain ~14-15 wt.% YAG, while the theoretical YAG content for Series III ranged from 14 wt.% (IIIa) to 34wt.% (IIIe)

4.2 SAMPLE PREPARATION

The starting materials for the experiments were α-Si_3N_4, Al_2O_3, AlN, and Y_2O_3. All powders were of high purity, high surface area and low impurities (alkali) content, some specifications of these starting powders are given in Table 4 7 The compositions were prepared in 100 g batches by attrition milling α-Si_3N_4 with the additives in propanol for 0 5 h using high purity Si_3N_4 media. Details on the milling techniques are given elsewhere [85] The slurry was microwave dried to rapidly reduce the liquid content and avoid separation of the powders The remaining slurry was then oven dried at 120°C for a minimum of eight hours in order to remove any residual propanol The dried powders were granulated through a 240μm mesh to break up agglomerates Two-gram samples were uniaxially pressed at 17 MPa into 41mm x 7 5mm x 4mm bars Any excess moisture was then removed by heat

(theoretical)	Ia	Ib	Ic	Id
wt.% YAG	14 3	18.7	30.6	32 8
z value	0 5	0.7	0.9	1 0
ρ_{th}	3 23	3 25	3.28	3.30

Table 4 4 Theoretical z value, wt % YAG and density based on starting compositions for Series I.

(theoretical)	IIa	IIb	IIc	IId
wt.% YAG	14 3	14.3	14.6	14 6
z value	0 5	1.1	1.6	2 0
ρ_{th}	3 23	3 26	3.28	3.31

Table 4 5 Theoretical z value, wt.% YAG and density based on starting compositions for Series II

(theoretical)	IIIa	IIIb	IIIc	IIId	IIIe
wt % YAG	14 0	25 6	34 6	43 0	50 0
z value	0	0	0	0	0
ρ_{th}	3 20	3 22	3.24	3 26	3.28

Table 4 6 Theoretical z value, wt % YAG and density based on starting compositions for Series III.

	Supplier	Surface Area (m^2/g)	d_{50} (μm)	Purity (%)	Oxygen content (%)	Major Impurities
α-Si_3N_4	H.C. Starck LC12	~23	0 7 (max)	97 8	1 4	30 ppm Fe
AlN	H.C. Starck Grade C	~6	0 8-1.3	97 6	2 5	150 ppm Fe
Al_2O_3	Alcoa A16SG	~11	0 3-0 5	99 9	n/a	0 08wt % Na_2O 0 04wt % SiO_2 0 04wt % Fe_2O_3
Y_2O_3	Molycorp 5603	~39	~1.8	99 99	n/a	10 ppm CaO 10 ppm Na_2O 5 ppm Fe_2O_3

Table 4.7. Characteristics of starting material based on manufacturer's specifications. (n/a not available)

treating the bars at 500°C for one hour. The bars were then isostatically pressed at 340 MPa before sintering to maximize the green density.

4 3 SINTERING PROCESS

Pressureless sintering of the specimens was performed in a graphite resistance furnace under a slight nitrogen overpressure of 0.1 MPa. The bars were placed horizontally in a boron nitride crucible (to avoid slumping) along with a powder bed composed of 50/50 mixture (by weight) of boron nitride and composition Ia. The boron nitride prevents the silicon nitride from fritting, the Si_3N_4 + additive powder prevents both weight loss and additive mobility The optimum sintering temperature and time were assessed for each composition, based on (i) maximization of the fired density , (ii) complete α to β transformation, and (iii) minimization of weight losses The reduction of porosity and complete α to β transformation are important in terms of improving the mechanical properties of the sintered body (see Section 2 6) A minimum sintering temperature of 1400°C is required for the conversion to take place, however, a higher temperature is necessary to eliminate as much closed porosity as possible, as discussed in Section 2.3 Weight losses must also be avoided to ensure that the composition has not shifted out of the desired β-YAG-Al_3O_3N triangle

The sintering temperatures ranged from 1600°C to 1800°C for one to two hours and are listed in Table 4 8 - 4 10 Sample dimensions and weights were recorded before and after sintering, as well as an evaluation of density and porosity of the fired specimens as outlined by ASTM C373 [86] This method, also known as the Archimedes Method, allows for the direct measurement of

	Ia	Ib	Ic	Id
T (°C)	1800	1800	1600	1600
t (h)	1	1	1	1

Table 4.8. Sintering conditions for Series I.

	IIa	IIb	IIc	IId
T_{sinter} (°C)	1800	1800	1700	1700
t_{sinter} (h)	1	1	1	1

Table 4.9. Sintering conditions for Series II.

	IIIa	IIIb	IIIc	IIId	IIIe
T (°C)	1800	1800	1800	1700	1700
t (h)	1	1	2	2	2

Table 4.10. Sintering conditions for Series III

bulk density, open porosity and apparent density; and an indirect measurement of closed porosity based on the theoretical density.

4.3.1 The Archimedes Method

The sintered samples were boiled in water for two hours, and then allowed to cool in the water for a minimum of six hours. The wet weight in air (W) and the wet weight suspended in water (S) were measured. The samples were then oven dried at 120°C for eight hours, and the dry weight (D) measured. The following were then calculated:

$$Apparent\ density = \rho_A = \frac{D}{D-S} \tag{4.1}$$

$$Bulk\ density = \rho_B = \frac{D}{W-S} \tag{4.2}$$

$$Percent\ open\ porosity = \frac{W-D}{W-S} \times 100 \tag{4.3}$$

$$Percent\ closed\ porosity = \frac{\rho_{th} - \rho_A}{\rho_{th}} \times 100 \tag{4.4}$$

$$Percent\ relative\ density = \frac{\rho_B}{\rho_{th}} \times 100 \tag{4.5}$$

The theoretical density, ρ_{th}, of the samples was based on the volume fraction of glass and Sialon of each composition. As expected, these densities increased with increasing glass volume since the density of Y-Sialon glass (3.7-

3.9 g.cm^{3-}) is greater than that of Si_3N_4 (3.18 g.cm^{3-}); these values are listed in Tables 4.4-4.6.

4.4 HEAT TREATMENT PROCESS

The sintered samples were heat treated in a vertical tube furnace with a nitrogen flow rate of 31cm/min. The nitrogen gas was purified using a titanium getter. The samples were placed in a graphite crucible with a BN powder bed. Heat treatment was carried out at two temperatures, namely 1100°C and 1400°C for 10, 20 and 50 hours. The lower temperature of 1100°C was chosen as it is above the glass transition temperature of the glassy phase of ~950°C; while the higher temperature is below the lowest melting eutectic composition formed upon sintering.

Based on these results, an additional heat treatment was performed at 1400°C for 100 hours in an attempt to reach equilibrium and full devitrification of the glass to YAG. After heat treatment, the weight losses and density changes were again evaluated by the Archimedes Method

4.5 ANALYSIS

4.5.1 Phase Identification

All sintered and heat treated samples were individually milled in a steel-lined shatterbox to a particle size < 325μm. Diffraction patterns of each specimen were obtained using a Philips X-ray Automatic Powder 1700 Diffractometer with a goniometer, linked to a Digital Micro PDP-11 computer.

The samples were step-scanned using monochromatic CuK_α radiation at 40 kV and 20 mA . A step size of 0.020 degrees and a scan rate of 25 00 deg/sec were used to scan the samples through a 2θ of 15° to 80°, where the strongest

peaks of interest are found Peak shifts were corrected for using KCl as an internal standard. A sample scan is shown in Figure 4.3 with the α, β, and YAG peaks identified.

Phases present upon sintering and heat treatment were identified by comparing the patterns with those found in the JCPDS index available on the PDP-11, as well as using diffraction patterns manually entered into the user database.

4.5.2 α to β Transformation

The evaluation of the extent of α to β transformation upon sintering was according to the methods developed by Gazzara and Reed [87]. The procedure is based on the ratio of intensities of the strongest α and β silicon nitride peaks, which are found to be the (210) diffraction lines in both cases. The relationship between weight percent β and this ratio is given by:

$$\frac{I_{\beta_{210}}}{I_{\alpha_{210}} + I_{\beta_{210}}} \propto wt.\%\beta \qquad (4.6)$$

where I is the intensity of the peak.

The peaks were identified using the "Peak Search" program available on the PDP-11. The backgrounds were subtracted from the intensities, and the resulting counts for α(210) and β(210) were substituted into Equation 4.6 A sample calculation is given in Appendix B. Using the calibration curve developed by Gazzara et Reed (Figure 4.4), the weight percent β in the samples were obtained from the calculated ratio of intensities.

4.5.3 YAG Content

In order to quantify the amount of YAG formed upon heat treatment, calibration curves of wt.%YAG versus intensity of peak were obtained based on the three strongest YAG diffraction lines which did not overlap with other

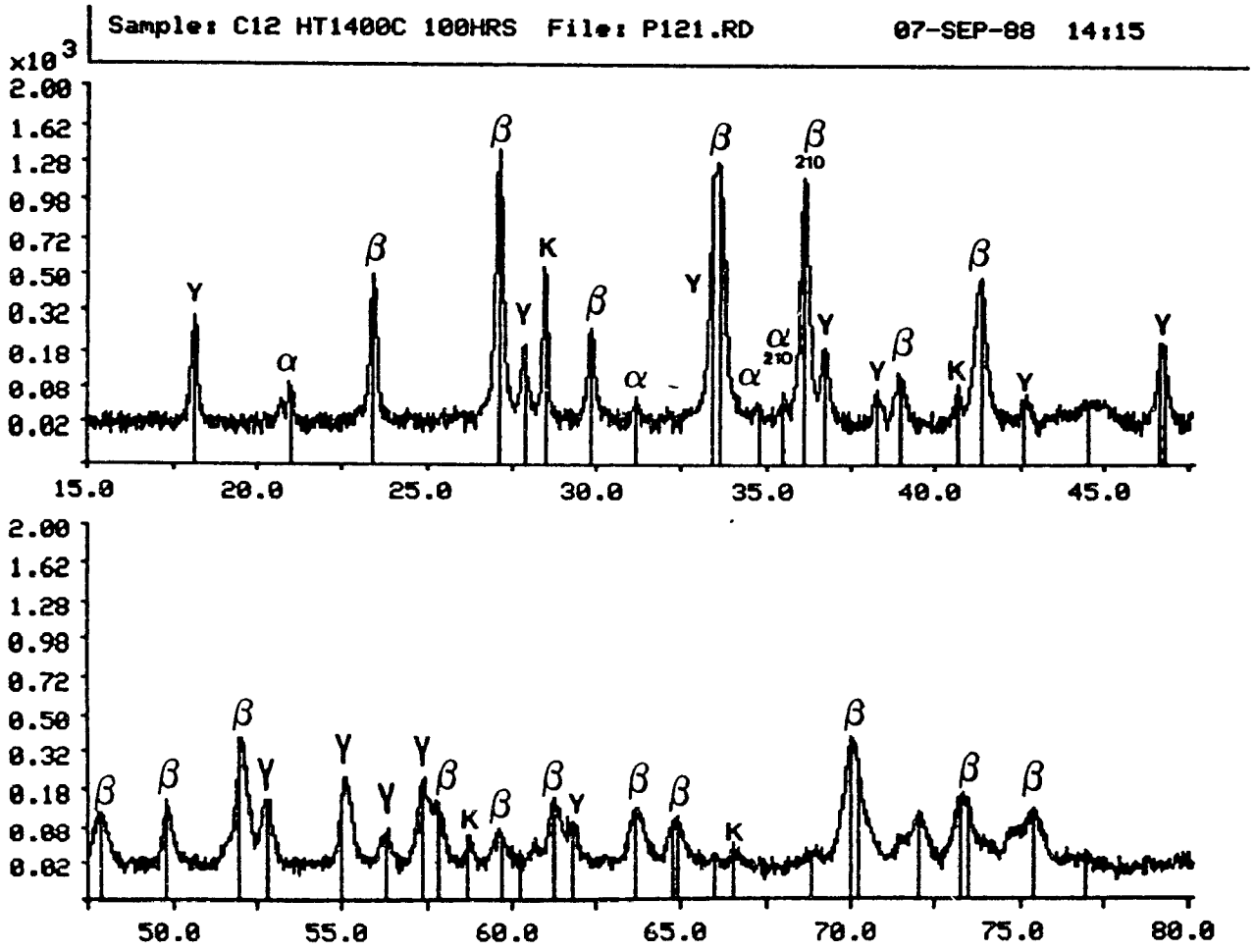

Figure 4.3. X-ray diffraction pattern of as-sintered Id:
α - α-Si_3N_4; β' - β'-Sialon; Y - $Y_3Al_5O_{12}$
K - KCl

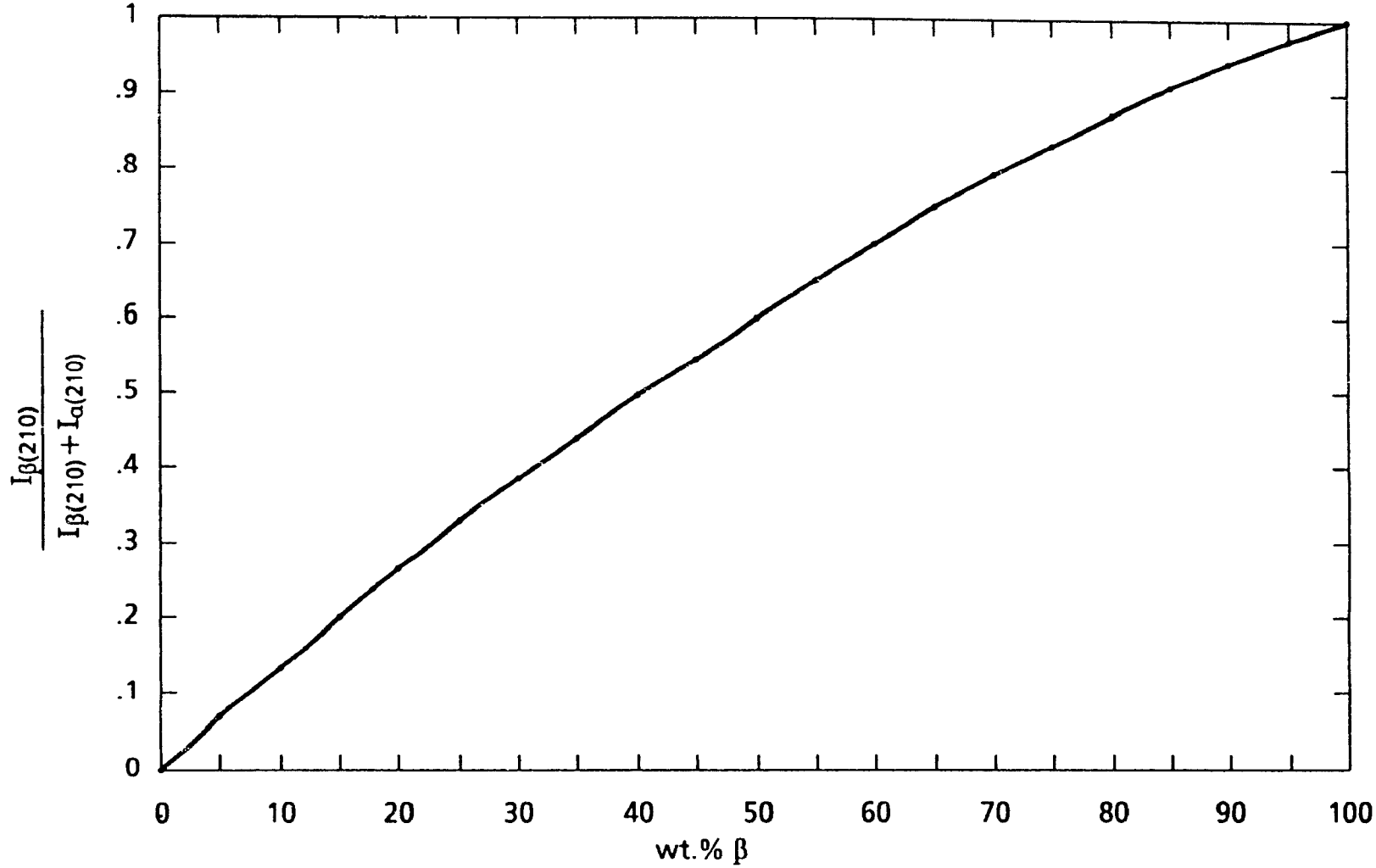

Figure 4.4. Calibration curve for wt.% β in sample [87].

phases present, namely β'-Si_3N_4 or β'-SiAlON. The lines chosen were the (211), (400) and (640) reflections, each line having an intensity (I/I_o) ≥ 30%. These diffractions lines were the same ones used by Greil et al [62] in their determination of YAG content. Samples were prepared by adding increasing amounts of YAG (5-50 wt %) to β-Si_3N_4. Calibration curves for each of the diffraction lines were based on the known weight percent of YAG in the sample (x-coordinate) and the ratio of intensities of the YAG lines and the (210) line of β-Si_3N_4 (y coordinate), which is given by:

$$y\ coordinate = \frac{I_{YAG_{(i)}}}{I_{YAG_{(i)}} + I_{\beta_{(210)}}} \qquad (4.7)$$

where I is the peak intensity (background subtracted), and i is the (211), (400) or (640) diffraction line. Calibration curves for these lines are shown in Figures 4.5-4 7.

For each of the heat treated samples, the ratio of intensities was calculated for all three YAG lines, using the above relationship The weight percent YAG for each diffraction line was interpolated from the calibration curve, and the average of the three YAG contents calculated. The error associated with the intensity measurements were less than 2% A sample calculation of the YAG content is given in Appendix B

4.5 4 Measurement of z Values

The extent of solid solution substitution, or the z value, within the β-Si_3N_4 lattice was determined indirectly by x-ray diffraction As discussed in Section 2.4, the z value is linearly dependent upon the lattice parameter These dimensions, in turn, can be obtained directly by x ray diffraction

For an HCP system such as Si_3N_4, the general relationship between the Miller indices (hkl)and cell dimensions (a and c) is [88]

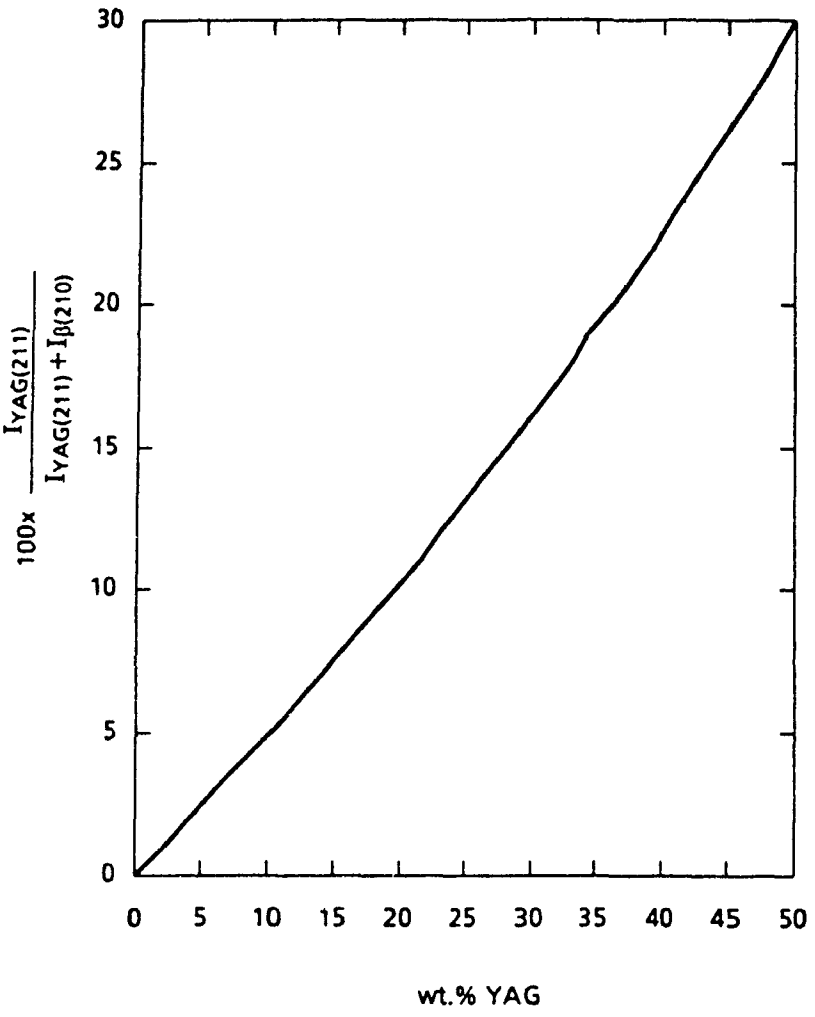

Figure 4.5 YAG calibration curve for (211) diffraction line.

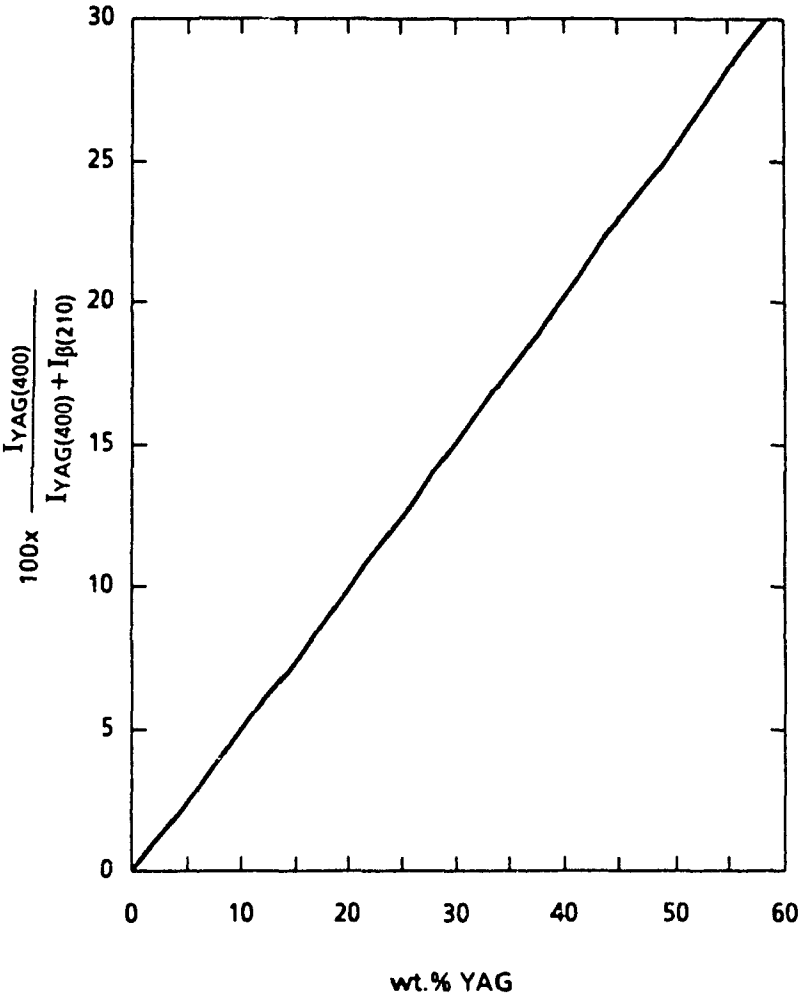

Figure 4.6. YAG calibration curve for (400) diffraction line.

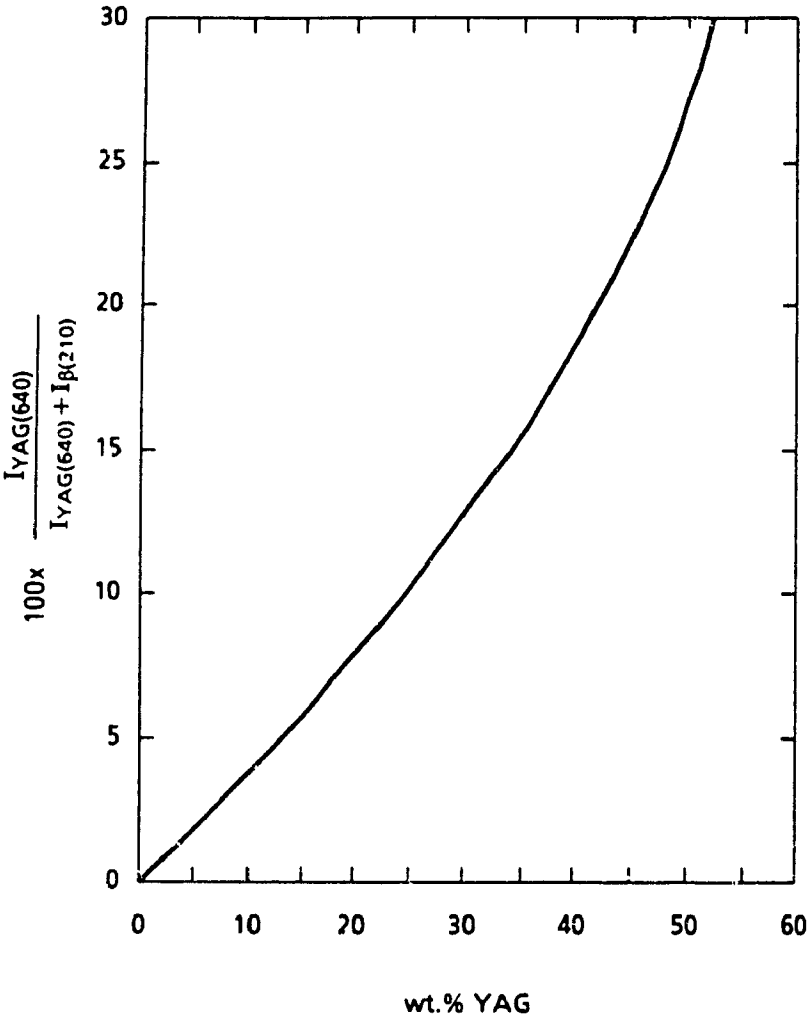

Figure 4.7. YAG calibration curve for (640) diffraction line.

$$\sin^2\theta = \frac{\lambda^2}{4}\left[\frac{4}{3}\,\frac{(h^2+hk+k^2)}{a^2} + \frac{l^2}{c^2}\right] \qquad (4\ 8)$$

where θ = angle of reflection

$(\lambda^2)/4$ = 0 594 for CuKα radiation

As $(\lambda^2/4)$ is a constant, and θ is associated with a particular diffraction (hkl) line, then a and c can be calculated by solving simultaneous equations A sample calculation for the lattice cell dimensions is given in Appendix B

Using the calibration curves in Figure 4 8, the *a* and *c* values were interpolated to give a z value related to each parameter, i e a *z* value based on the *a* parameter, and a *z* value based on the *c* parameter These values were then averaged to give a mean z value for the composition

The criteria for choosing the diffraction lines of β-Si_3N_4 for lattice parameter calculations were such that the lines (i) did not overlap with other phases possible within the system, (ii) were at as high an angle as possible in order to reduce the error, and (iii) were strong enough to be detected in all samples The diffraction lines which fit these criteria were the (212), (231), (330) and (411)

4.5.5 Grain Morphology

Grain sizes and aspect ratios of sintered and heat treated (1400°C/100h) samples were obtained through scanning electron microscopy The samples first were mounted in resin and diamond polished down to 1 μm using a LECO VP-150 Vari/Pol Automatic Polisher The resin was mechanically removed and any residual resin was burned off in air at 500°C from the specimens These were then etched in molten KOH at ~360°C for 15-25s The specimens were gold coated and studied on a JEOL T-300 Scanning Electron

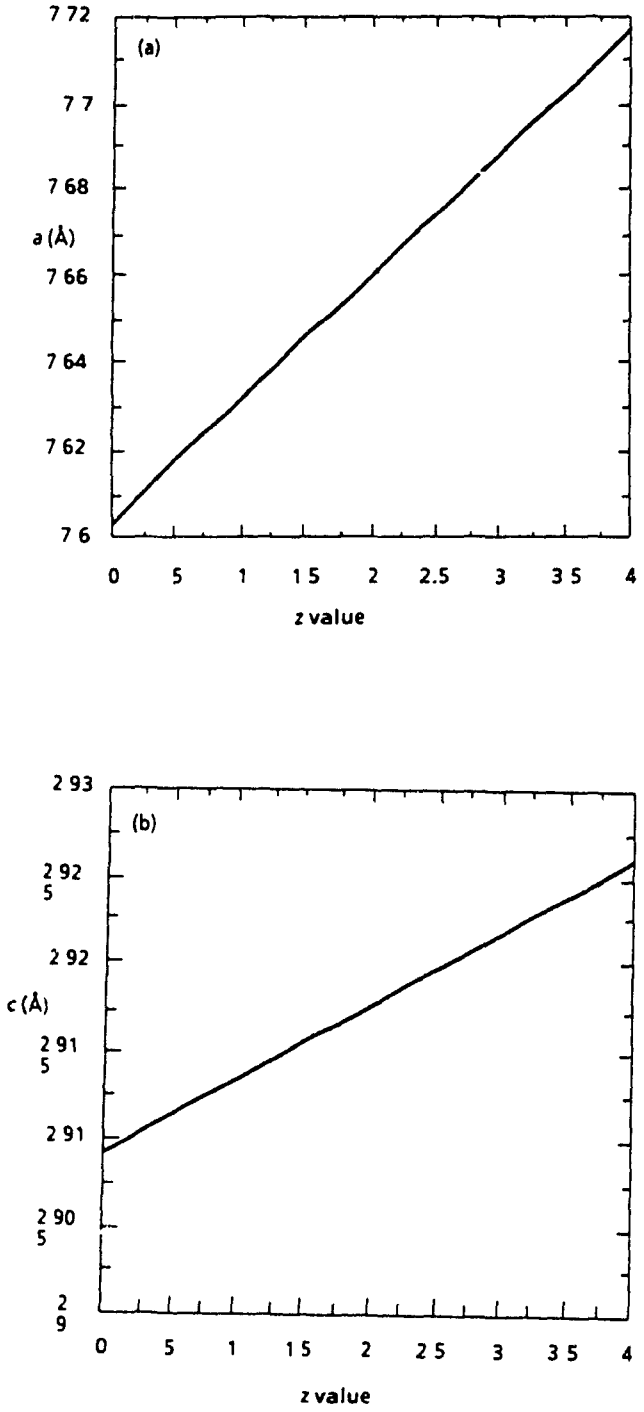

Figure 4.8. Calibration curves for z value determination based on:
(a) *a* parameter; and (b) c parameter.

Microscope. The samples were tilted 30° in order to enhance the contrast between the grains. From micrographs taken, the average grain size and aspect ratio of each composition was determined based on 60 grains, using the grain boundary intercept method[89].

4.5.6 Analysis of Triple Points

Based on the extent of devitrification and crystallized phases found by x-ray diffraction, specific sintered and heat treated samples were chosen to study the grain boundary microstructure by high resolution electron microscopy (HREM). These samples are listed in Table 4.11.

SAMPLES		wt.% YAG		% devitrified
As Sintered	Heat Treated	theoretical	calculated	
	IIIa	14	0	0
Ia	Ia	14.3	0	0
IIIb	IIIb	26	3	10
IIb	IIb	14.6	7	34
	Id	33	33	100

Table 4.11 Samples studied by TEM, showing extent of devitrification.

The heat treated samples were chosen such that they ranged from 0-100% devitrification to YAG The following aspects were studied (i) location of YAG pockets; (ii) location of residual glass

Sample preparation involved: (i) cutting the ~1-2 mm specimens into 3 mm discs using a GATAN Model 601 ultrasonic disc cutter, (ii) dimpling the discs on both sides to a final thickness of 5×10^{-3} mm with a South Bay Technology Model 510 dimpler; and (iii) a final thinning stage by Argon ion milling with

an Ion Tech Ltd ion mill The samples were then coated with a light carbon film High resolution electron microscopy was performed on a JEOL 2000FX transmission electron microscope on which microdiffraction, selected area diffraction and lattice imaging were possible.

Semi-quantitative analysis of the triple points in a sample which showed no devitrification after 100 hours of heat treatment at 1400°C (Ia) was obtained by energy dispersive spectrometry (EDS) using a LINK detector attached to a JEOL 1200 STEM. The technique allows for the precise determinaton of Al, Si and Y contents, and to a lesser degree of accuracy, O and N in samples However, due to severe overlapping of the low energy peaks (i.e C from the coating, and N), semi-quantitative results were obtained for the cations (Al^{3+}, Si^{4+}, Y^{3+}).

The method used for quantification was based on the Cliff-Lorimer equation[90].

$$\frac{at\ \%A}{at\ \%B} = K_{AB}\ \frac{I_A}{I_B} \qquad (4.9)$$

where at.%A = atomic percent of element A

at %B = atomic percent of element B

K_{AB} = Cliff-Lorimer or K-factor

I_A = x-ray intensity of element A

I_B = x-ray intensity of element B

The technique, however, is based on the assumption that the analyzed film is "infinitely thin", whereby the effects of x-ray absorption and fluorescence can be neglected and that the generated x-ray intensity leaving the film are identical For more detail about the method and inherent errors, refer to Ref 90 and 91

Mullite ($3Al_2O_3\ 2SiO_2$) and YAG ($Y_3Al_5O_{12}$) standards were used to determine the K factor for Y/Al and Si/Al The integrated intensities of the cation peaks were measured and, knowing the K factors, the atomic ratios were then calculated from Equation 4.9 A sample calculation is given in Appendix C. The Cliff-Lorimer method was also used to show the variability in z value within a sintered sample, based on the Si/Al cation ratios A sample calculation is also given in Appendix C.

Since the nitrogen content in the glass pockets was below the detection limit and suffered severe overlap from carbon, another method was used to obtain the anion (N/O) ratios of glasses in as sintered and heat treated samples which either showed no devitrification (Ia) or partial devitrification (IIb) Triple points and grain boundaries of these samples were analyzed by electron energy loss spectroscopy (EELS) This technique is the study of the electron energy distribution of electrons which have interacted with the specimen. The method allows for semi-quantification of light elements such as O, and N A software package available on the Tracor system, attached to the TEM, allowed for quantification of the anions based on a "best-fit" of the curves. For a more detailed study of this technique see References 8 and 90, and 91.

4.6 MECHANICAL PROPERTIES

Strength measurements were obtained for all sintered samples Some bars which had been heat treated at 1400°C for 100 hours were also tested These were compositions within Series II which had a constant liquid content Strength measurements of IIIb were also obtained as this composition had a similar liquid content to IIb In this way, it could be determined whether

strength is depended upon the amount of glass present or the composition of the glass A minimum of seven bars for each composition were tested.

Modulus of rupture bars of sintered and heat treated samples were prepared as follows The bars were ground to a final 240μm diamond finish, and the edges bevelled. Four-point testing was performed at room temperature on an Instron Model 1362 tensile tester A crosshead speed of 0 5 mm/min and a load cell of 10 kN were used The experimental set-up is illustrated in Figure 4.9 The sample dimensions were approximately 6 mm x 2 mm x 35 mm, the length of sample under tension (L) was 30 mm, and under compression (P) was 15 mm Strengths of the bars (σ_{MOR}) were calculated according to the equation.

$$\sigma_{MOR} = \frac{3Pa}{bd^2} \qquad (4.10)$$

where P = load

a = span between the top and bottom blades

b = sample width

d = sample thickness

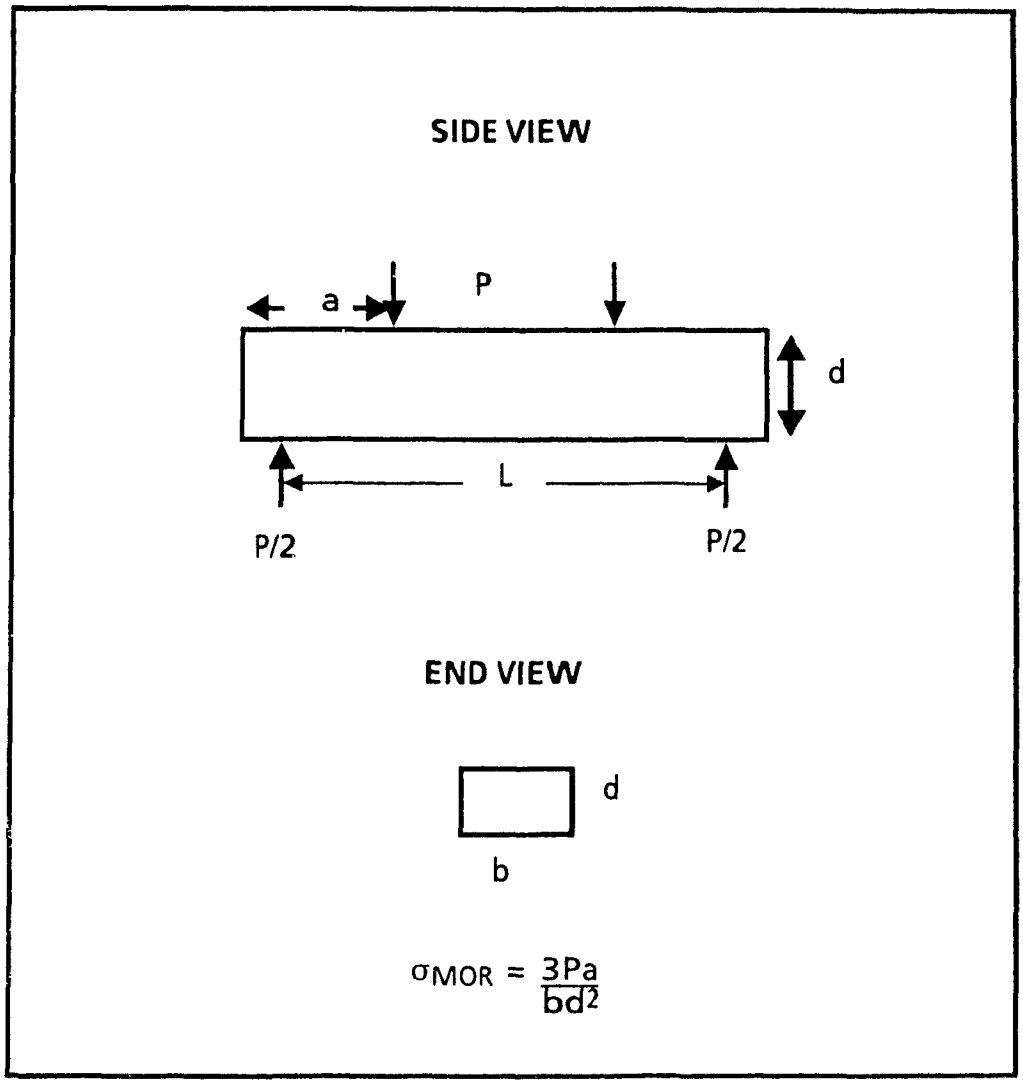

Figure 4.9. Schematic of modulus of rupture loading, illustrating sample dimensions, and loading method [46]

CHAPTER 5

RESULTS AND DISCUSSION

5 1 THE SINTERING STAGE

5 1 1 Sintered Densities and Weight Losses

Full densification is essential in producing sintered components of high strength, since porosity is a source of crack nucleation and therefore provides a mechanism for brittle failure to occur The resulting fired densities along with weight losses of the compositions that were studied are given in Tables 5 1-5.3 for Series I-III In almost all cases, the specimens were >95% dense, values which are fairly typical for low pressure sintered silicon nitride Weight losses upon sintering were kept below 2%, however, composition IIe, which had a very high additive content (32 wt.%), suffered severe bloating due to decomposition of the silica in the liquid phase, according to the reaction [15]

$$Si_3N_{4(s)} + 3SiO_{2(l)} = 6SiO_{(g)} + 2N_{2(g)} \qquad (5\ 1)$$

The thermodynamics of the reaction between Si_3N_4 and SiO_2 show that the equilibrium SiO partial pressure at sintering temperatures $\geq$ 1650°C can be significant

Volatilization of samples can also be attributed to the decomposition and oxidation of Si_3N_4 These effects were minimized through the use of a powder bed of a similar composition to the samples, as well as the use of a slight overpressure of nitrogen The importance of a powder bed in reducing weight losses was demonstrated by Ekstron et al [92], who found that an active powder bed containing constituents of the specimens (i e Al, Si, N, O)

	Ia	Ib	Ic	Id
Wt.% additives	11.26	17 94	25 93	31 97
T_{sinter} (°C)	1800	1800	1600	1600
t_{sinter} (h)	1	1	1	1
Fired density (g cm^{-3})	3 15	3 19	3 25	3 25
Relative (%)	96 5	96 1	97 3	94 4
% Weight loss	0 8	1 8	1 3	1 3
β/α x100	92	100	100	95

Table 5 1 Fired densities and weight losses for compositions within Series I

	IIa	IIb	IIc	IId
Wt.% additives	11 26	17 99	24 49	31 06
T_{sinter} (°C)	1800	1800	1700	1700
t_{sinter} (h)	1	1	1	1
Fired density (g cm^{-3})	3 15	3 18	3 16	3 15
Relative (%)	96 5	97 6	96 5	95 1
% Weight loss	0 8	0 9	0 9	1 0
β/α x100	92	100	100	96

Table 5 2 Fired densities and weight losses for compositions within Series II

	IIIa	IIIb	IIIc	IIId	IIIe
Wt % additives	5 41	12 57	19 39	25.93	32 17
T_{sinter} (°C)	1800	1800	1800	1700	1700
t_{sinter} (h)	1	1	2	2	2
Fired density (g cm^{-3})	2 95	3 19	3 28	3 24	n/a
Relative (%)	92 5	99 1	99 9	99 5	n/a
% Weight loss	0 3	0 1	0 6	0 1	n/a
β/α x100	100	100	100	95	88

Table 5 3 Fired densities and weight losses for compositions within Series III (n/a not available due to severe bloating)

was far more effective than using a passive powder bed such as BN since a partial pressure equilibrium between the sample and the bed is achieved in the former.

Overall, the weight losses suggest that there is only minor compositional shift occurring during sintering and, therefore, the desired compositions were achieved. This is in agreement with Spacie et al [63] who obtained desired single crystalline phases upon sintering only when the weight losses were kept below 2% at a sintering temperature of 1650C-1850°C in a nitrogen atmosphere However, other authors were unable to achieve single crystalline phases during sintering: Sanders et al [50] observed weight losses as high as 8% in samples sintered at 2140°C for 1 hour at 2 5 MPa These severe weight losses can be attributed to a shift of the overall composition away from the β'-Sialon region as a result of volatilization, despite the use of a nitrogen overpressure. Furthermore, the boron nitride discs used to separate specimens were not successful in preventing weight losses since convection of volatile species is possible in the absence of the physical barrier of a packing bed.

5.1.2 Phases Formed upon Sintering

As the aim of this research work was to produce a two-phase (β + YAG) system through heat treatment, it was essential that the sintered samples contained only β as the crystalline phase plus an amorphous glass prior to devitrification The presence of any untransformed α-Si_3N_4 leads to a decrease in mechanical strength and toughness due to its grain morphology [81,93]. This is because, as discussed in Section 2 6, α-Si_3N_4 is equiaxed in nature whereas β-Si_3N_4 is acicular The high aspect ratio of β grains means that more energy is required for crack propagation, producing a more tortuous intergranular crack path

X-ray diffraction of the sintered samples showed only one crystalline phase, namely β, in almost all cases, the exceptions being Ia, Id and IId, which contained residual α silicon nitride (< 8 % α). The incomplete transformation of these samples is associated with volatilization (causing slight compositional shifts) and/or low sintering temperatures. IIIe contained only 88% β upon sintering; in view of this and the fact that the sample had undergone severe bloating, this composition was not used in subsequent experiments

Spacie et al [63] found that compositions rich in Al formed small amounts of polytypoids with negligible weight losses, typically 12H and/or 15R. The compositions used in this study contained only a limited amount of aluminum, most of the compositions were close to the Si_3N_4 corner of the phase diagram shown in Figure 4.1, and therefore the likelihood of forming polytypoids was minimal

Other authors[23,41] have reported difficulties in achieving a single crystalline phase system upon sintering. In most cases, formation of crystalline phases other than β can be attributed to the following:

1. reaction kinetics at different temperatures.
2. changes in thermodynamic equilibrium as a function of temperature.
3. precipitation of second phases from liquids or glass phases on cooling.

The presence of residual α-Si_3N_4 indicates that the system has not yet reached equilibrium [41] In general, as the sintering temperature is increased, the more likely it is that β-Si_3N_4 will be the only crystalline phase upon sintering since transformation of α to β is thermodynamically favorable at temperatures greater than 1400°C (see Section 2.3.4). Although full densification can be achieved with incomplete conversion, residual α

indicates that the fabrication conditions were insufficient to allow completion of this transformation [82]

The cooling rate can affect the extent of long-range diffusion, that is, whether enough time is available for ions to reorganize into a structured network such as a crystal Hence, the faster the cooling rate from the sintering temperature, the less likely devitrification of the glass Based on the theory of glass formation (Section 2 5 1 2), it can be said that the cooling rate after sintering was high enough to prevent the crystallization of glass Thus, the viscosity of the liquid phase as it was being cooled was high enough (due to the presence of N) to prevent the rearrangement of the species into a structured network Hence, the formation and growth of crystals was avoided, resulting in a glass upon cooling of the liquid It should therefore be possible to devitrify this YSialon glass if proper heat treatment conditions are applied

In cases where multi-crystalline phases are present after sintering, it is impossible to achieve only β + YAG when heat treating at temperatures below 1400°C. This is principally because these secondary crystalline phases only become liquid at temperatures above 1600°C [63] and would therefore always be present when the heat treatment is carried out below their melting points In other words, to obtain a two-phase system upon heat treatment, only β-Sialon and glass must be present after sintering It is this glassy phase which is subsequently devitrified to form YAG

5.1 3 Z Value

The extent of aluminum and oxygen substitution within the Si_3N_4 lattice, which is quantified by the z value, is determined most easily by measurement of the lattice parameters of the unit cell through x-ray diffraction.These observed values were compared with the predicted values for all three series

of compositions in Figures 5 1-5 3 (The predicted z values of the compositions were calculated based on the equivalent percents of ions in the starting materials, a sample calculation is given in Appendix B)

The graphs (Figures 5 1-5 3) represent the effect of additive content on the z value of each series As was expected, the predicted z values in Series I and II show an increase with increasing additive content, since the amounts of Al^{3+} and O^{2-} ions available for substitution increase with additive content (See Tables 4 4-4 6) Throughout Series III, the predicted z value remains at zero as these compositions lie on the Si_3N_4-YAG tie line However, the calculated z values did not correlate well with the predicted values As seen in Figures 5 1 and 5 2, most of the observed values (solid line) for Series I and II were below the predicted values (dashed line); some of the higher additive compositions within Series III (Figure 5 3) had calculated z values of upto 1 3, implying that these compositions actually do not lie along the Si_3N_4-YAG tie line It can therefore be postulated that, in all three series, the system had not reached equilibrium under the sintering conditions used in the present study

The substitution of Al and O does occur within the silicon nitride lattice, however the extent of substitution is not easily controlled during sintering In Series I and II, the calculated z values were below the predicted data That is, less aluminum and oxygen ions have diffused within the silicon nitride but remain in the liquid phase, and hence in the glass on cooling

Compositions within Series III, on the other hand, show the existence of Al and O within the Si_3N_4 lattice, this should not have occurred based on the calculated starting compositions and, since they lie on the Si_3N_4-YAG tie, should have resulted in β-Si_3N_4 + glass upon sintering The fact that Al and O substitution has taken place implies that the compositions have undergone

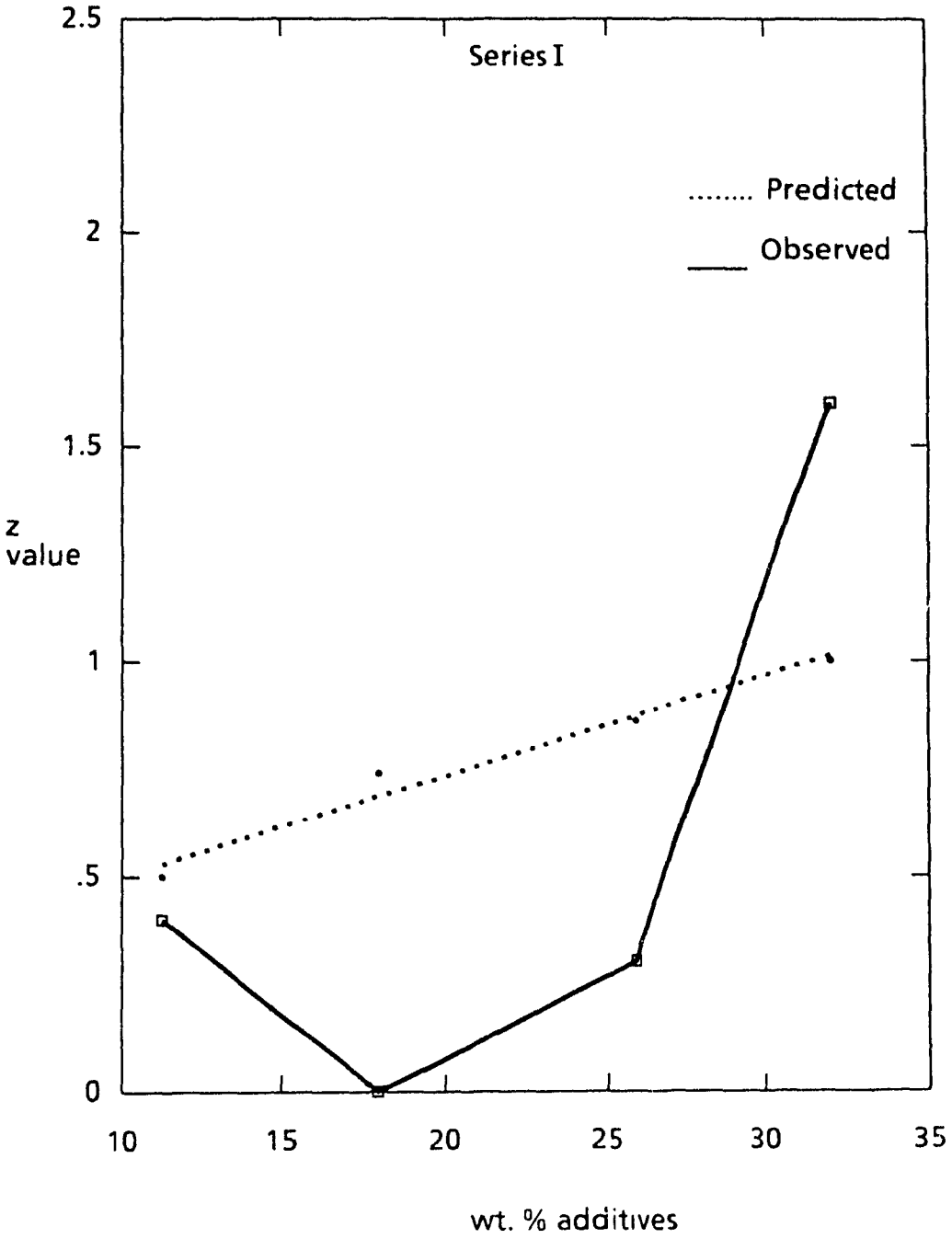

Figure 5.1. Effect of additive content on predicted and observed z values of Series I

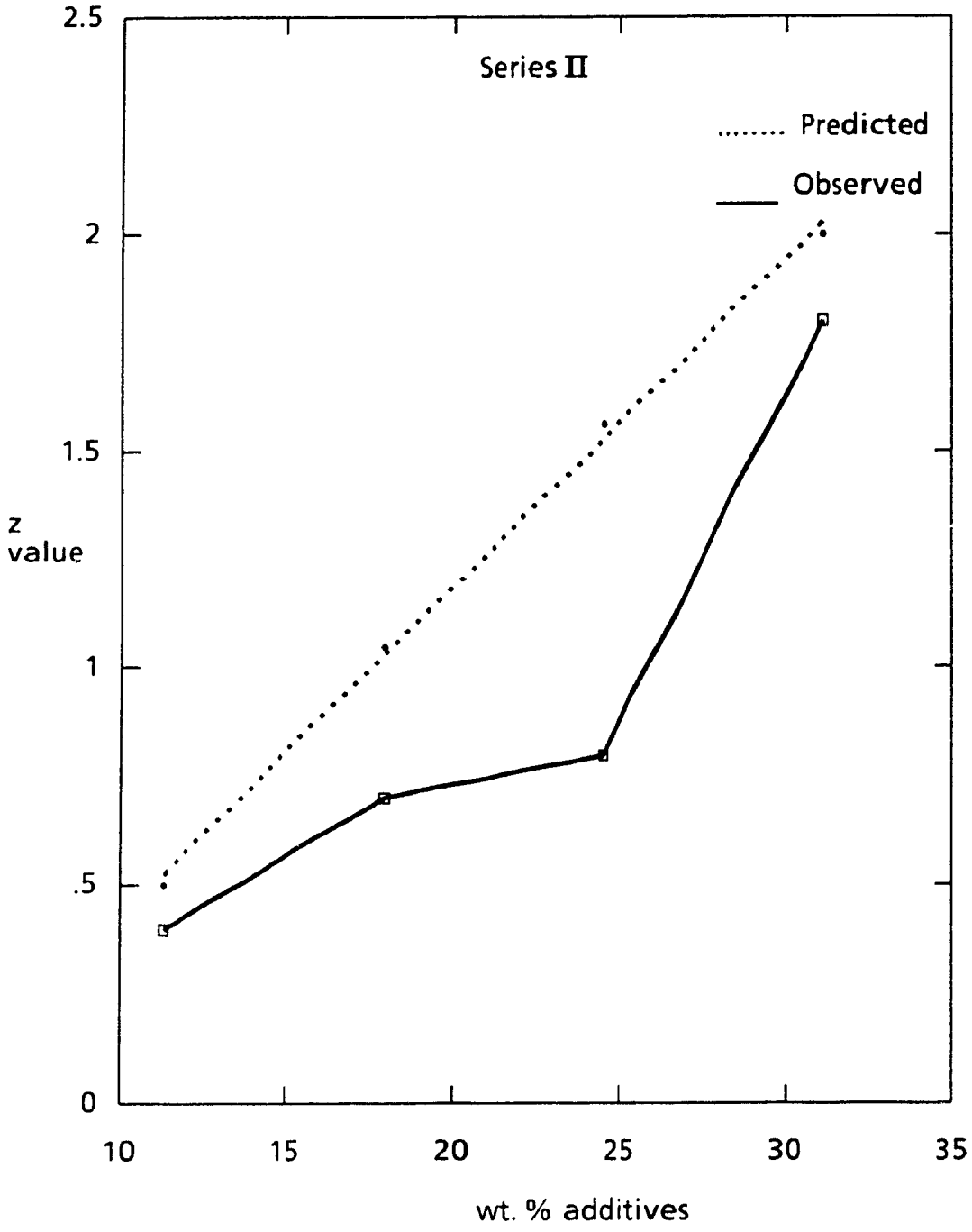

Figure 5 2 Effect of additive content on predicted and calculated z values of Series II.

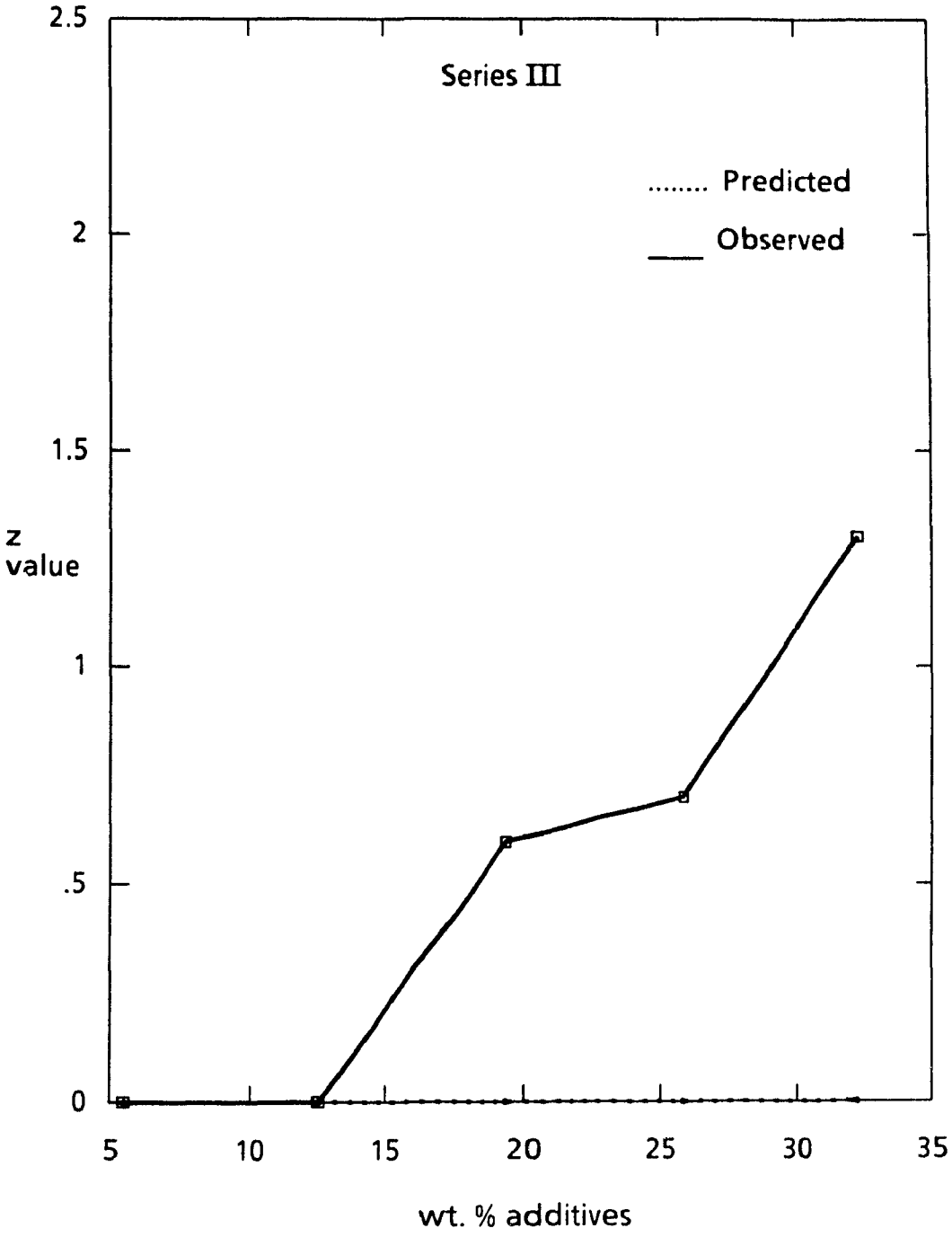

Table 5.3. Effect of additive content on predicted and observed z values of Series III.

an equilibrium shift from the starting material and that the residual glass phase is somewhat depleted of Al and O

Although many authors [54,94] discuss the effect of z values on the properties of sialons (i e with respect to grain growth), there are no reports which have studied the variability of substitution in terms of transformation, liquid volume present, and grain size as discussed in this thesis. Lee et al [94] observed that the z value increased with increasing α to β transformation, however, as the conversion was incomplete, with some samples containing as much as 95% α, equilibrium of the system cannot have been attained In their study, sintering was performed at 1600°C-1650°C for anywhere from 1 5 minutes to 16 hours Their ability to reliably evaluate the z value is therefore doubtful The peak intensities used for the lattice parameters as per Gauckler [95] for samples containing 2% β would be very low if not immeasurable That is, for 100% β-Si_3N_4 the intensities of the peaks measured in this study range from 2-14% of I/I_{max}, so for a sample containing only 2% β', these intensities would be below the detection limit. Also, they based their z value on only the c lattice rather than the average of both the *a* and c lattice parameters without any apparent justification for this

As concluded by Haviar and Johannesen [96], few experimental details about sample preparation, analysis of compositions and unit cell determinations are ever reported in literature and so, it is difficult to make comparisons between results of different studies

5 2 THE HEAT TREATMENT STAGE

As outlined in Section 4.1, the three series of compositions were heat treated at 1100°C and 1400°C for 10, 20, 50 and 100 hours in order to

establish the ideal annealing conditions. This heat treatment optimization was based on the following criteria:

1 the formation of $Y_3Al_5O_{12}$ (YAG) as the major or, if possible, only devitrification product (determined by XRD), and

2. the maximum devitrification of the glassy phase to form YAG

The extent of devitrification was evaluated by a comparison of the observed amount of YAG formed (by XRD) and the theoretical amount (based on the starting compositions and assuming that complete devitrification to β + YAG was achieved) Series I and III should show an increasing YAG content with increasing additive content, while Series II should have a constant amount of YAG with increasing additive content, since the liquid content was kept constant

In all cases, the weight losses were minimal due to the low annealing temperatures, and it could be assumed that no significant compositional shift occurred due to volatilization during the process, according to Eq 5 1 Therefore, the predicted amount of YAG based on the starting compositions was a valid means of assessing the expected extent of devitrification

5.2.1 Weight Losses and Densities

Weight changes after heat treatment at 1100°C and 1400°C were within ± 1.5%. Thus, the same argument discussed in the previous section is still valid and the compositions should lie within the predicted area of the phase diagram.

A slight increase in density (up to 3% in some compositions) was also observed in some compositions after heat treatment As discussed in Section 2.5.2.1, crystallization of a glass is often accompanied by a small volume change due to specific gravity differences between the crystal and the parent glass. In this case, the density of YAG (4 5 g cm^{-3}) is much greater than that

of a Y-Sialon glass (3 8-4 0 g cm^{-3}), resulting in a volume shrinkage and thus an increase in the overall density.

A more important phenomenon associated with the crystallization process is the difference between the thermal coefficients (α) of the glass and YAG No data is available for the thermal expansion coefficients of a Y-Sialon glass, however Hyatt and Day [73] report that the thermal expansion coefficient of Y-aluminosilicate glasses range from 3 1-7 0x10^{-6} C^{-1}, which would imply that the values for Y-Sialon glasses would be slightly lower This is because nitrogen will bond tetrahedrally to Si, the overall covalent bond strengths in the glass are stronger [97], leading to lower thermal expansion The values of α for YAG is 8 2x10^{-6} C^{-1}, which is considerably larger than that of the glass This gradient can have deleterious effects on the mechanical properties of the ceramic, especially at elevated temperature (see later).

5 2.2 Phase Formed after Heat Treatment

Tables 5 4-5 6 list the phases present after heat treatment at 1100°C and 1400°C for the different annealing times At 1100°C several crystalline phases are formed such as $Y_2Si_2O_7$, mullite, melilite and YAG; however, in all compositions, these were found in relatively small amounts, e g <5w/o for compositions containing ~11w/o additive, and ~15w/o for high additive (33w/o) compositions ; this implies that in most cases little of the glass phase had crystallized It is therefore clear that this lower temperature is inadequate for devitrification, especially for the formation of YAG, and that other crystalline phases are more stable at this temperature

Thomas and Ahn [98] found that devitrification at 1100°C of nitrogen containing glasses was at best very sluggish compared to pure oxide glasses, and attributed the slower rates of nucleation of the Y-Sialon glass to the presence of nitrogen, which decreases the tendency for the glass to devitrify

	Ia		Ib		Ic		Id	
	1100°C	1400°C	1100°C	1400°C	1100°C	1400°C	1100°C	1400°C
A/S	β,α, +	β,α	β	β	β +	β +	β, α	β, α
10h	β YS	β	β tr YAG +	β, tr YAG +	β YAG +	β YAG +	β YAG YS +	β YAG
20h	β YS	β, tr YAG	β YS + tr YAG	β YAG	β YAG +	β YAG +	β YAG +	β YAG
50h	B,YS tr YAG M +	β, tr YAG	β YAG tr YS +	β YAG	β YAG YS +	β YAG +	β YAG YS +	β YAG
100h		β		β YAG +		β YAG +		β YAG +

Table 5.4. Series I - Phases formed upon heat treatment
YS- $Y_2Si_2O_7$
YAG - $Y_3Al_5O_{12}$
M- melilite
+ -trace unknown

	IIa		IIb		IIc		IId	
	1100°C	1400°C	1100°C	1400°C	1100°C	1400°C	1100°C	1400°C
A/S	β,α, +	β,α	β +	β +	β	β	β, α	β, α
10h	β YS	β	β tr YAG +	β, tr YAG +	β M YS	n/a	β M +	β M +
20h	β YS	β, tr YAG	β tr YAG +	β tr YAG	β M +	β tr YAG M	β M YS +	β M tr YAG
50h	B,Y tr YAG M +	β, tr YAG	β YS tr YAG +	β tr YAG	β YS +	β YAG Y, M	β YS +	β YAG M
100h		β		β YAG		β YAG M		β YAG M +

Table 5.5 . Series II - Phases Formed Upon Heat Treatment.
YS - $Y_2Si_2O_7$
YAG - $Y_3Al_5O_{12}$
M - melilite
+ - trace unknown
n/a - not available

	IIIa		IIIb		IIIc		IIId		IIIe	
	1100°C	1400°C	1100°C	1400°C	1100°C	1400°C	1100°C	1400°C	1100°C	1400°C
A/S	β +	β +	β +	β +	β	β	β	β	β α	β α
10h	β YS tr YAG	β YS +	β YAG Y +	β YS tr YAG	n/a	β YAG	n/a	β YAG	n/a	β YAG
20h	β YS tr YAG +	β YS tr YAG +	β YS tr YAG +	β YS tr YAG +	n/a	β YAG	n/a	β YAG	n/a	β YAG
50h	β tr YAG M +	β, tr YAG +	β YS tr YAG M +	β YS YAG	n/a	β YAG +	n/a	β YAG	n/a	β YAG
100h		β		β YS YAG		β YAG		β YAG		β YAG

Table 5.6. Series III - Phases Formed Upon Heat Treatment.
YS - $Y_2Si_2O_7$
YAG - $Y_3Al_5O_{12}$
M - melilite
+ - trace unknown
n/a - not available

presence of nitrogen, which decreases the tendency for the glass to devitrify. They reported that 24 hours of heat treatment at 1100°C resulted in stable crystalline phases other than YAG being formed (such as $Y_2Si_2O_7$ and mullite), as was the case in the present study. They attributed the formation of these phases to the slow nucleation kinetics of YAG at this low temperature.

The number of phases crystallized at a heat treatment temperature of 1400°C is more limited. In almost all compositions, YAG was present as the major devitrification product and was found in significant amounts. Some exceptions to this are Ia and IIIa which showed no devitrification to YAG even after 100 hours of heat treatment Both these compositions had low additive content and would therefore be greatly affected by any shift in additive composition. An underestimation of the oxygen content, and hence the silica content (introduced by processing), in these phases would greatly affect the glass composition. Small changes in the SiO_2 content would shift the compositions out of the field of interest (β + YAG) in the system The effect of this shift will be discussed in a subsequent section (Section 5.6.1.1)

The presence of mullite in alumina-rich compositions IIc and d and yttrium silicate ($Y_2Si_2O_7$) in some low additive (IIIb) compositions together with YAG can be explained in terms of the phase diagram for the system (refer to Figure 2 26) Compositions IIc and d lie close to the Al_3O_3N phase and are rich in Al_2O_3, they would therefore be more likely to form an Al_2O_3-based crystalline product Composition IIIb , in which $Y_2Si_2O_7$ was detected, may have had an excess of SiO_2 present, which would shift the composition out of the Si_3N_4-$Si_2Al_4O_4N_4$-YAG field and into the adjacent SiO_2-rich side where $Y_2Si_2O_7$ is the most likely phase to form.

5.3 OPTIMIZATION OF HEAT TREATMENT CONDITIONS

5.3.1 Temperature

A heat treatment temperature of ~1400° is required to allow for nucleation and growth of YAG crystals, at the lower temperature of 1100°C, other phases (i.e. $Y_2Si_2O_7$) with higher rates of nucleation and growth than YAG will tend to form. The choice of a higher annealing temperature is also supported by comparing the amount of YAG formed at 1100°C and 1400°C, shown in Figure 5 4 At 1400°C, the nucleation of YAG is visible after 0-10 hours of heat treatment, whereas at the lower temperature of 1100°C, 20-50 hours of annealing is required for the detection of YAG Also, after 100 hours at 1400°C, approximately three times more YAG is formed than after the same time at 1100°C, i e 33wt % vs. 11wt % YAG, respectively This improved devitrification at the elevated heat treatment temperature was observed in almost all cases.

Successful crystallization of the glassy phase to YAG in sialons has been shown to occur at 1400°C Greil et al [62] found that with solid solutions compositions of z = 0 4-1.5, i e similar to the theoretical substitution levels in this study, crystallization was only observed below 1450°C which is close to the lowest liquid composition in this system[45,74], and with a maximum rate of devitrification at 1380°C Butler et al [54] relate the crystallization of YAG over $Y_2Si_2O_7$ to the level of polytype addition At low substitution levels, they found the major crystallization product to be the disilicate, together with a considerable amount of residual glass, while at high levels of polytype, the major crystallization phase was YAG, with a minimal amount of residual glass However, the study is vague in that there is no indication of the starting material composition nor the annealing conditions This relationship between the substitution level and YAG formation was not

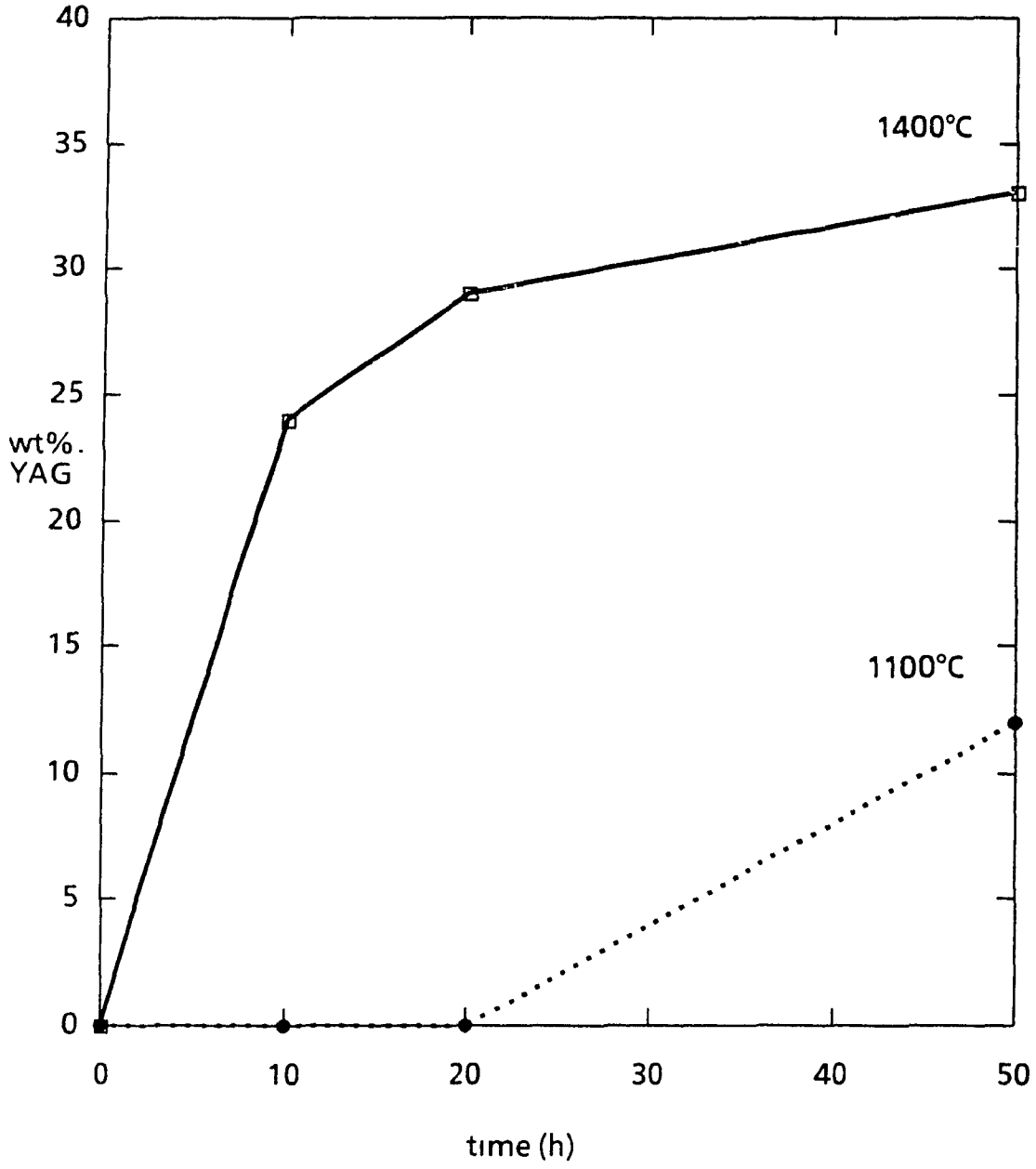

Figure 5.4. Effect of heat treatment temperature on the amount of YAG formed.

observed in this study. In fact, devitrification of the glass to YAG occurred at substitution levels from z = 0 up to 1.8.

5.3.2 Time

The length of heat treatment time determines the degree of grain growth of nucleated crystals within the glassy phase. As discussed in Section 2.5.1.1, the volume fraction of glass crystallized is related to time ($V \propto t^{\frac{1}{2}}$) The volume fraction of glass crystallized was generally found to increase with heat treatment, however, the time exponent, which in theorey should be 0.2', varied between 0.06 and 0.5, indicating fluctuations in the rate of crystallization.

Figures 5.5 to 5 7 show the effect of heat treatment time at 1400°C on the amount of YAG formed for Series I, II and III, respectively. Compositions within Series I show a stabilization in devitrification after 20-50 hours of heat treatment, whereas 50-100 hours are required for most of the compositions in the other two series. Therefore, it is assumed that the system has reached equilibrium in Series I in that no more glass will devitrify under these conditions Composition Ia shows some devitrification to YAG after 10 hours annealing, but no YAG formation after longer periods of time This can be attributed to sample variation as only one sample for each heat treatment time was used for analysis All compositions within Series II and some within Series III (c and d) do not show signs of having reached equilibrium after 100 hours as the plateau observed in Series I is non-existent, once again this may be due sample to sample variation, but is more likely because of a non-equilibrium state of the system

In summary, it can be concluded that the ideal heat treatment temperature for achieving (β + YAG) is 1400°C. The annealing time, however, is composition-dependent, ranging from 50 hours for Series I to

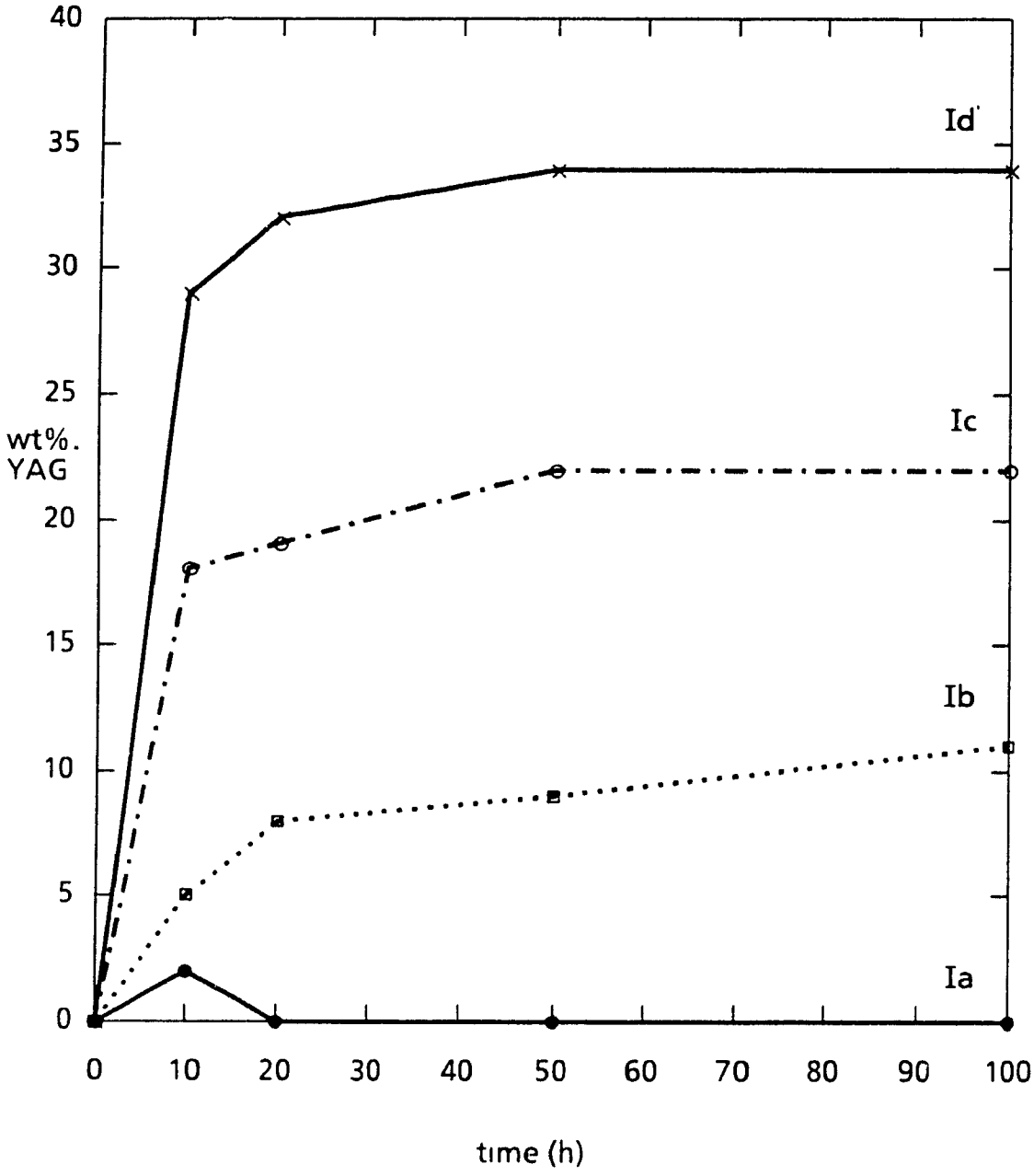

Figure 5.5 Effect of heat treatment time (1400°C) on the amount of YAG formed in Series I.

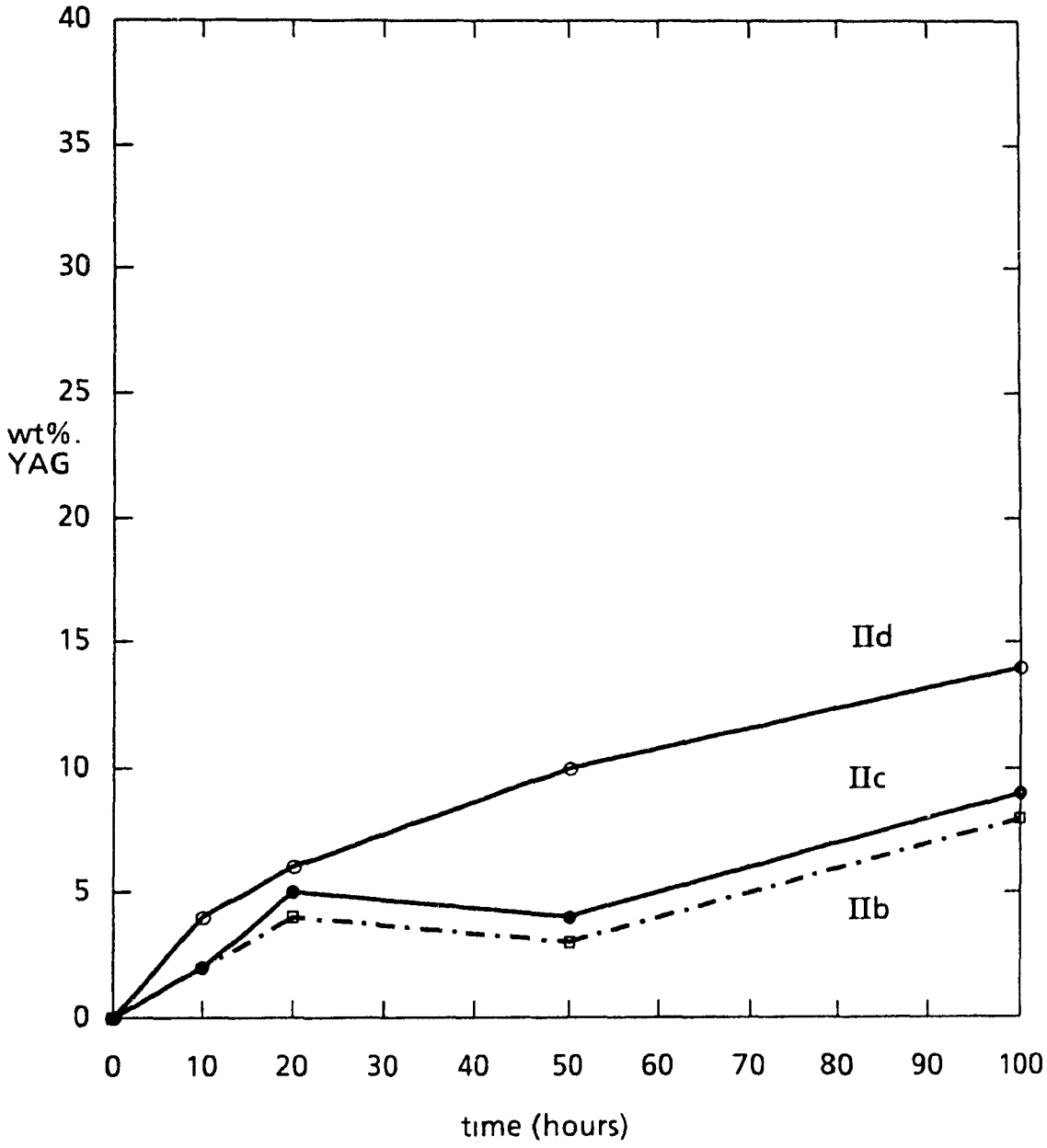

Figure 5.6. Effect of heat treatment time (1400°C) on the amount of YAG formed in Series II.

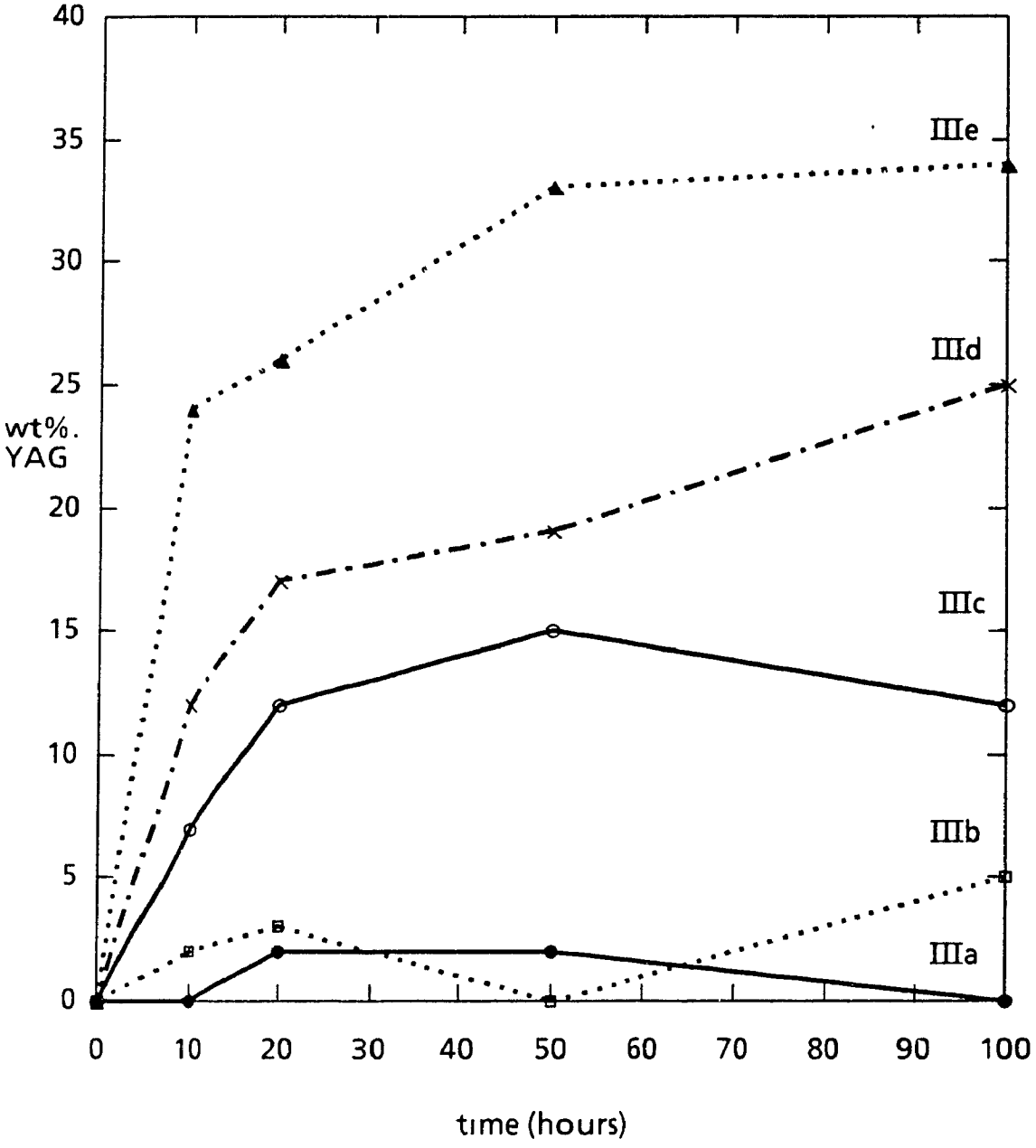

Figure 5.7 Effect of heat treatment time (1400°C) on the amount of YAG formed in Series III.

more than 100 hours for most of Series II and III. (these would require longer heat treatment times for the system to reach equilibrium). However, after 100 hours, all compositions within these two series contained mainly β and YAG, and no other crystalline phases were observed in significant amounts (i.e.<5%).

5.3.3 Z value

As discussed in Section 2.5.1.4, the devitrification of the Y-Sialon glass to YAG should result in a decrease in z value as excess Si and N from the glass diffuse back into the Si_3N_4 lattice, according to Equation 2.20. Lewis et al. [98] found that the major effect of heat treatment was a decrease in the overall substitution level due to this diffusion process. However, Hohnke and Tien [74] found a decrease in lattice parameters with annealing time and attributed it simply to compositional changes in the β phase.

The variation of the z value with heat treatment time is illustrated for two of the compositions in Figures 5.8 and 5.9. The extent of substitution varies extensively with annealing time Even after 100 hours of annealing, the z values do not correlate with the theoretical values based on compositions and assuming β' + YAG formation only This randomness in *z* value with heat treatment time was observed in all compositions Therefore, it can be concluded that the z value cannot be predicted based on the starting compositions of the samples since the effect of heat treatment on the extent of solid solution substitution is quite variable, with no visible trends observed. In addition, the Sialon system does not reach equilibrium, in some cases even after 100 hours of heat treatment.

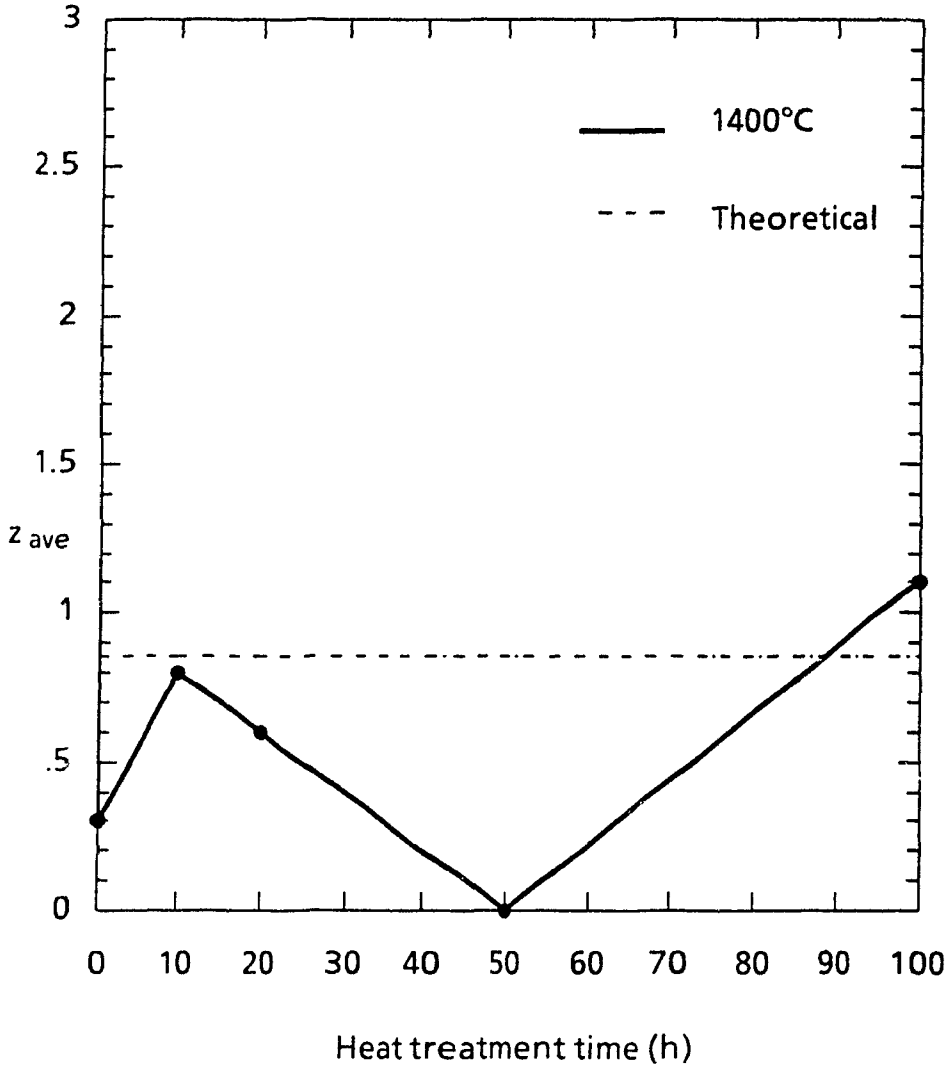

Figure 5 8 Average z value vs heat treatment time at 1400°C for IIc.

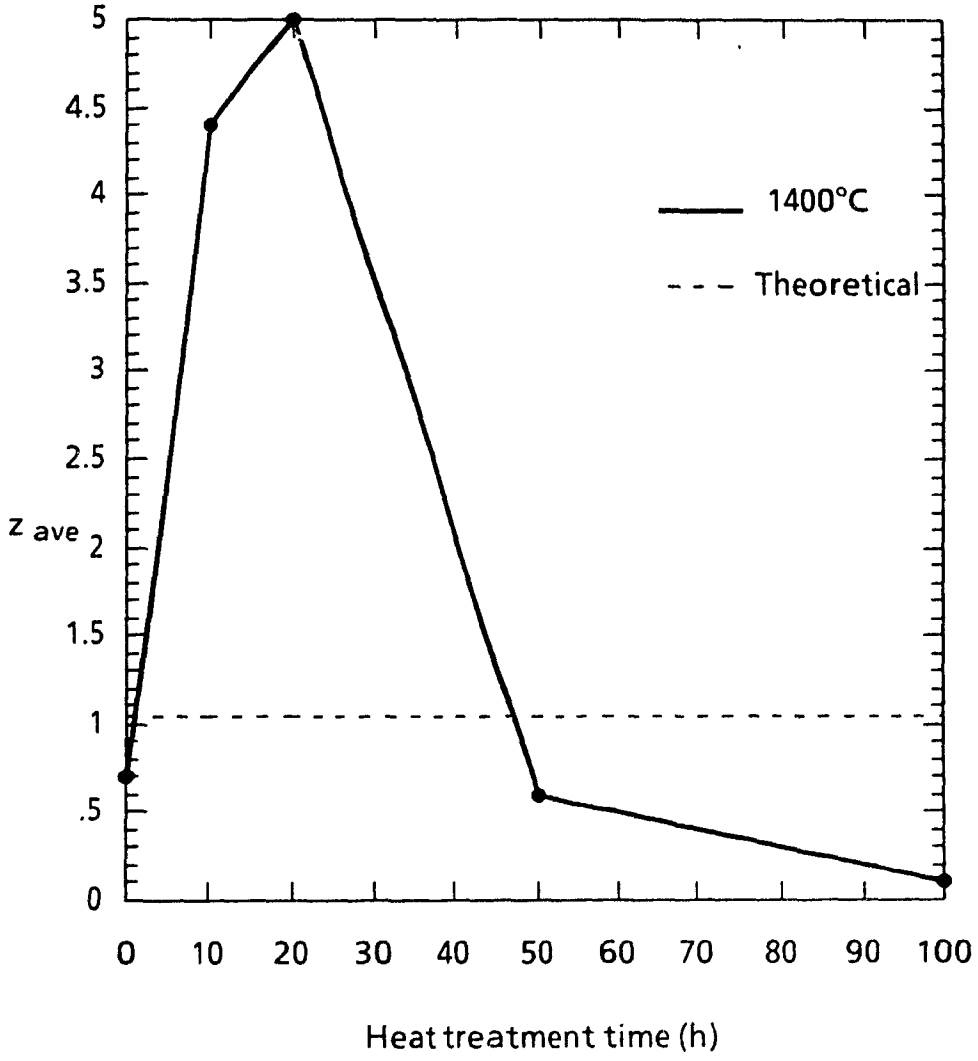

Figure 5.9. Average z value vs. heat treatment time at 1400°C for IIb.

It must also be emphasized that these z values were based on one sample per heat treatment time, thus some variation in z value was expected But despite this, the z values calculated were much below the theoretical values.

5 4 THE EFFECT OF ADDITIVE CONTENT ON DEVITRIFICATION

The extent of devitrification, or YAG formation, was evaluated in terms of the additive content of the compositions for samples heat treated at 1400°C for 100 hours Figure 5 10 illustrates this effect. Ia, the lowest additive content of Series I, showed no signs of devitrification, even after 100 hours of annealing. Conversely, Id, a high additive composition, underwent full devitrification after only 50 hours The order of increasing additive content within this series is Ia<Ib<Ic<Id. This ascending order is also reflected in the increasing extent of devitrification (wt.% YAG formed)in all three series

The effect of additive content on YAG formation was analyzed in terms of the amount of Y^{3+} and Al^{3+} present (shown in Figure 5 11) since these are the cations that are required in the formation of YAG ($Y_3Al_5O_{12}$) Three conclusions can be drawn from this graph·

1 the more abundant the Y^{3+} and Al^{3+} cations, the greater the amount of YAG formation IIb contains 21e/o of these cations and undergoes 34% devitrification, whereas IIe contains 34e/o Y^{3+} + Al^{3+}, and is almost fully devitrified (95%).

2 The formation of YAG is independent of the amount of liquid phase Series II, which has a constant liquid volume with increasing additive content, undergoes similar devitrification behaviour to Series I and II, which both had increasing liquid content with additive content.

3 Devitrification does not depend upon the z value (refer to Section 5.3). After heat treatment, no distinct trend was observed in z values

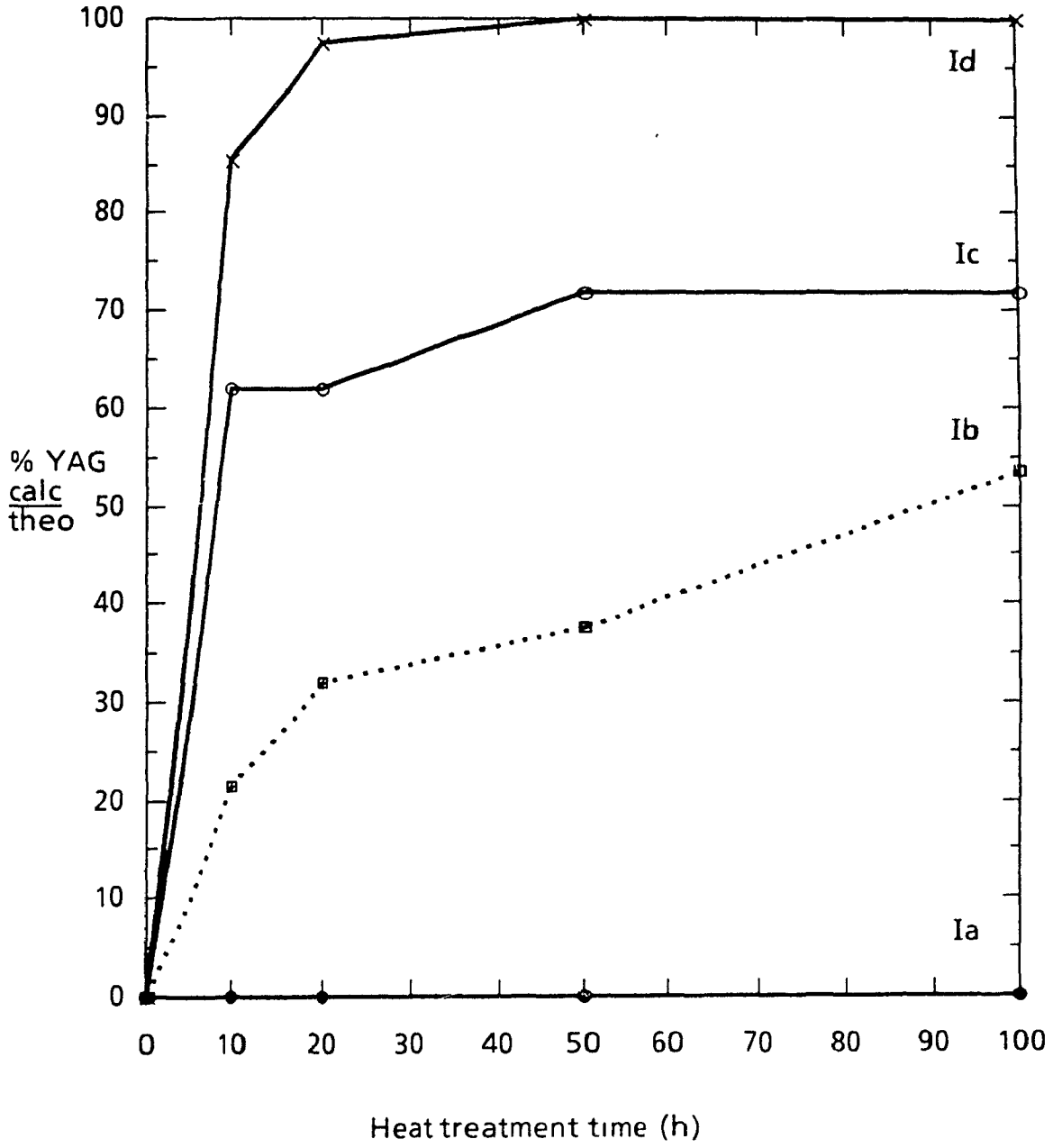

Figure 5.10. Effect of heat treatment time at 1400°C on the extent of devitrification of glass to YAG

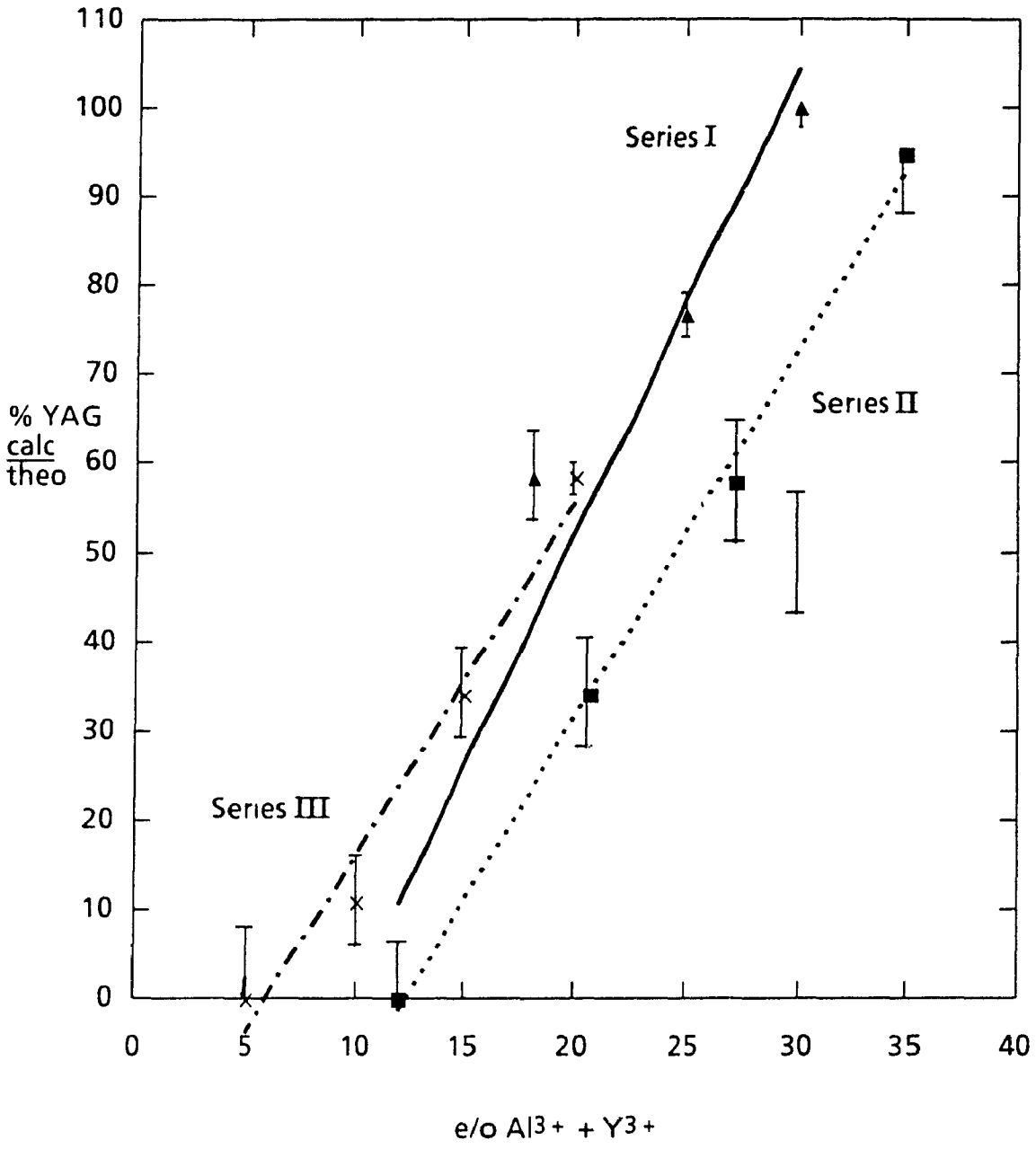

Figure 5.11. Effect of $Al^{3+} + Y^{3+}$ on devitrification of YAG at 1400°C for 100 hours.

Therefore, the z value cannot be related to the devitrification process since there is no correlation between the kinetics of crystallization and the extent of substitution (see Figures 5 8-5 10)

The third conclusion is in disagreement with some authors Greil et al [62] found that the total amount of crystallized glass was strongly dependent on the β'-solid solution composition They found that devitrification of the glass to YAG was accelerated by increasing the Al and O content of the solid solution composition Also, Butler et al. [54] related the crystallization of YAG with little residual glass to high substitution levels, but as mentioned earlier, the report is ambiguous in terms of heat treatment conditions There are no other reports available which study the effects of composition on devitrification to YAG Thus, a comparison of results is not feasible

5.5 GRAIN MORPHOLOGY

The microstructures of sintered compositions were studied by scanning electron microscopy Low additive content samples were found to have larger and more acicular grains than high additive content compositions which were more spherical in nature (Table 5 7) This is seen when comparing Ia (11w/o additives) with Id (32w/o additives) shown in Figures 5.12 and 5 13, respectively The grain structure of Ia is highly acicular in nature, with an average grain size of 0 7 μm, as opposed to Id which shows a more equiaxed and finer structure, with an average grain size of 0 3μm This difference in morphology can be explained primarily by the differences in sintering conditions Ia was sintered at 1800°C while Id was sintered at a lower temperature of 1600°C, both for 1 hour The higher sintering temperature allows for a decrease in the viscosity of the liquid and a higher diffusion rate for precipitation and grain growth of β-Si_3N_4 It would also

Composition	Sintering Temp. (°C)	Ave. Grain Size (μm)	Morphology
Ia	1800	0.7	5
Ib	1800	0.6	4
Ic	1600	0.3	2
Id	1600	0 3	2
IIa	1800	0 7	5
IIb	1800	0 5	5
IIc	1700	0 4	3
IId	1700	0 4	3
IIIa	1800	0.7	5
IIIb	1800	0 7	5
IIIc	1800	0 7	5
IIId	1700	0 5	2/3
IIIe	1700	0 5	2/3

Table 5 7. Particle morphology of sintered compositions 1 = equiaxed, 2 = equiaxed/acicular, 3 = acicular/equiaxed, 4 = acicular, 5 = highly acicular,

Figure 5.12. Microstructure of Ia, containing 11w/o additives.

Figure 5.13 Microstructure of Id, containing 32w/o additives

follow that the low additive compositions would have a higher strength than the high additive content compositions, as the morphology of the former is more desirable in terms of improved mechanical properties

The observed increase in grain size with sintering temperature is in agreement with Ekstrom et al. [92] who found that at low sintering temperatures (1600°C), the grain size was smaller and more equiaxed than at high sintering temperatures (1800°C), where the presence of larger elongated grains with high aspect ratios predominated Tani et al. [99] also observed an increase in grain size of hot pressed Si_3N_4 with increasing sintering temperatures: the grains grew to 5, 20 and 40 μm at 1600°C (2MPa), 1900°C (3MPa) and 2000°C (4MPa), respectively, but maintained the same aspect ratio of ~ 10

5 6 TRANSMISSION ELECTRON MICROSCOPY

In the previous sections, the effect of heat treatment on various compositions was studied on a macroscopic level; the phases present, the z value, and the extent of devitrification were obtained on bulk samples by x-ray diffraction However, detailed chemical information and microstructural characterization can only be obtained by transmission electron microscopy[100] In the present study, a combination of microscopy and analysis techniques (TEM, STEM, EDS and EELS) were used It must be emphasized here that electron microscopy involves the analysis of very small volumes of samples which may not always be representative of the bulk sample Also, EDS results obtained are at best semi-quantitative due to inherent errors in the technique (i e absorption, overlap) For a more in-depth analysis of errors see Reference 90 Thus electron microscopy

techniques used in this study were only to substantiate results obtained by bulk analysis of the samples

5 6.1 Analysis of the Devitrification Process

Three groups of samples (Table 5 8) were studied by TEM, based on the

Sample	Theoretical wt % YAG	Calculated wt % YAG (by XRD)	% Devitrified
Ia	14 3	0	0
IIIa	14 0	0	0
IIb	14 6	7	34
IIIb	25 6	2 3	11
Id	32 8	32 8	100

Table 5 8 TEM samples studied based on extent of devitrification

extent of devitrification that occurred after 100 hours at 1400°C, they were

(i) samples which showed no devitrification (Ia, IIIa)

(ii) samples which were partially crystallized (IIb, IIIb)

(iii) samples which were fully devitrified to YAG (Id)

As was seen in Section 5 4, the extent of devitrification was dependent upon the amount of additives present Low additive compositions showed poor devitrification while those with high additive content were fully devitrified. Therefore, high resolution electron (HREM) was used to determine the differences in sample composition and microstructural morphologies which result in different degrees of devitrification

Some authors [61,102] have postulated that devitrification of glass pockets is dependent upon the size of the pockets Falk and Dunlop [61] found that in samples heat treated in air at low temperatures, smaller glass pockets did not

either wollastonite and Y_2SiO_5 after 6 hours at 1100°C, or N-apatite and $Y_2Si_2O_7$ after 24 hours at 1200°C. At higher temperatures (1400°C), where the predominant crystallization phase was $Y_2Si_2O_7$, they found large volumes of glassy phases remaining in the sample, the presence of which they attributed to the formation of a liquid phase within the SiO_2-Y_2O_3-Al_2O_3 system during devitrification It must be emphasized that these heat treatments were done in an oxidizing environment rather than an inert atsmosphere as in the present study. This may account for the fact that no YAG was formed under any circumstances in air. Furthermore, no liquid phase formation was observed in this study during the devitrification of YAG. Also crystallization of the glass to YAG was not found to be dependent on pocket size Rather devitrification of glass pockets seemed to be more environment-dependent (see Section 5 6.1.2).

5 6.1 1 Poor Devitrification

Figures 5 14 shows the typical high resolution microstructure of a low additive sintered sample (IIIa) The hexagonal nature of the Si_3N_4 grains is very clear, also, there is quite a large range of grain sizes observed, from 0.7μm down to 0 1μm which may be either not fully developed precipitated β grains or more probably a sample thinning artifact These grains are also completely wetted by the Y-Si-Al-O-N glass phase, with pockets forming at the triple points The grain boundary phases are undoubtedly glass as their diffraction patterns are typical of an amorphous phase, with the diffuse rings (Figure 5 15) The size of the glass pockets is also variable

Neither IIIa nor Ia underwent any detectable devitrification Energy dispersive spectroscopy (EDS) of Ia as sintered material showed very high Si content in the glass pocket (Figure 5 16, Table 5 9). implying that these glasses, which are rich in SiO_2, and therefore would be harder to devitrify

Figure 5.14. Microstructure of IIIa, containing 5w/o additives.

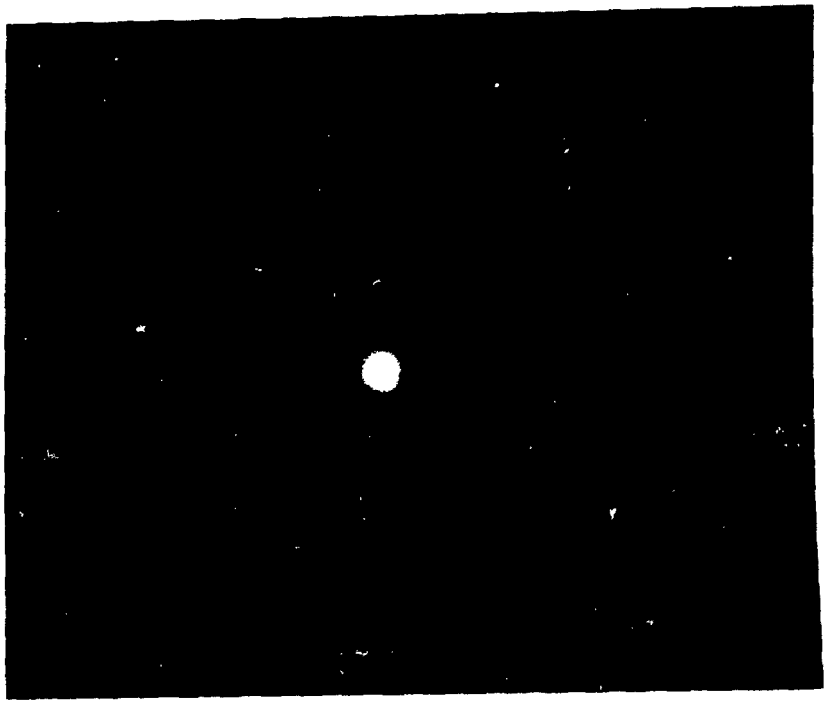

Figure 5 15 Selected area diffraction of glass pocket.

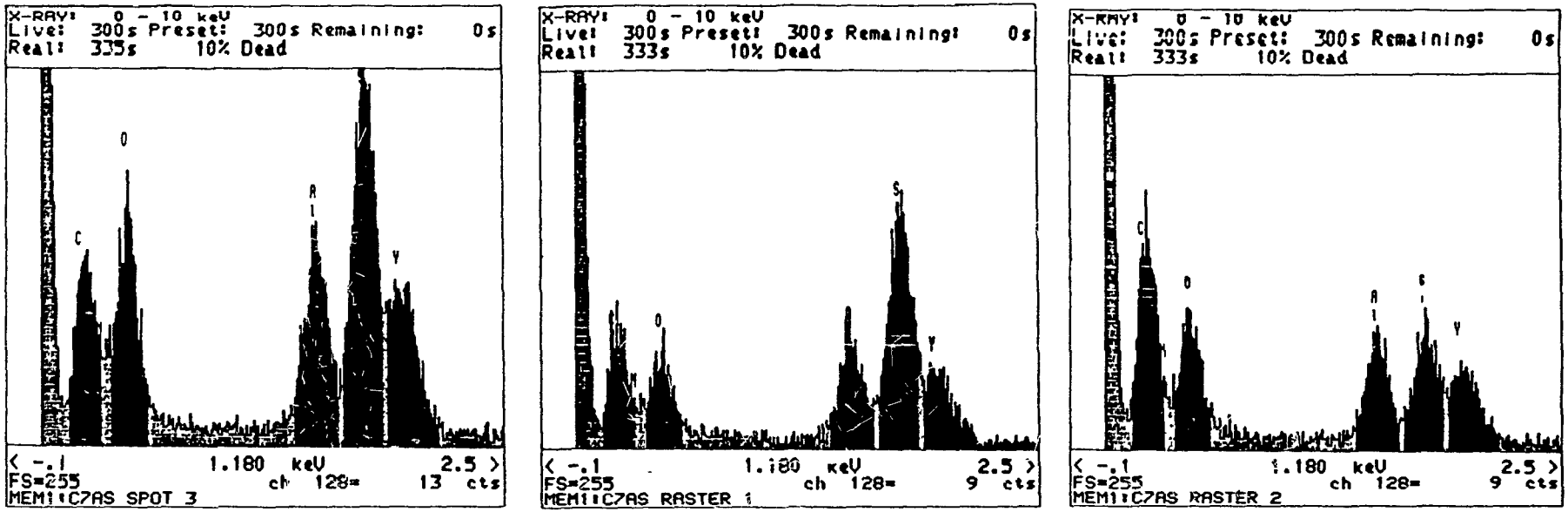

Figure 5.16. Energy dispersive spectra of as-sintered glass pockets (Ia).

	Equivalent %		
	Y^{3+}	Si^{4+}	Al^{3+}
IaAS	20 20 15	53 45 61	22 35 24
IaHT	17 21 22	62 46 50	21 33 28

Table 5.9. Equivalent % cations in Ia sintered (AS) and heat treated (HT) for 100 hours at 1400°C

The chemical composition of the heat treated glass pockets (Figure 5.17, Table 5.9) were comparable to the as sintered glass pockets, with compositional variation from pocket to pocket indicating that heat treatment had very little effect on the grain boundary phases. Once again, these were very high in silicon, and explain why crystallization was not attained.

Since the starting compositions were carefully controlled, this excess Si or SiO_2 detected by EDS must have been introduced during processing in the form of surface oxide on the powders. As the additive content of Ia and IIIa is very low (11 and 5wt.%, respectively), a few percent excess SiO_2 would have a far greater effect on the glass composition than in high additive content samples. This, therefore, explains the lack of devitrification in the low additive compositions.

The belief that pocket size has an effect on devitrification, as proposed by Raj and Lange[101] and Falk and Dunlop[35] was not observed here, since no crystalline pockets were found, irrespective of size. Therefore, the lack of devitrification in these low additive samples is primarily explained by the

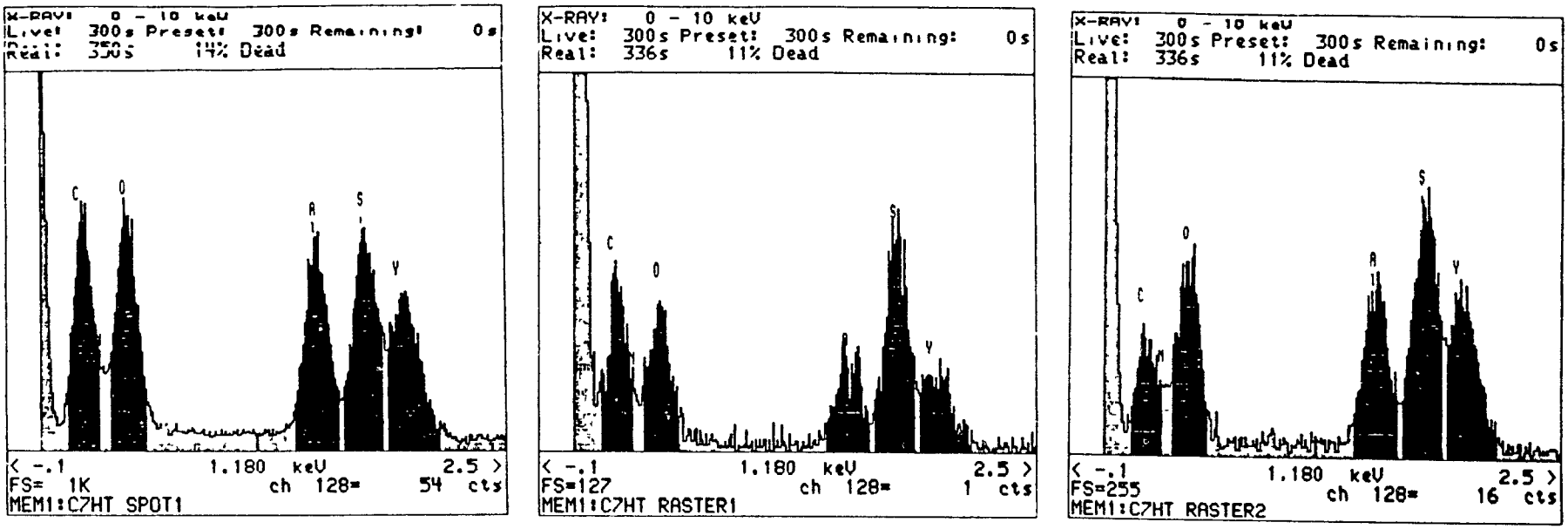

Figure 5.17. Energy dispersive spectra of heat treated (1400°C/100h) glass pockets (Ia).

crystalline pockets were found, irrespective of size Therefore, the lack of high Si content of the grain boundary phase stabilizing the glass with insufficient amounts of Y, Al and O being available to form YAG

The compositions of the glasses (Table 5 9), lie within the glass-forming region shown in Figure 5 18, and are far away from the desired YAG phase on the Y_2O_3-Al_2O_3 tie line. Therefore, devitrification of these glasses to YAG is not feasible

5.6.1.2 Partial Devitrification

Compositions which showed partial devitrification were studied to determine where crystallization occurred, i e whether YAG formation was dependent on Si_3N_4 grain size or the size of pocket or whether it was due to compositional variation within the sample

Figure 5 19 is a micrograph of a general area within a moderate additive content composition (IIb) which was annealed at 1400°C for 100 hours EDS of the pockets within the region was performed to determine whether or not the pocket was crystallized to YAG Crystallized regions are highlighted on the figure All pockets were found to be devitrified to YAG, therefore, crystallization was viewed as being independent of pocket size EDS was also performed on the area adjacent to the one illustrated in Figure 5 19, and is shown in Figure 5 20 Although some YAG pockets were found, glass was identified within most of the region Once again, the pockets which did not devitrify were of variable sizes.

It can therefore be concluded from this that devitrification of glass occurs in localized areas Compositional variation exists within regions of the sample, whereby crystallization of only certain pockets of the right chemical composition will occur One explanation to account for this compositional variation within the sample is inhomogeneous mixing of the starting

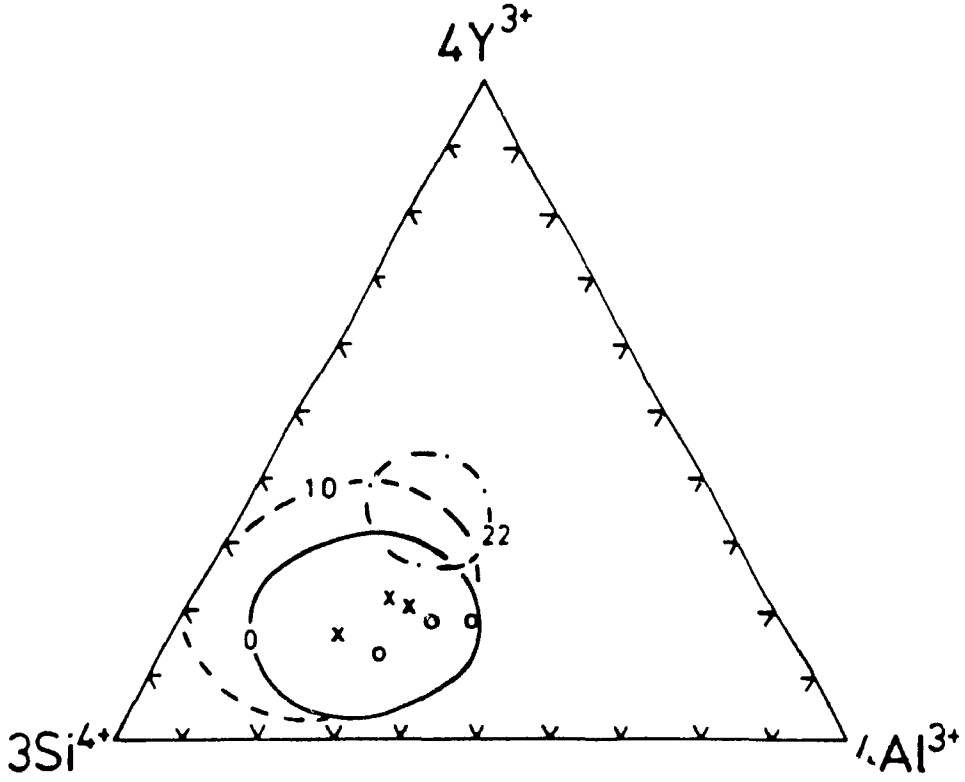

Figure 5.18. Glass compositions determined by EDS of as-sintered (o) and heat treated (x) compositions.

Figure 5 19 Microstructure of IIb showing crystallized YAG pockets

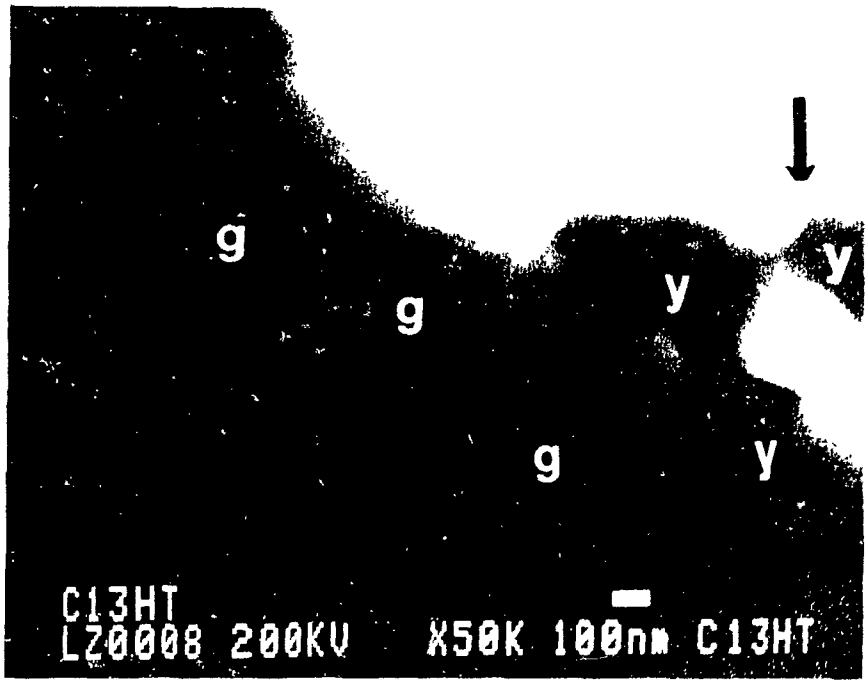

Figure 5 20 Microstructure of IIb showing crystallized YAG pockets

materials This could result in glass pockets which are richer in Si and hence harder to devitrify than those with low Si content. In the heat treated samples, the glass pockets which did not devitrify to YAG were generally found to be quite high in Si, with the amount of Y and Al being quite variable The influence of glass composition on the ease of crystallization was also observed by Lewis et al [99], who found that silicate liquid of high viscosities, i e high Si, as in this study have high viscosities at temperatures below the the equilibrium liquidus for the garnet phase and require prolonged heat treatment for crystallization

Another finding which supports the belief of compositional variation of the liquid phase is that the Al/O content within the Si_3N_4 lattice varied from grain to grain, as seen in the EDS results in Table 5 10 In the two β grains

	Al Si	z value
β-Si_3N_4	1 1 5	2 4
β-Si_3N_4	1 3 6	1 3

Table 5 10. Variation in z value with β grains.

analyzed, the z value varied from 1 3 to 2 4 This would suggest that the liquid surrounding the β grains was not homogeneous, being richer in Al and O in some regions, and therefore more available for substitution On the other hand, sintered glass regions which are Al and O rich would be more favored to form YAG on annealing This variation in liquid composition is possibly due to the similar particle sizes of the starting material, which after mixing, could concentrate in areas so as to produce pockets or areas which are rich in Al (and others rich in Y) The large availability of Al would

therefore result in a greater substitution within surrounding β' grains Conversely, liquid areas which are rich in Y, for example, would tend to result in low substitution of Al into neighbouring β' grains

Compositional inhomogeneity of β grains was also observed by Bonnell et al. [103] They found that the Al content of small β grains was lower than that of the large grains and attributed this variation to differences in equilibrium rates of the grains That is, the smaller grains, with a higher surface-to-volume ratio, equilibrate faster than the larger grains as the samples cool Also, the initial glass composition, which is Al rich, will be compatible with a highly substituted silicon nitride As Al continues to be absorbed into the Si_3N_4, the glass becomes less rich in Al and will be in local equilibrium with Si_3N_4 at a lower Al content The authors assumed that the largest grains were the first to nucleate, and therefore had the highest Al content

It is generally believed [65] that YAG forms as a single crystal around the Si_3N_4 grains Greil et al [62] reported that after crystallization, single YAG regions could be detected at triple points They determined that during the devitrification stage, only a few YAG nuclei grow, resulting in large single phase regions of YAG having the same orientation, such that the triple points were all interconnected Lewis et al [99] also found that over very large electron-transparent areas (10-30 β grain diameters) the garnet phase had a constant crystallographic orientation Thus, few nuclei form within the large volume of material, these nuclei are believed to be internal microcavities rather than β'-glass interfaces which result from a compositional influence

The formation of single garnet crystals in large areas of sample was also observed in this study Figure 5 21 shows the general area of β + YAG, selected area diffraction (SAD) of the devitrified regions shown in Figure

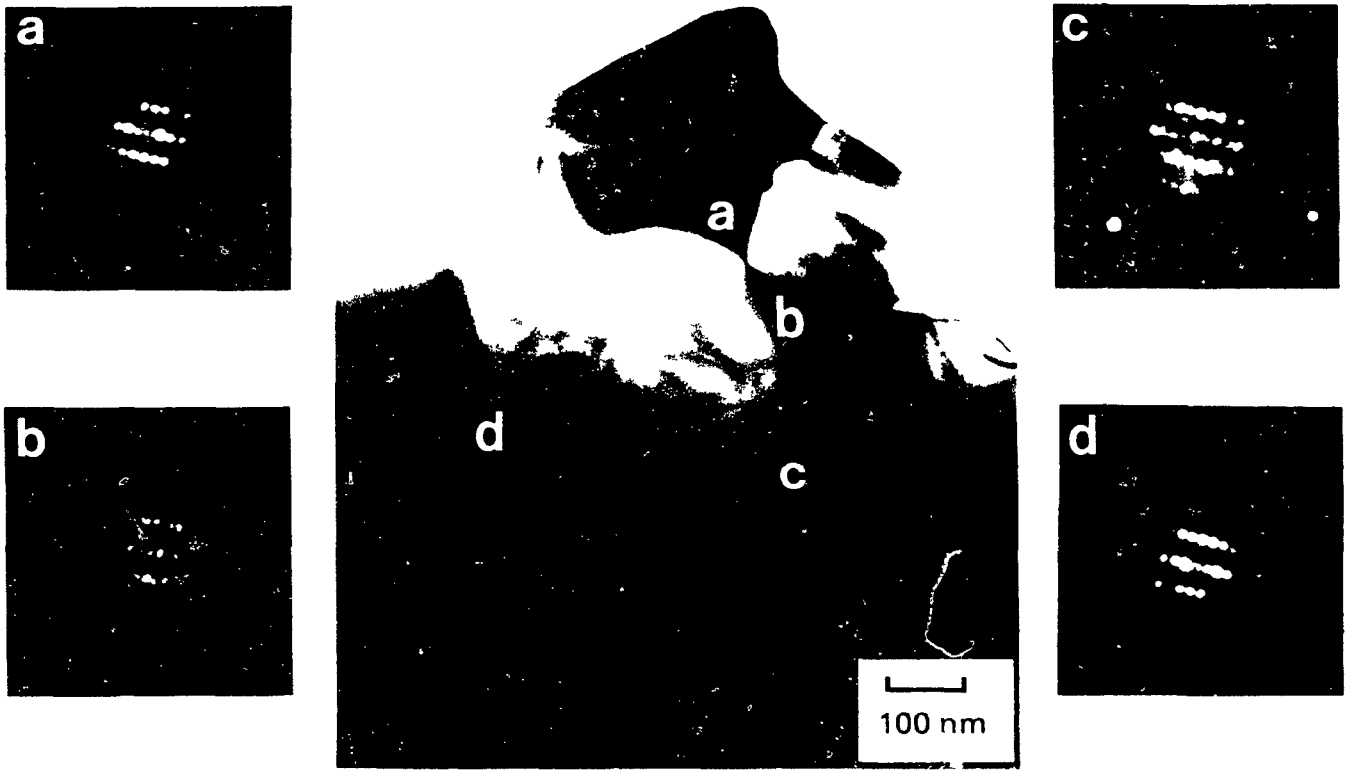

Figure 5.21. Crystallized YAG pockets around β grain, showing single crystal formation: (a)-(d) selected area diffraction of YAG pockets showing same orientation.

5.21(b-d) show the pockets to be of the same orientation, and that the YAG forms as a single crystal around the β grain

5.6.1 3 Fully Devitrified Samples

Compositions which showed full devitrification as verified by x-ray diffraction were also studied by HREM (Id, IId) It is generally accepted (Falk & Dunlop)[61] that an amorphous phase always remains along the grain boundary interfaces of grains This was also observed in the present study where even in fully devitrified samples, an amorphous grain boundary phase was always present, as seen in Figure 5 22, (the glass band is highlighted by white arrows) HREM of two adjacent Si_3N_4 grains show that the lattice fringes almost go up to the edges of the grain but are separated by an amorphous band 1-2 nm thick

Petzow and Greil [104] reported that grain boundaries and morphologies were dependent on the amount of liquid phase present The grain boundaries of compositions which had a large liquid volume were straight, whereas in low liquid content structures, the grain boundaries were typically curved and overlapping This was not seen in the samples studied here Little difference in grain boundary characteristics is observed between IIa (Figure 5 23) which contains 11w/o additives, and IId (Figure 5 24), with 32w/o additives

Devitrification of the Y-Sialon glass to YAG was found to be primarily dependent on composition In samples which showed no devitrification to YAG, the glasses were found to be extremely high in Si (a glass-stabilizer), believed to have been introduced during powder processing In partially devitrified samples, crystallization of the glass was composition-dependent in that crystallization of YAG occurred in distinct areas, and was independent

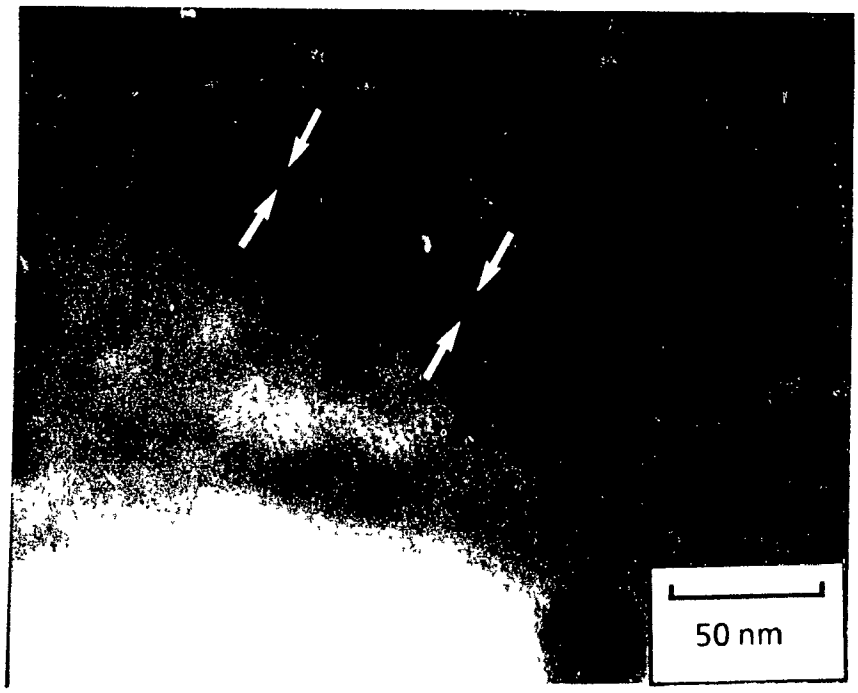

Figure 5 22 HREM of β-β interface separated by a thin amorphous band.

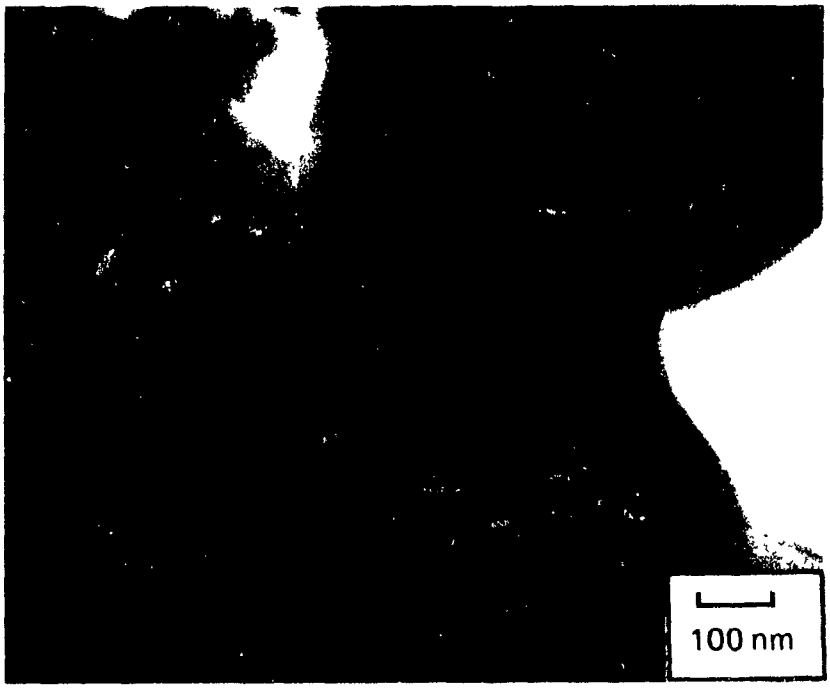

Figure 5.23. Low additive composition showing straight grain boundary edges.

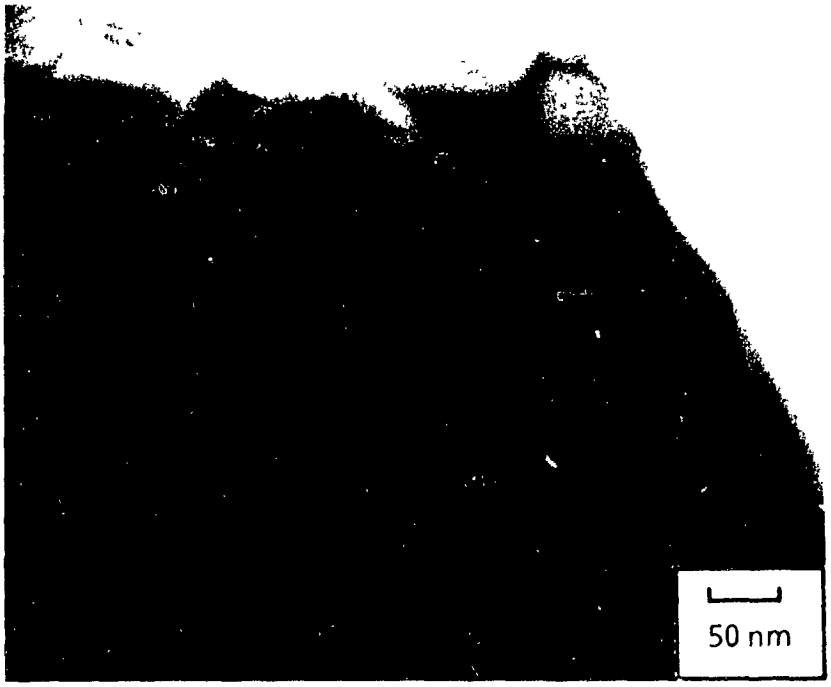

Figure 5 24 High additive composition showing straight grain boundary edges

of pocket size In fully devitrified samples, an amorphous grain boundary phase always remained between the β-β and β-YAG interfaces.

5.6 2 EELS Analysis

As discussed in Section 5 1 3, some authors believe that heat treatment of sialons results in the diffusion of Si and N from the glass back into the Si_3N_4 grains EELS analysis of two as-sintered and heat treated samples 1400°C/100h (IIa and IIb) unequivocally show the presence of N in the glass phase after annealing (Figures 5.25 and 5.26) Both compositions contained substantial amount of nitrogen with respect to oxygen, upon heat treatment (Table 5 11) Although it was not possible to establish the atomic ratios of all

	AS SINTERED		HEAT TREATED	
	O (e/o)	N (e/o)	O (e/o)	N (e/o)
IIa	97	3	36	64
IIb	46	54	46	54

Table 5 11 Anion ratios in as sintered and heat treated samples

the elements, the anion ratios (N·O) in Table 5 11 do show up to 64e/o N in one of the samples. It can be said that heat treatment does not allow for the total diffusion of Si and N back into the Si_3N_4 lattice, leaving a glass containing only Y, Al and O Nitrogen does exist in the glass phase after sintering, as was observed by other authors in bulk glasses [68-72] During liquid phase sintering, the Si and N from α-Si_3N_4 dissolve in the liquid phase and reprecipitate as β-Si_3N_4, thus, the presence of residual N in the glass is not unusual

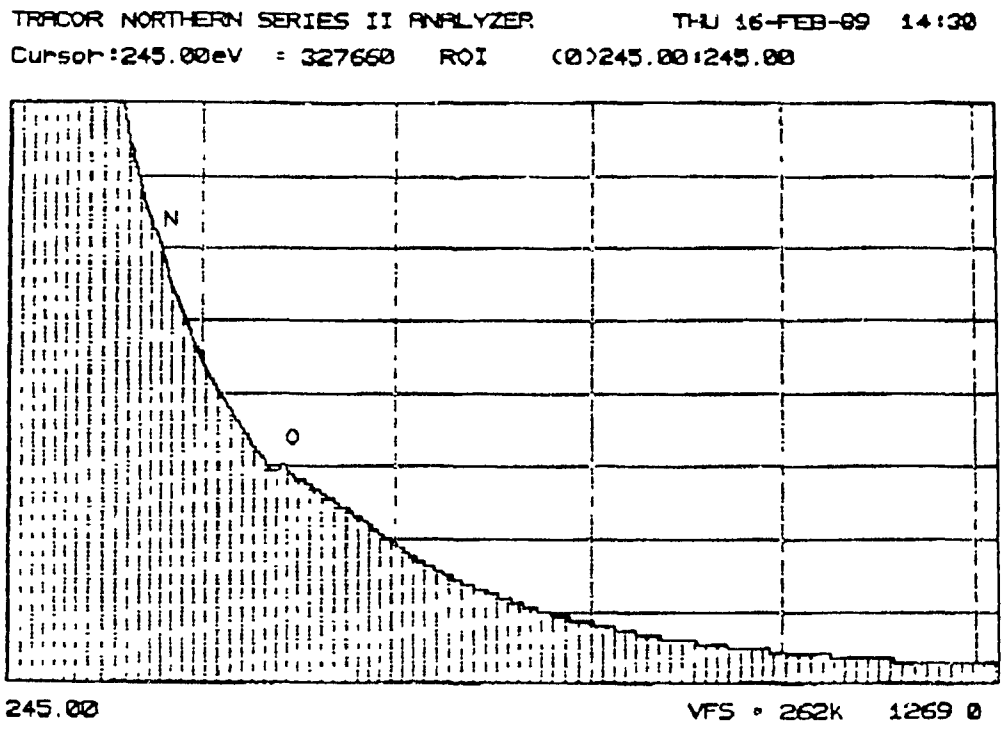

Figure 5.25 EELS of as-sintered Ib, showing the presence of nitrogen.

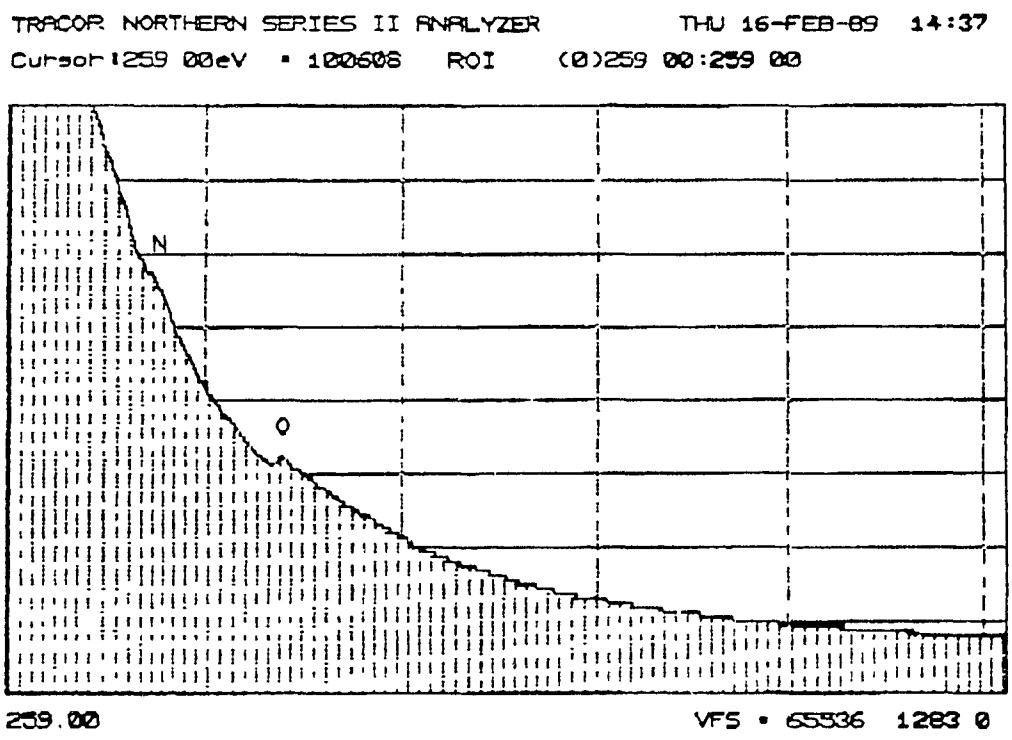

Figure 5.26 EELS of heat-treated Ib, showing the presence of nitrogen.

5 7 MECHANICAL PROPERTIES

As reviewed in Chapter 2, the grain structure of a material greatly influences its mechanical properties In general, a more acicular grain structure is desired over an equiaxed morphology as crack propagation is more difficult in the former More importantly, the room temperature strength depends on the volume and nature of the grain boundary phase If the grain boundary phase is a glass, then the strength will be primarily dependent on the volume fraction of glass present On the other hand, crystallization of the grain boundary phases will result in a lowering of the room temperature strength, but improved high temperature creep resistance

Room temperature strengths of all sintered compositions are listed in Table 5 12 The results (Figure 5 27-5 29) show a general decrease in strength with increasing additive content Composition Ia, which contained ~11wt % addtives, had the highest strength (602MPa) IIIb, with a similar amount of additives (~13wt %) had a comparable strength of 596MPa The lowest additive composition, IIIb (~5wt.%) had a lower strength than Ia and IIIb This decrease can be explained by the fact that this composition only achieved a relative density of 92 5%, compared with 96 5 and 97 8% for Ia and IIIb, respectively Thus, residual pores within the microstructure of IIIa act as critical defects and lower the strength of the material. Pugh et al [81] classified residual pores as (a) agglomerates causing differential shrinkage, (b) pores resulting from burn-out, and (c) density inhomegeneities leading to poor sintering

The general decrease in strength with additive content is attributed to the larger volume fraction of glass present As discussed in Section 2 6, the glass is weaker than the parent β-Si_3N_4, and its volume will in turn affect the

Sample	σ (MPa)
Ia	602
Ib	565
Ic	536
Id	453
IIb	545
IIc	483
IId	498
IIIa	488
IIIb	596
IIIc	633
IIId	555
IIIe	365

Table 5.12. Average room temperature strength of as-sintered compositions

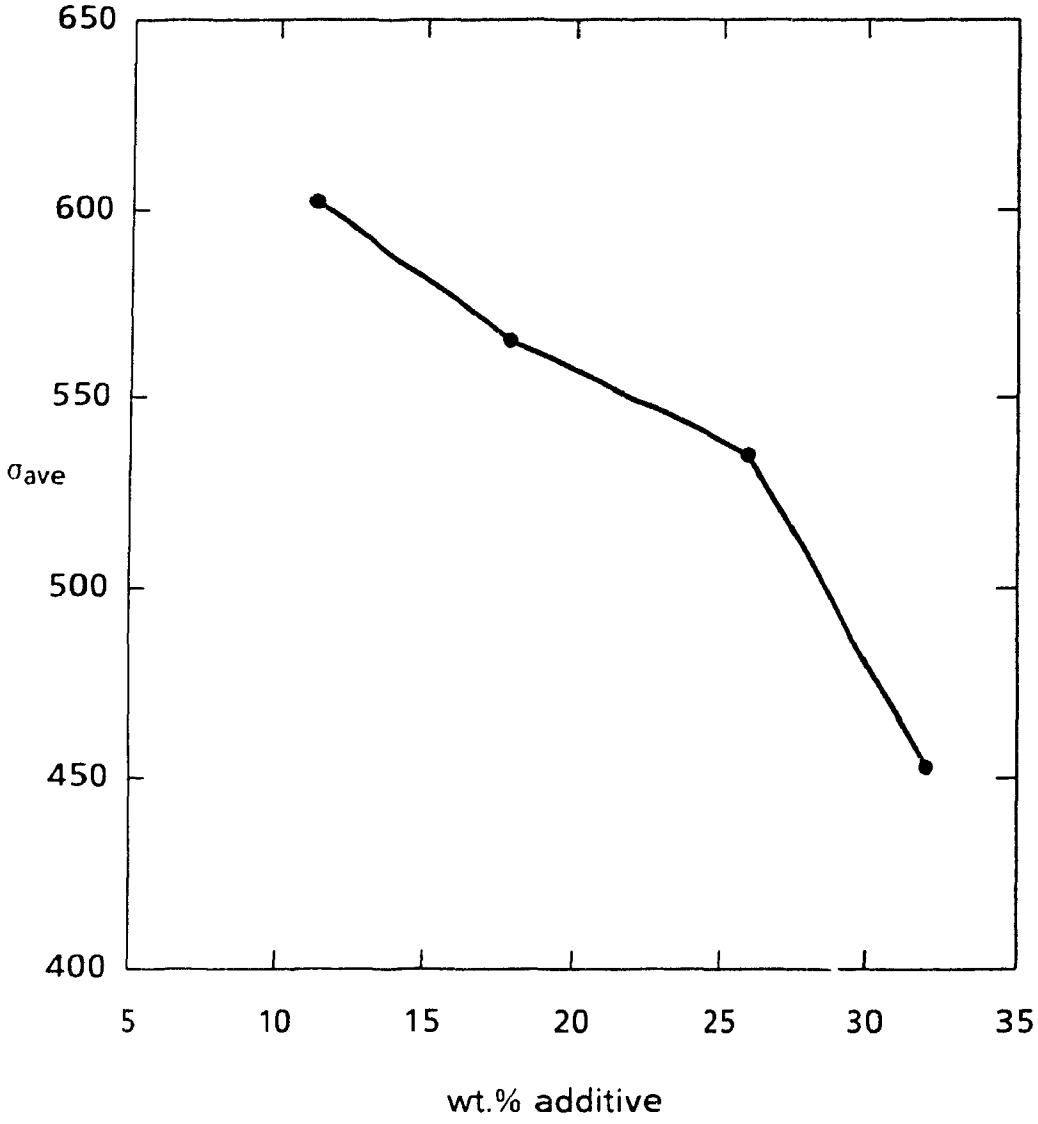

Figure 5 27 Effect of additive content on room temperature strength for Series I.

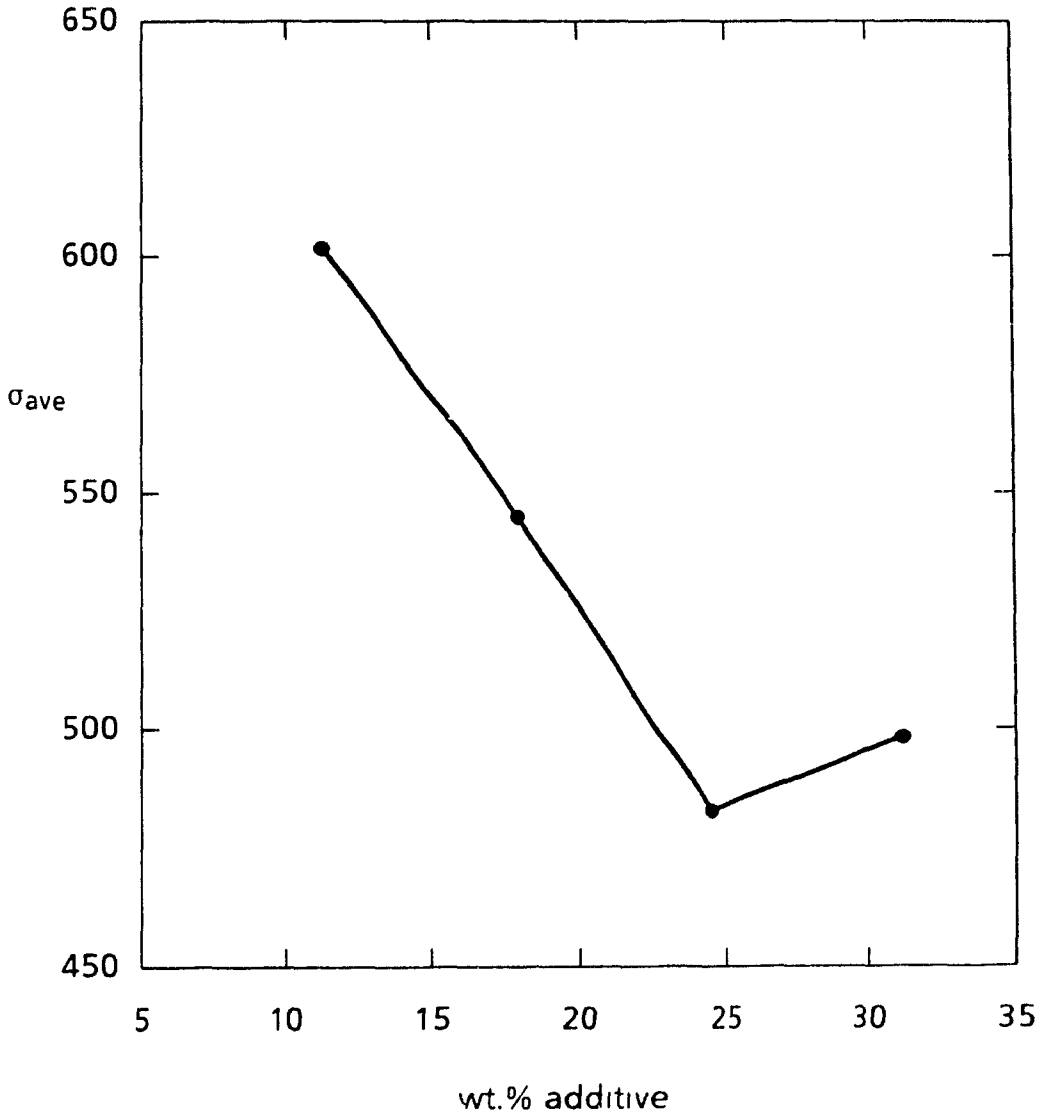

Figure 5.28 Effect of additive content on room temperature strength for Series II.

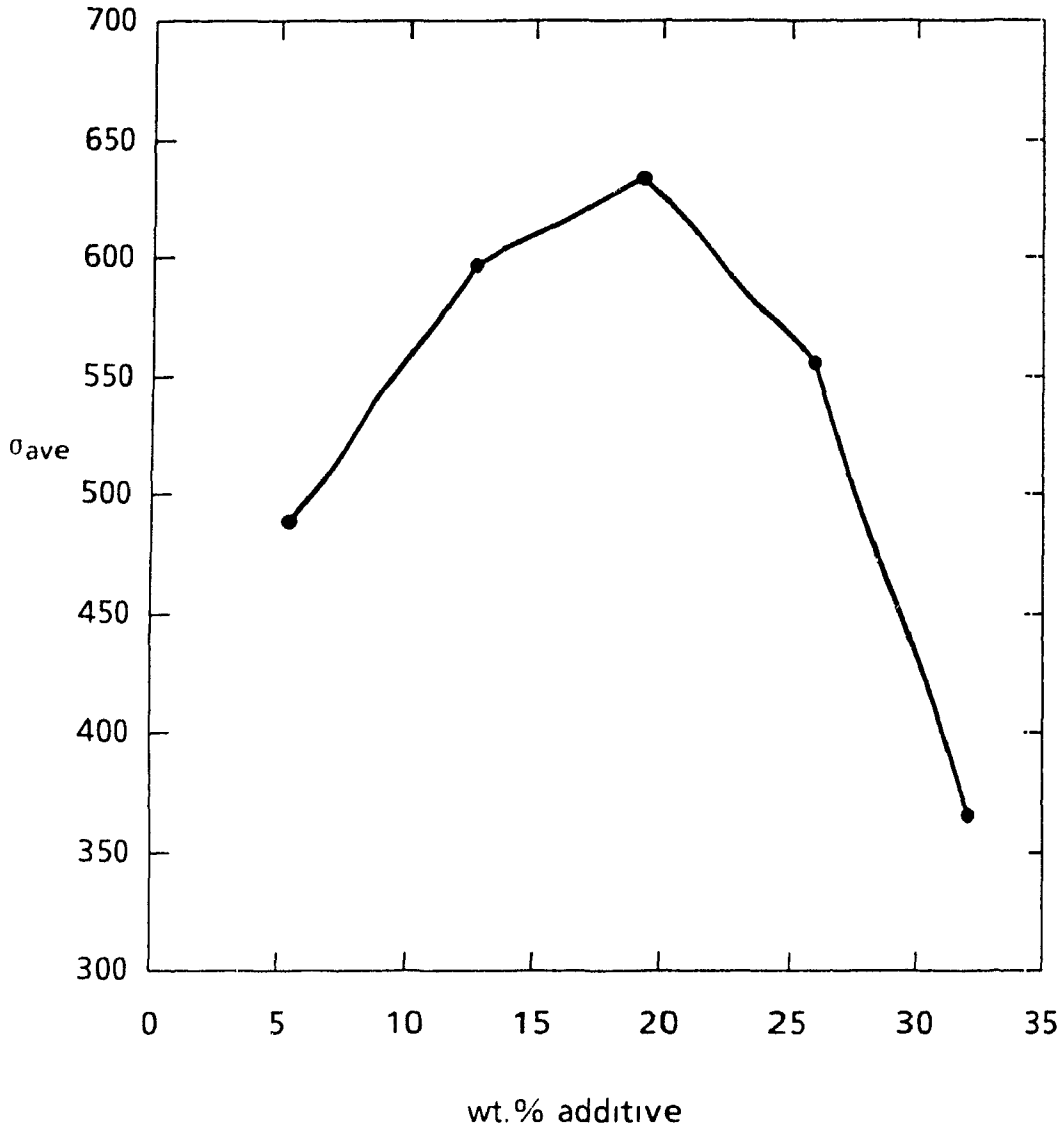

Figure 5.29 Effect of additive content on room temperature strength for Series III

resulting strength of the material. This decrease in strength with glass content was also observed by Das and Mukerji [80] who showed a similar deterioration in strength with glass content.

Figure 5.30 shows the strength differences between as sintered and heat treated samples. It is clear that heat treatment has a deleterious effect on strength for all compositions studied. The percent decrease in strength generally increases with additive content. Ia (11wt %) showed a 5% decrease, while the strengths of IIb (18wt %) and IIc (25wt %) decreased by ~65%, and IId (32wt.%) a 40% reduction. As all the compositions within this series had an equal theoretical amount of YAG (14.6wt %), this difference in strength reduction is associated with the amount of YAG crystallized. IIIb, of similar additive content to Ia, showed a similar reduction of strength upon heat treatment. The strength decreased from 596 MPa to 515 MPa (a 10% decrease), with no devitrification of the glass observed.

Figure 5.31 shows the effect of devitrification (or YAG content) on strength. Ia showed the highest strength in the series of heat treated samples; no YAG was detected (0% devitrification) in the compositions with heat treatment, thus the grain boundary phase remained a glass, and did not greatly affect the strength (only a 5% reduction in strength with annealing was observed). A significant decrease in strength was observed in IIb, which was 34% devitrified: the strength dropped from 573 MPa (as sintered) to 158 MPa. Thus this dramatic decrease in strength with heat treatment is linked to the crystallization of some glass pockets to YAG. IIc and IId showed similar decreases in strength with heat treatment, however, a slight increase in strength with increasing devitrification was observed. IIb, which contained 34% YAG had a strength of 158MPa, The strengths of IIc (54% devitrified) and IId (95% devitrified)were 178 MPa and 242 MPa, respectively. This slight

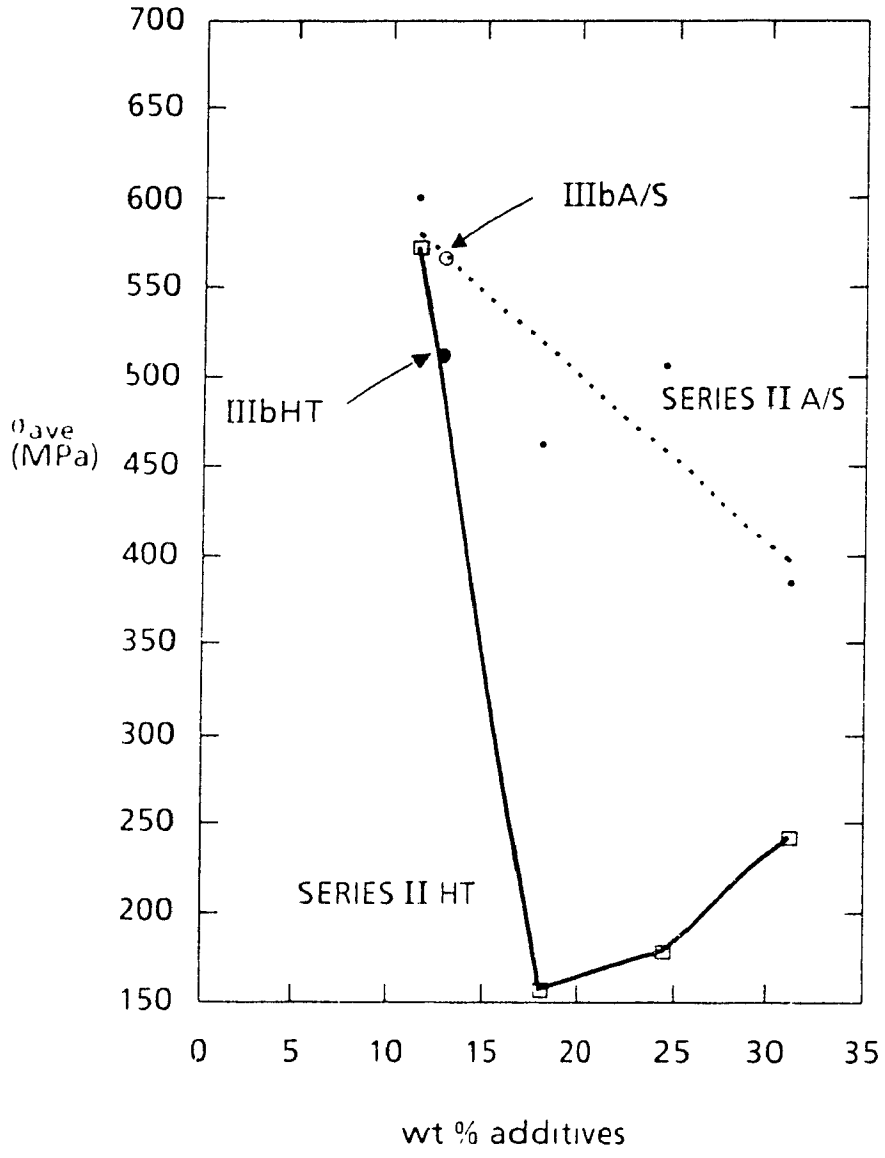

Figure 5 30 Effect of heat treatment on average room temperature strength of compositions in Series II
A/S - as sintered; HT heat treated 1400°C, 100 hours.

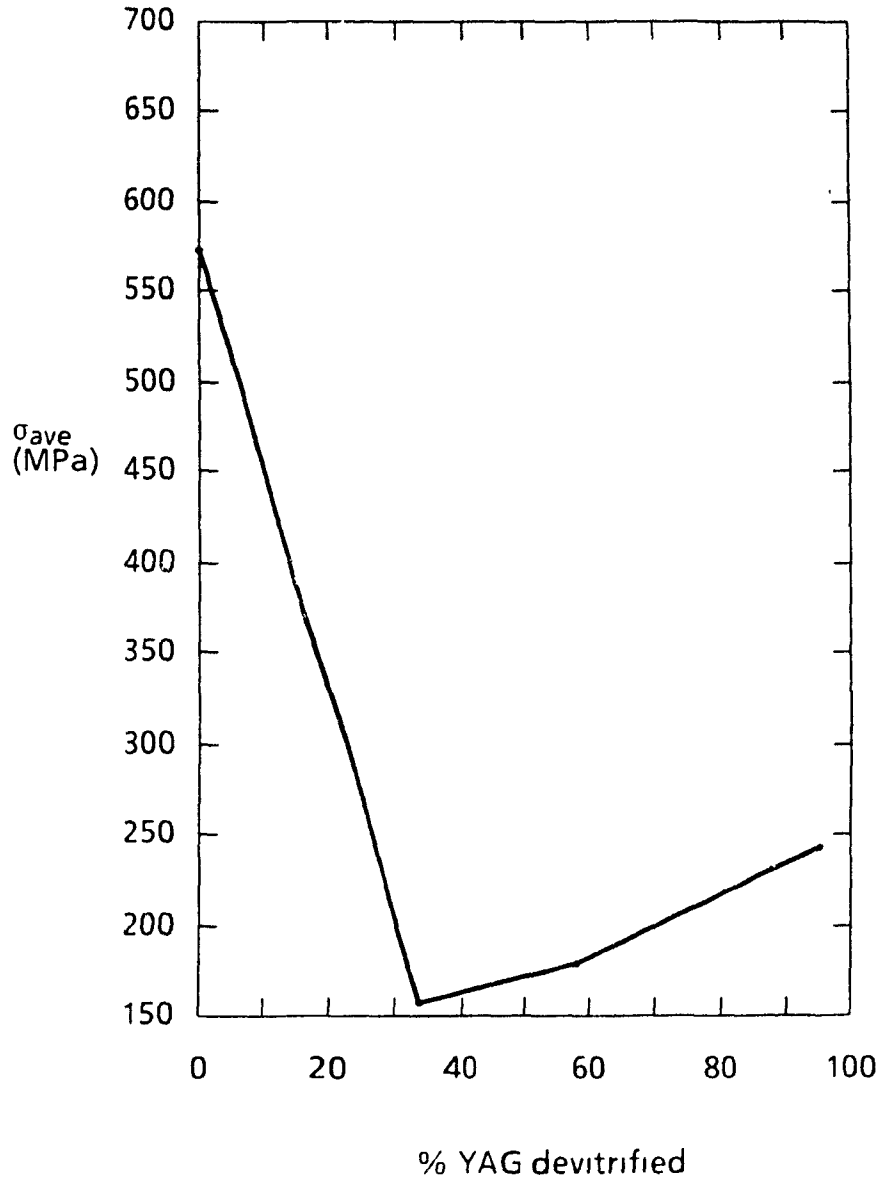

Figure 5.31. Effect of devitrification on average room temperature strength of Series II

increase in strength with devitrification cannot necessarily be associated with YAG formation Rather, it is most probably due to the more refined grain structure observed with the higher additive compositions As discussed in Section 5 6, the grain size was found to decrease with increasing additive content, due to the lower sintering temperatures used Thus, IIb had an average grain size of 0 5μm,while IIc and d a grain size of 0 4μm

The significant drop in strength with the formation of YAG is associated with property changes which occur during devitrification of the YSialon glass As discussed in Section 2 5 1 3, crystallization of a glass is most often accompanied by significant changes in the thermal expansion coefficients and densities Greil et al [62] found that residual stresses induced by the difference in thermal expansion of β-Sialon (3 3 x 10^{-6}°C^{-1}) and YAG (8 2 x 10^{-6}°C^{-1}) result in stresses at the YAG-β' interface that are not totally relieved as is the case of the partially crystallized material Lee et al [105] stated that the volume change associated with crystallization (between the glass and the crystalline phase) imposes a strain on the Si_3N_4 grains, deforming them and causing dislocations to form In their work, they found that extending the heat treatments tended to reduce the dislocation densities brought about by the crystallization due to the density difference of $Y_2Si_2O_7$, probably through annealing No regions of high dislocation densities were observed in the heat treated samples, nor were they expected, since the samples under study were too thick to make such observations, areas where these are typically seen must be extremely thin However, the formation of YAG is thought to result in the formation of micropores brought on by the differences in thermal expansion coefficients between the β grains and the YAG

Bonnell et al [65] attributed strength reduction upon crystallization to high residual stresses developed due to thermal expansion mismatch between Si_3N_4 and the garnet phase They proposed that cracks could develop in regions of concentrated tensile stress, causing the observed decreases in strength and toughness However, they were unable to distinguish between the contribution to this by the morphology of the grains and residual stresses imposed by the associated volume change upon crystallization

Hayashi et al [52] observed a similar decrease in strength upon devitrification of the glassy phase, and attributed this degradation to changes of specific volume of the grain boundary phases and the difference of thermal expansion coefficients between Si_3N_4 and crystallized phases They found strength decreases of ~19% with devitrification primarily to melilite and a 23% reduction when the major devitrification phase was $YSiO_2N$.

As discussed in Section 2 5 1, the devitrification of glass is also accompanied by a difference in density between the crystalline phase and the parent glass The density of YAG (4 55g cm^{-3}) is significantly higher than that of the YSialon glass (~3 9g cm^{-3}), thus its formation is accompanied by a substantial volume change (17%) It is postulated here that as the YAG is crystallized, the shrinkage associated with its formation is so great that the YAG crystals formed are no longer bonded to the parent Si_3N_4 grains Rather, the crystals sit at the triple points, being supported by surrounding β grains (Figure 5 32) As the volume shrinkage associated with the formation of YAG from the glass is so great, it is hardly surprising that the YAG becomes detached from its neighbouring Si_3N_4 grains

Few YAG crystals were identified in the thin section of the TEM samples The majority of them were found nestled in among β grains, as in Figure

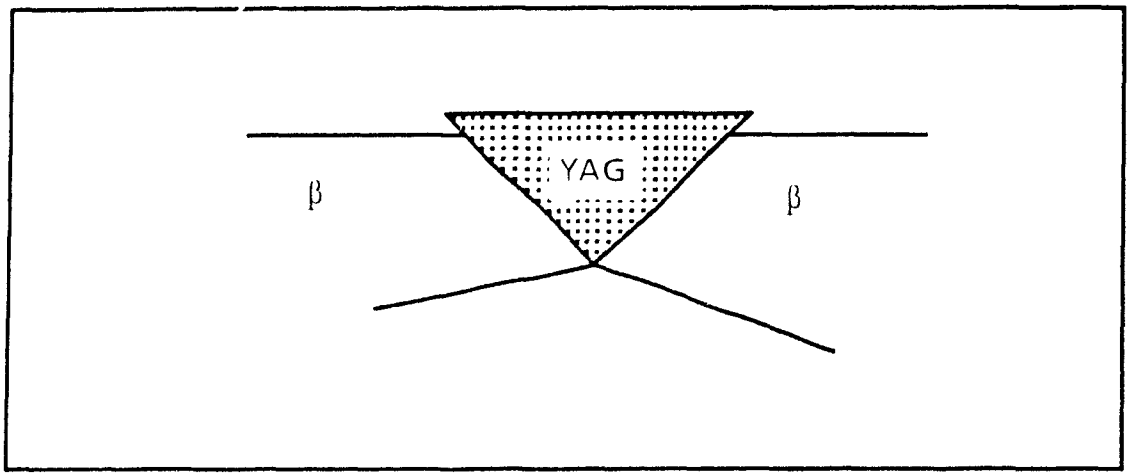

Figure 5 32 Schematic of YAG pocket supported by β grains

5 33(a) Since the YAG crystals are thought to be supported by surrounding β grains, overlap of the YAG over the β grain should exist Figure 5 33(b) shows the lattice fringes of YAG overlapping the β grain to the right of it This lattice fringe overlap was identified in numerous triple points

5 7 1 Micropore Coalescence

As discussed above, it was found that upon devitrification of the glassy phase, the YAG crystals formed become detached from the β matrix It is suggested that micropores are formed within the grain boundary phase due to the specific volume change associated with the crystallization of YAG from the glass These pores, in turn, will act as flaws which weaken the grain boundary phase such that under an applied stress, the pores will coalesce and act as a path for crack propagation A similar effect is observed in ductile metals, and is called microvoid coalescence [106] Thus, the overall effect of this micropore coalescence is a deterioration in the room temperature strength of the silicon nitride, as was observed in this study devitrification of the glass lead to a decrease in strength of up to 40%

(a)

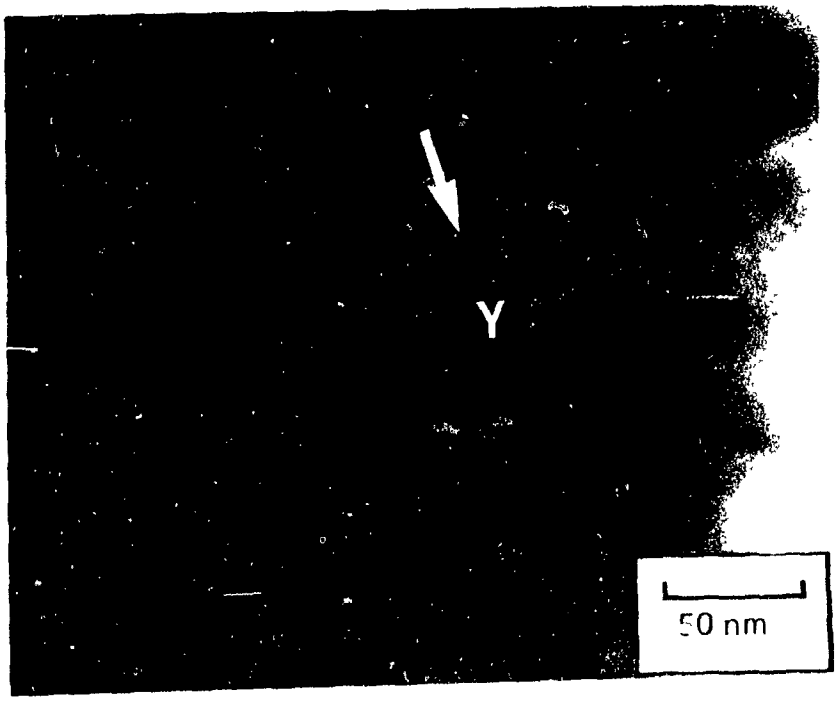

(b)

Figure 5.33. (a) general microstructure of heat treated IIb
(b) HREM of YAG and β overlap.

5 7 2 The YAG Phase

Some authors [99] have proposed that the yttrium aluminum garnet phase exists as an oxynitride, $Y_3(Si,Al)_5(O,N)_{12}$, they based this substitution on EDS results, which showed the presence of Si and N within the garnet phase It has been suggested [11] that any replacement of oxygen by nitrogen in YAG is extremely limited What was probably observed, in most cases, was the overlap of YAG with β', as observed in this study· when *x*-ray analysis was performed on the YAG crystals (Figure 5 34), Si and N were also detected, since there was interference in the EDS analysis from the underlying β' grains (as in the schematic shown in Figure 5 32) It is suggested that the existence of Si and N in YAG previously observed is due to this phenomenon. Butler et al [54] also detected Si and N in EDS analysis of YAG crystals, but they did not suggest their substitution in the garnet phase However, they did not offer any explanation for the presence of Si and N in the YAG

As discussed in Section 5 6 1 3, an amorphous grain boundary phase always remains between β/β grains, however, no reports deal with the presence of residual glass between YAG and β grains at triple points Butler et al [54] proposed that at a critical level of polytype addition, YAG grows into the glassy phase and excess silicon and nitrogen diffuse into the β' phase, resulting in a microstructure of β' and YAG Figure 5 35(a) is a HREM of a YAG crystal partially attached to the adjacent β grain Lattice fringes of the YAG clearly meet those of the β in the top part of Figure 5 35(b), with no glass detected Thus, all of the Si and N present in the triple point prior to devitrification to YAG diffused into the surrounding β grains upon crystallization

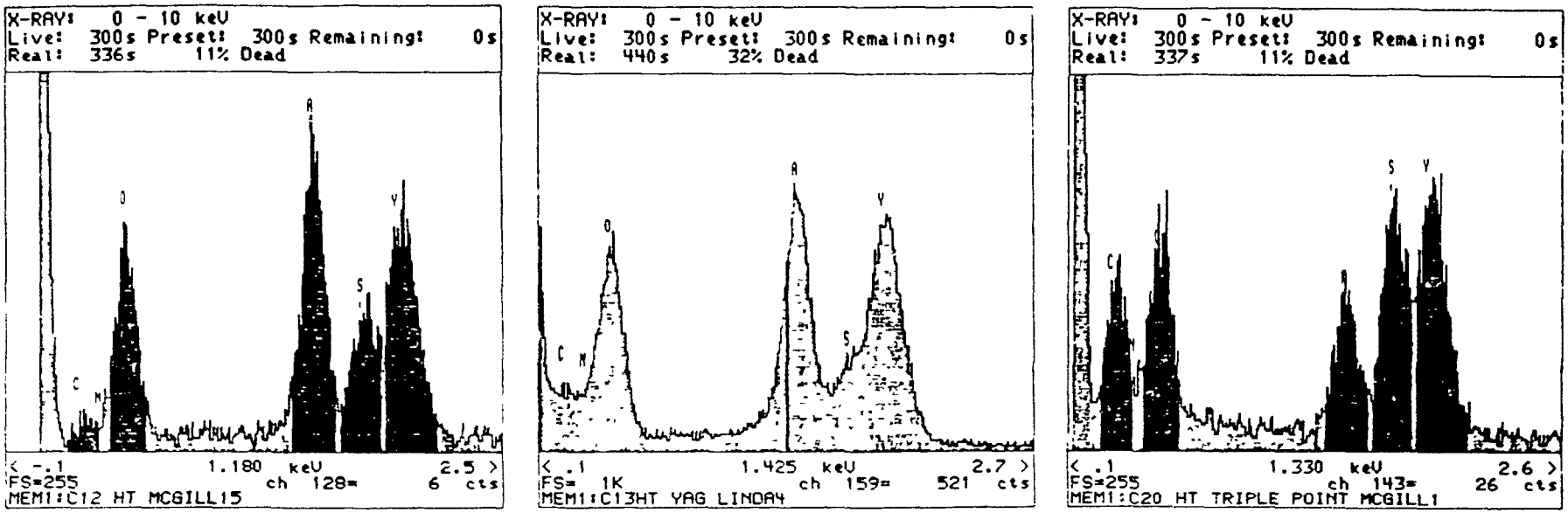

Figure 5.34 Energy dispersive spectra of various YAG triple points, showing the presence of Si and possibly N.

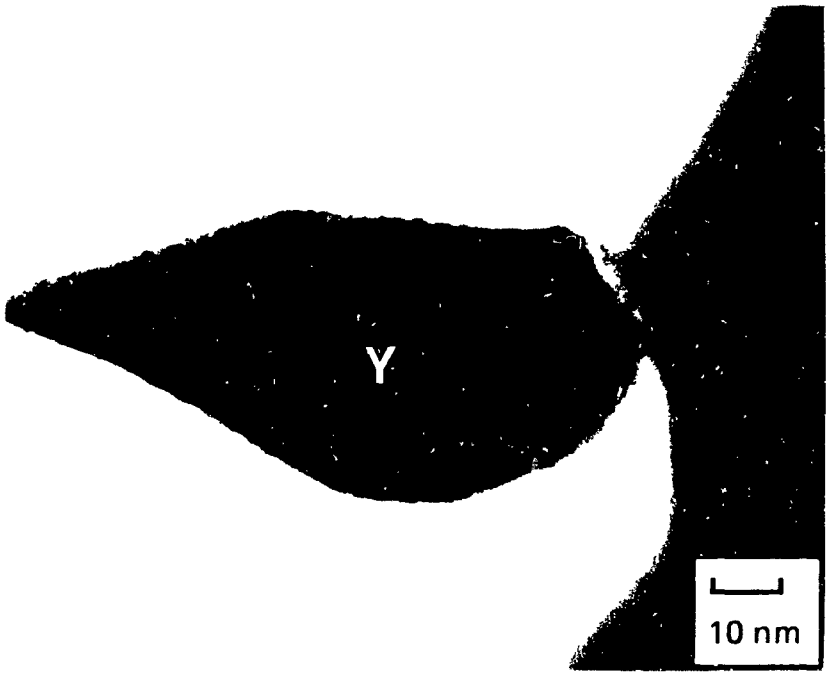

(a)

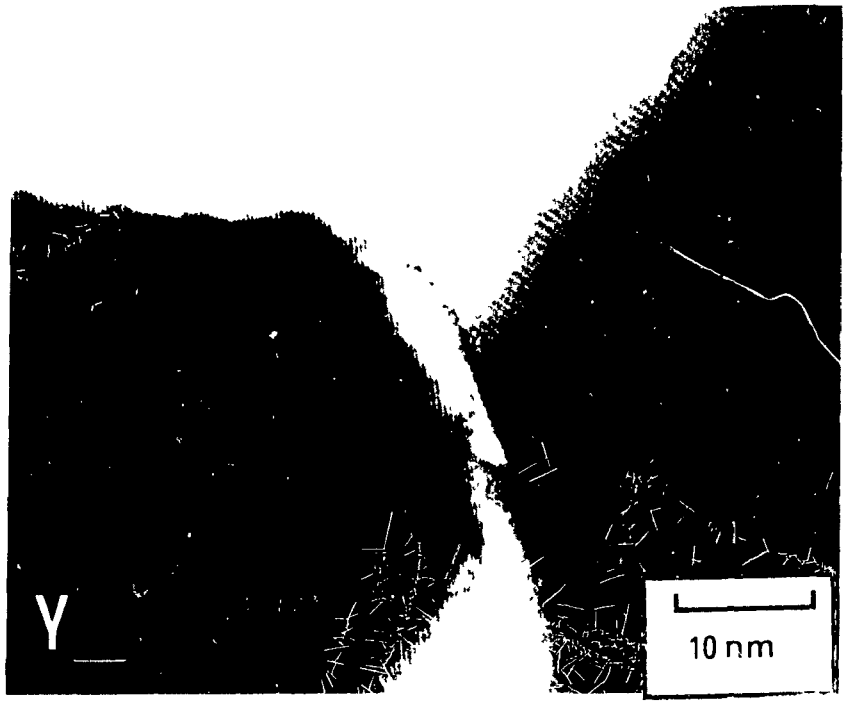

(b)

Figure 5 35. (a) bright-field image of IIb, the triangular grain being YAG; (b) HREM of YAG/Si_3N_4 overlap

CHAPTER 6

CONCLUSIONS AND TOPICS FOR FURTHER RESEARCH

This research work involved the systematic study of grain boundary control in sialon systems, by compositional control of the grain boundary phase and crystallization of the glass to a refractory phase. Three series of compositions with varying additive contents were sintered to near theoretical density; no crystallization of the grain boundary phase was observed on cooling from the sintering temperature. Different annealing conditions, i.e. heat treatment times and temperatures, were then applied to maximize devitrification of the Y-SiAlON glass to $Y_3Al_5O_{12}$.

6.1 CONCLUSIONS

6.1.1 Achieving β' + YAG

(i) Compositional control of the starting materials is essential in achieving a two-phase system of β and glass upon sintering, with complete α to β transformation.

(ii) The extent of Al and O substitution within the Si_3N_4 lattice could not be predicted.

(iii) A heat treatment temperature of ~1400°C is required to crystallize the amorphous YSiAlON glass to the stable $Y_3Al_5O_{12}$ (YAG) phase. Lower annealing temperatures result in the formation of other phases since they have higher rates of nucleation and growth and are more thermodynamically stable at that temperature.

(iv) The extent of devitrification to YAG is dependent on the composition of the glass. For full crystallization high Y^{3+} and Al^{3+} contents are required. The Si^{4+} content must be minimized as it tends to stabilize

the glass, making devitrification difficult. Thus, compensation for silicon and oxygen in the starting material (surface SiO_2 on Si_3N_4) and due to oxidation during processing of the powders are required

(v) The crystallization of YAG is found to occur in localized areas and is thought to be due to poor dispersion of the additives, resulting in micro-compositional variations from region to region in the microstructure.

(vi) The residual glass pockets which did not devitrify were found to be high in silicon Nitrogen was also present in the glass phase after heat treatment, implying that diffusion of Si and N from the glass to β is incomplete or the oxynitride glass is more stable with respect to the surrounding β grains

6.1.2. The Properties of YAG

(i) YAG crystallizes as a single crystal around the β grains, with no residual glass being observed

(ii) Crystallization of the triple points is independent of pocket size Rather, devitrification of the pockets is composition-dependent pockets high in Si will tend to remain amorphous due to the stability of the glass phase

(ii) The room temperature strength of sialons decreases significantly with devitrification to YAG This is predominantly due to the volume shrinkage associated with the formation of YAG from the glass, and results in the debonding of the YAG grains from the β' matrix

(iii) The room temperature strengths of devitrified SiAlONs are also affected by the grain morphology a refined grain structure (i e

acicular particles of ~0 3μm) in devitrified samples improves the mechanical properties.

6 2 FURTHER RESEARCH

(i) Improving the dispersion techniques to homogenize the additives is essential to improving the extent of devitrification of the glass to YAG This might require using non-powder additives since the particle size of the additives are similar to that of the Si_3N_4

(ii) Further work on high temperature properties of devitrified samples should be performed to monitor the effect of the extent of crystallization on the creep rates

(ii) Devitrification of YSiAlON glasses to other refractory phases which form with lower volume shrinkages should be studied, i e. $Y_2Si_2O_7$ The lower shrinkages should therefore result in improved mechanical properties of the SiAlON, as the effect of micropore coalescence would be reduced

REFERENCES

1. H.M. Conway, NACA CV No 4D10, September (1943)
2. R.A.L. Drew, Canadian Metallurgical Quarterly, 27 [1], (1988), 59
3. L.M. Sheppart, Advanced Ceramic Materials, 3[4], (1988), 309
4. G Ziegler, J Heinrich, and G. Wotting, J Mat Sci , 22, (1987), 3041
5. D J Godfrey, Proceedings of the British Ceramic Society, July 1978, 1
6. K H Jack and W I Wilson, Nature (Phys. Sci), 238 [80], (1972), 23
7. Y Oyama and O Kamigaito, Japan Journal of Applied Physics, 10 [11], (1971), 1637
8. R N. Katz, and G E Gazza, in "Nitrogen Ceramics", edited by F L Riley, (Noordhoff-Leyden, 1977), 417
9. R.L Coble, Journal of Applied Physics, 32[5], (1961), 787
10. K. Jack, in "Progress in Nitrogen Ceramics", edited by F L Riley, (Matinus-Nijhoff, 1983), 45
11. D Hardie and K.H Jack, Nature, 10, (1957), 332
12 K Blegen, Special Ceramics 6, (1975), 223
13 S. Wild, P Grieveson, and K Jack, Special Ceramics 5, 1972, 385
14. K H. Jack, Journal of Materials Science, 11, 1976, 1135
15. F.F. Lange, International Metals Review, 247[1], 1
16. H F. Priest, F C. Burns, G L. Priest and E.C Skaar, J Am Ceram Soc , 56, (1973), 395
17. A J Edwards, D P Elias, M W Lindley, A Atkinson, and A J Moulson, J Mat. Sci , 9, (1974), 516
18 E T. Turkdogan, P M. Bills, and V.A. Tippett, J Appl Chem , 8, 1958, 296
19 F.L Riley, in "Nitrogen Ceramics", edited by F L Riley, (Noordhoff-Leyden, 1977), 265
20 F.S Galasso and R D Veltri, J Am Ceram Soc , 1[1], (1981), C-15
21 M B Trigg, D B. Ellson, M W A Stewart, W Sinclair, A M MacDonald, and A.S. Blicblau, Materials Forum, 10[3], (1987), 208

22 D W Richerson, "Modern Ceramic Engineering· Properties, Processing, and Use in Design", Marcel Dekker, Inc., N.Y , 1982

23 B Nyberg, L K L Falk, R. Pompe and R.Carlsson, 2nd International Proceedings of Ceramic Materials and Composites for Engines, edited by W Bunk & H Hausner, (Travemunde, 1986), 154

24 W D Kingery, J Appl Phys , 30[3], (1959), 301

25 S Baik and R Raj, J Am Ceram Soc , 68[5], (1985), C-124.

26 W D Kingery, , H K Bowen, and D R. Uhlman, "Introduction to Ceramics", Wiley Pub Co , 2nd ed , (1976),

27 S Hampshire and K H Jack, Special Ceramics 7, (1981), 37

28 F F. Lange, in "Nitrogen Ceramics", edited by F L Riley, (Noordhoff-Leyden, 1977), 288

29 F F Lange, J. Am. Ceram. Soc , 56[10], (1973), 518.

30 S Prochazka and W O Rocco, High Temp. High Pressures, 10[1], (1978), 87

31 T Yamada, M Shimada and M Koizumi, J. Am. Ceram Soc J , 60[12], (1981), 1281

32 Y Miyamoto, K. Tanaka, M. Shimada, and M Koizumi, 2nd International Proceedings of Ceramic Materials and Composites for Engines, edited by W Bunk & H. Hausner, (Travemunde, 1986), 271.

33 A Rae, D Thompson and K Jack, Proc. Army Materials Technology Conf , 'Ceramics for High Performance Applications II, J J Burke, E N Lenoe and R N Katz (eds), (1978), Chestnut Hill, Mass , Brook Hill Publ Co , 1039

34 L.J Bowen, R J Weston, T G Carruthers, R J Brook, J Mat Sci. 13, (1978), 341.

35 D R Clarke and G. Thomas, J Am Ceram. Soc , 66 (1983), 114.

36 W Braue, G. Wotting, and G Ziegler, Brit Ceram. Special Ceramics 37, 71

37 K.H. Jack, Trans J Brit Ceram Soc , 72, (1973), 376

38 F P Hall and H Insley, "Phase Diagrams for Ceramists", Publication of the Am Ceram Soc. Int , 1972

39. Karyama, Inomato, J Am. Ceram. Soc , 57, 1978, 11119

40 K H Jack, Metals Tech , 9, 1978, 297

41. D.P. Thompson, Proc. 21st Conf. on Ceram. Science, Penn State, R Tressier (ed.), July 1985

42. I.K. Naik, L.J Gauckler, and T Y Tien, J Am Ceram Soc , 61[7-8], (1981), 332.

43. R.A.L. Drew, S Hampshire and K H. Jack, Special Ceramics 7, D Taylor and P. Popper, (eds.), Proc. Brit Ceram Soc. No 31, (1981), 119

44. S Wild, P. Grieveson, K H. Jack and J J Latimer, Special Ceramics 5, (1972), 377.

45. S Hampshire, R A.L. Drew and K.H Jack, J Am Ceram Soc , 67 (1984), C-46.

46 D W. Richerson, Am. Ceram J , 52[7], (1973), 561

47. G.E. Gazza, J Am Ceram Soc , 56, (1973), 602

48. A. Rae, D Thompson, N Pipkin and K Jack, Special Ceramics 6, (1973), 347

49 C.H Drummond III, W E Lee, W A Sanders and J D Kiser, Ceram Eng Proc., 9[9-10], (1988), 1343

50. W.A. Sanders and D M Mieskowski, Ceram. J , 64[2], (1985), 304

51. M. Mitomo, J Mat. Sci , 11, (1978), 1103

52. T. Hayashi, H Munakata, H Suzuki, and H Saito, J Mat Sci 21, (1986), 3501.

53. D.P Rowcliffe and P J Jorgensen, SRI Int Final Tech Report, NSF Grant No. AER 75-14896 (1977).

54. E. Butler, R.J Lumby, A Szweda, and M H Lewis, Proc of Int Symp on Ceram Components for Engines, edited by S Somiya, E Kanai, and K Ando (KTK Scientific, Tokyo, 1983), 159

55. K.H Jack, in "Nitrogen Ceramics", edited by F L Riley, (Noordhoff-Leyden, 1977), 109

56. H F Priest, G G. Priest, G E. Gazza, J Am Ceram Soc , 60[1-2],(1977), 81

57. S. Prochazka and W A Rocco, in "Nitrogen Ceramics", edited by F L Riley, (Noordhoff-Leyden, 1977),

58. D R. Clarke, F F Lange and G D Schnittgrund, J Am. Ceram Soc , 65[4], (1982), C-51

59. I.K. Naik and T Y Tien, J Am Ceram. Soc , 62[11-12], (1979), 642

60 A Tsuge, K Nishida and M Komatsu, J Am. Ceram Soc. , 58[7-8], 1975, 323

61 L K L Falk and G L Dunlop, J Mat Sci 22, (1978), 4369

62 P Greil, J C Bressiani, and G Petzow, Proc of Int Symp on Ceram Components for Engines, edited by S Somiya, E Kanai, and K Ando (KTK Scientific, Tokyo, 1983), 229

63 C J Spacie, N S Jameel and D P Thompson, Proc. of Int. Symp on Ceram Components for Engines, edited by S Somiya, E Kanai, and K Ando (KTK Scientific, Tokyo, 1983), 343

64 G Leng-Ward and M H Lewis, Mat Sci & Eng , 71, (1985), 101

65 D Bonnell, T Y Tien, and M. Ruhle, J Am Ceram Soc , 70[7], (1987), 460

66 Annual Book of ASTM Standards, Section 15, Vo 15.02, American Society for Testing and Materials, (1986), C162

67 P W McMillan, "Glass Ceramics", 2nd ed , Academic Press, J P Roberts, P Popper (eds), London, (1979), 7

68 D R Messier, Int J High Tech Ceram 3, (1987), 33

69 K H Jack, in "Nitrogen Ceramics", edited by F L Riley, (Noordhoff-Leyden, 1977),257

70 R E Loehman, J. Am Ceram Soc , 62[9-10], (1979), 491.

71 S Hampshire, R A L Drew, K.H Jack, Physics and Chem of Glasses, 26[5], (1985), 182

72 R A L. Drew, Nitrogen Glasses, in Research Reports in Mat. Sci , P.E Evans (ed), Series I, Parthenon Press, 1986

73 M J Hyatt and D E Day, J Am Ceram Soc , Oct. 1987, C-284

74 H Hohnke and T Y Tien, in "Progress in Nitrogen Ceramics", edited by F L Riley, (Matinus-Nijhoff, 1983), 101

75 R A L Drew, S Hampshire and K H Jack, in "Progress in Nitrogen Ceramics", edited by F L Riley, (Matinus-Nijhoff, 1983), 323

76 H Unuma, T Kokubo, and S Sakka, J Mat Sci , 23, (1988), 4399

77. M F Ashby and D R Jones, "Engineering Materials An Introduction to their Properties and Applications", Int Series on Mat. Sci and Tech , Vol 34, Oxford, 1980, p 122

78 J Singh, Adv Ceram Mat , 3[1], (1988), 18

79 L F Bowen and T G Carruthers, J Mat. Sci Letters 13, (1978), 684 687

80. P K Das and J Mukerji, Adv Ceram Mat , 3[3], (1988), 238

81 M D Pugh, L C Zarnon and R A L Drew, Japan Fine Ceramics Center Workshop IV, Nagoya, Japan, February 1988

82 J L Iskoe, F F Lange and E S Diaz, J Mat Sci , 11, (1976), 908

83 H Tanaka, and Y Hoshizo, Proc of Int Symp on Ceram Components for Engines, edited by S Somiya, E Kanai, and K Ando (KTK Scientific, Tokyo, 1983), 296

84 Technology Update in Amer Ceram Soc J , Vol 68, No 4, April 1989, 846

85 L C Zarnon and R A L Drew, J. Am Ceram Soc , 72[3], (1989), 495

86 Annual Book of ASTM Standards, Section 15, Vo 15 03, American Society for Testing and Materials, (1986), D3800

87 C P Gazzara and D R Messier, J Am Ceram Soc , 56, (1970), 777

88 B D Cullity, "Elements of X-Ray Diffraction", Addison-Wesley Publ Co , Inc , Reading Mass , 1978, 335

89 N Furushiro, Y. Takayama, S Hori, Mat Trans JIM, 30[1], (1989), 27

90 J I Goldstein, D B Williams, and G Cliff, "Principles of Analytical Electron Microscopy", D C Joy, A D Romig Jr , and F I Goldstein (eds), Plenum Press, N Y , 1986, 157

91 G Thomas and M J Goringe, "Transmission Electron Microscopy of Materials," Wiley-Interscience Publications, 1979

92 T Ekstrom, N Ingelstrom, R Grage. M Hatcher, T Johansson, J Am Ceram. Soc , 71[12], (1988), 1164

93 E M Rabinovich, L Harel, and R Fisher, in "Nitrogen Ceramics", edited by F L Riley, (Noordhoff-Leyden, 1977), ,71

94 D K. Lee, S J L. Kang, D N Yoon, J Am Ceram Soc , 71[9], (1988), 803

95 L J Gauckler, S Prietzel, G Bodemer and G Petzow,in "Nitrogen Ceramics", edited by F L Riley, (Noordhoff-Leyden, 1977), 529

96. M Haviar and Ø Johannesen, Adv Ceram Mat , 3(4), 1988, 405

97 H O Mulfinger, J Am. Ceram Soc , 49 (1962), 462

98 G Thomas and C Ahn, J Am Ceram Soc , Nov 1982, C-185

99 M H Lewis, A R Bhatti, R J Lumby, and B North, J Mat Sci , 15, (1980), 103

100 E Tani, S. Umebayashi, K Kishi, K Kobayashi, and M Nishijima, Am. Ceram Soc Bull, 65[9], (1986), 1131

101 W Sinclair, and M B Trigg, Materials Forum, 10 [3], (1987), 202

102 R Raj and F F Lange, Acta Metallurgica, 29, 1981, 1993

103 D D Bonnell, M Ruhle, T Y Tien, J Am. Ceram Soc , 69[8], (1986), 623

104 G Petzow and P Greil,Proc of Int Symp on Ceram Components for Engines, edited by S Somiya, E Kanai, and K Ando (KTK Scientific, Tokyo, 1983), 177

105 W E Lee, C H Drummond III, and G E Hilman, Ceram Eng Sci Proc 9 [9-10], (1988), 1355

106 Metals Handbook, "Mechanical Testing", J R Davis et al (ed), 9th ed , Vol 8, American Society for Metals, Metals Park, Ohio, 1985

APPENDICES

APPENDIX A

CONVERSION OF EQUIVALENT PERCENT TO WEIGHT PERCENT COMPONENTS OF SIALON FOR IIb

(i) Converting e/o ions to at.% elements

	cation			anion	
	Y^{3+}	Si^{4+}	Al^{3+}	O^{2-}	N^{3-}
equivalent % (e/o)	2	88	10	10	90
divide by valency	3	4	3	2	3
= atomic ratios	0 67	22	3 3	5	30
atomic %	1 1	36 1	5 5	8 2	49 2

(ii) At % elements in components

	Y	Si	Al	O	N
Si_3N_4		42 36		2 76*	54 68
AlN			50 5	3 4*	46 1
Y_2O_3	40			60	
Al_2O_3			40	60	

* based on manufacturer's data

(iii) Conversion of at % to wt.% component

Si_3N_4

at % Si = 36 1

at % O = $\frac{36\ 1}{42\ 36}$ x 2 76 = 2.35 O remaining = 8 2 - 2 35 = 5 85

at.% N = $\frac{36.1 \times 54\ 68}{42\ 36}$ = 46.6 N remaining = 49 2 - 46 6 = 2.6

mole % Si_3N_4 = 36.1 + 2 35 + 46 6 = 85 05%

AlN

at % N = residual N = 2 6

at % Al = 2 6 x $\frac{50\ 1}{46.1}$ = 2 83 Al remaining = 5 5 - 2 83 = 2 67

at.% O = 2.6 x $\frac{3\ 4}{46\ 1}$ = 0 19 O remaining = 5 85 - 0 19 = 5 66

mole % AlN = 2 6 + 2 83 + 0.19 = 5.62%

Y_2O_3

All Y comes from Y_2O_3 only

at.% Y = 1 1

at % O = 1.1 x $\frac{60}{40}$ = 1 65 O remaining = 5 66 - 1 65 = 4 01

mole% Y_2O_3 = 1.1 + 1 65 = 2.75

Al_2O_3

Al remaining comes from Al_2O_3

at % Al = 2.67

at % O = $\frac{60}{40}$ x 2 67 = 4 01 = O remaining from above

mole% Al_2O_3 = 2 67 + 4 01 = 6 68

(iv) Converting mole% to weight%

	Si_3N_4	AlN	Y_2O_3	Al_2O_3
mole%	85 05	5 62	2 75	6 68
x M W /100	141 4	41	225 8	102
	120 26	2 30	6 21	6 81
wt %	88 7	1 7	4 6	5 0

DETERMINATION OF YAG CONTENT AND Z VALUE

The following assumptions were made in calculating the amount of YAG formed and z values for IIb, based on the above data: only β' and YAG are present upon devitrification, and that all the Y^{3+} present is used to form $Y_3Al_5O_{12}$ The amount of Al^{3+} and O^{2-} used to form the garnet phase can also be calculated

One mole of $Y_3Al_5O_{12}$ contains 20 atoms: 3 atoms of Y, 5 atoms of Al and 12 atoms of O Since there are 1 1 a/o of Y present (see table above), then the moles of YAG formed are

$$\frac{1\ 1\ \text{a/o} \times 20\ \text{atoms in } Y_3Al_5O_{12}}{3\ \text{atoms of Y in } Y_3Al_5O_{12}} = 7.3\ \text{mole \% (m/o) YAG}$$

Then, the amount of Al used to form YAG is.

$$\frac{7\ 3\ \text{m/o YAG} \times 5\ \text{atoms Al in } Y_3Al_5O_{12}}{20\ \text{atoms in } Y_3Al_5O_{12}} = 1\ 8\ \text{mole \% (m/o) YAG}$$

Therefore, the amount of Al remaining in the SiAlON is:

5 5a/o Al	- 1 8 a/o Al	= 3 6 a/o Al
in starting material	used in YAG	remaining in SiAlON

The z value is equal to the number of atoms of Al in 1 mole of β'. There are 14 atoms per mole of β' SiAlON, since the atomic percent Al is known, the z value can also be determined

3.6 a/o Al in SiAlON x 14 atoms per mole of SiAlON = z value = 0 5

Therefore, the chemical formula for the β' SiAlON is

$$Si_{5\ 5}Al_{0\ 5}O_{0\ 5}N_{7\ 5}$$

The molecular weight of YAG = 593 6 g/mole

and the molecular weight of $Si_{5\ 5}Al_{0\ 5}O_{0\ 5}N_{7\ 5}$ = 281 g/mole

Therefore:

0.073 mole YAG (593.6 g/mole) + (1-0 073 mole β') 281 g/mole = 303 9 g

and the wt % YAG in the composition is:

$$\frac{0.073 \text{ mol } (593\ 6 \text{ g/mole})}{303.9 \text{ g}} \times 100 = 14\ 3 \text{ wt \% YAG}$$

APPENDIX B

α TO β TRANSFORMATION

The following data was obtained by x-ray diffraction for composition Id (sintered)

Phase	(hkl)	2θ	Intensity (counts)
α	210	35 3000	88
β	210	36.0825	1160

The weight percent β in the sample is determined by the following equation

$$\frac{I_{\beta 210}}{I_{\alpha 210}+I_{\beta 210}} = \frac{1163}{88+1163} = 0\ 93$$

From the calibration curve in Figure 4 4, the ratio of intensities is interpolated to give the weight % β in the sample In this case, wt % β = 88%

YAG CALCULATION FOR IC

The following data was obtained by x-ray diffraction for composition Ic

Phase	(hkl)	2θ	Intensity (counts)
YAG	211 400 640	18.1125 29 6750 55 4175	188 172 106
β	210	36 1100	1310

Using the ratio of intensities for each YAG diffraction line, the wt % YAG can be interpolated from the calibration curves in Figures 4.5-4 7

$$\frac{I_{YAG211}}{I_{YAG211}+I_{\beta 210}} = \frac{188}{188+1310} \Rightarrow 27 \text{ wt \% YAG}$$

$$\frac{I_{YAG400}}{I_{YAG400}+I_{\beta 210}} = \frac{172}{172+1310} \Rightarrow 24 \text{ wt \% YAG}$$

$$\frac{I_{YAG640}}{I_{YAG640}+I_{\beta 210}} = \frac{106}{106+1310} \Rightarrow 23 \text{ wt \% YAG}$$

DETERMINATION OF *a* AND *c*

The lattice parameters for β were calculated using the following equation

$$\sin^2\theta = \frac{\lambda^2}{4}\left[\frac{4}{3}\frac{(h^2+hk+k^2)}{a^2} + \frac{l^2}{c^2}\right]$$

where θ is the diffraction angle, $\lambda^2/4$ = 0 594, (h,k,l) are the Miller indices for the diffraction angle, and *a* and *c* the lattice parameters

For composition Ia

Diffraction line	2θ
212	75 5125
330	74 7625

Substituting into the above equation, and solving the equations simultaneously:

$$\sin^2 75\ 5125/2 = 0\ 594\left[\frac{4}{3}\frac{(2^2+2\times 1+1^2)}{a^2} + \frac{2^2}{c^2}\right]$$

$$sin^2 74\ 7625/2 = 0\ 594\left[\frac{4}{3}\ \frac{(3^2+3\times3+3^2)}{a^2} + \frac{0^2}{c^2}\right]$$

$$a = 7\ 609$$

$$c = 2\ 916$$

APPENDIX C

CATION RATIO DETERMINATION

The Y:Al:Si ratios were calculated based on the Cliff-Lorimer equation

$$\frac{at\,\%A}{at\,\%B} = k_{A/B}\,\frac{I_A}{I_B}$$

where at.% i is the atomic percent of element i, Ii is the intensity (or area) of the peak, and k is the k factor for the two elements.

The k factor for Y/Al and Si/Al were determined from YAG ($Y_3Al_5O_{12}$) and mullite ($3Al_2O_3.2SiO_2$) standards, respectively, as follows:

YAG

$$\frac{3\ \text{atoms Y}}{5\ \text{atoms Al}} = k_{Y/Al}\ \frac{916\ 85}{1042\ 16} \quad \text{and} \quad k_{Y/Al} = 0\ 682$$

Mullite

$$\frac{2\ \text{atoms Si}}{6\ \text{atoms Al}} = k_{Si/Al}\ \frac{566.00}{1436\ 82} \quad \text{and} \quad k_{Si/Al} = 0\ 846$$

For the sialon samples, the atomic ratios were calculated knowing the k factor and intensities of the elements as follows:

$$\frac{\text{at.\% Y}}{\text{at.\% Al}} = 0.682 \quad \frac{393.2}{421.2} \qquad \text{and} \qquad \frac{\text{at.\% Y}}{\text{at.\% Al}} = 0.637$$

$$\frac{\text{at.\% Si}}{\text{at.\% Al}} = 0.846 \quad \frac{968.6}{421.2} \qquad \text{and} \qquad \frac{\text{at.\% Si}}{\text{at.\% Al}} = 1.946$$

Multiplying by the respective valencies, the equivalent percents can thus be obtained:

	cations		
	Y^{3+}	Si^{4+}	Al^{3+}
atomic ratios	0 637	1.946	1
x valency	3	4	3
equivalents	1.91	7.78	3
equivalent %	15	61	24